# MODELING OF TOOL LIFE AND MICRO-MIST FLOW FOR EFFECTIVE MICRO-MACHINING OF 316L STAINLESS STEEL

A Thesis

by

SAURABH KAJARIA

Submitted to the Office of Graduate Studies of
Texas A&M University
in partial fulfillment of the requirements for the degree of

MASTER OF SCIENCE

December 2009

Major Subject: Mechanical Engineering

# MODELING OF TOOL LIFE AND MICRO-MIST FLOW FOR EFFECTIVE MICRO-MACHINING OF 316L STAINLESS STEEL

A Thesis

by

SAURABH KAJARIA

Submitted to the Office of Graduate Studies of
Texas A&M University
in partial fulfillment of the requirements for the degree of

MASTER OF SCIENCE

Approved by:

| | |
|---|---|
| Chair of Committee, | Wayne N. P. Hung |
| Committee Members, | Debjyoti Banerjee |
| | Jyhwen Wang |
| Head of Department, | Dennis L. O'Neal |

December 2009

Major Subject: Mechanical Engineering

# ABSTRACT

Modeling of Tool Life and Micro-mist Flow for Effective Micro-machining of 316L Stainless Steel. (December 2009)

Saurabh Kajaria, B.E., Visveswaraiah Technological University, India

Chair of Advisory Committee: Dr. Wayne N. P. Hung

Recent technological advancement demands new robust micro-components made out of engineering materials. The prevalent methods of manufacturing at micro-nano level are established mostly for silicon structures. Therefore, there is interest in developing technologies for micro-fabrication of non silicon materials.

This research studies microend-milling of 316L stainless steel. Machine tool requirement, tool modeling, cutting fluid evaluation, and the effect of cutting parameters are investigated. A machine tool with high rigidity, high spindle speed, and minimal runout is selected for successful micro-milling. Cumulative tool wear and tool life of these micro-tools are studied under various cutting conditions.

Ideal abrasive wear is observed when applying mist cooling; whereas inter-granular shearing is the major failure mode when flood cooling or dry cutting during micro-machining. Various experiments and computational studies suggest an optimal position of the mist nozzle with respect to a tool that provides maximum lubrication at the cutting edge. Mist droplets effectively penetrate the boundary layer of a rotating tool and wet the cutting edge and significantly improve the tool life.

# ACKNOWLEDGEMENTS

I would like to thank my committee chair and mentor, Dr. Hung, for providing an outstanding research environment and facility. This project would not have been possible without the vision, invaluable advice and guidance provided by Dr. Hung during the course of my research. I would also like to thank my committee members, Dr. Wang and Dr. Banerjee, for their guidance and support throughout the course of this research.

I would like to thank my colleague, Sujeev Chittipolu, in HAAS CNC Lab for helping me throughout the work. I really appreciate the contribution of Luke Bickston-Texas A&M University, David Williamson-Texas A&M University, Solomon Adera - Georgia Tech, Antony Polocaren -Penn State, Jonathan Howson- Texas A&M University and Grant Fox- Texas A&M University. Huge thanks also goes to my friends, students and the department faculty and staff for making my time at Texas A&M University a great experience.

I would like to thank our sponsor, Haas Automation Inc., MA Ford Inc and UNIST Inc. for their generous support without which the project would not have materialized.

Finally, thanks to my mother, father, brother for their love, encouragement and numerous sacrifices. I really owe this to my entire family.

TABLE OF CONTENTS

Page

# LIST OF FIGURES

FIGURE Page

FIGURE Page

# LIST OF TABLES

# LIST OF SYMBOLS

| | |
|---|---|
| D | Diameter of particle (m) |
| E | Modulus of elasticity ($N/m^2$) |
| F | Force (N) |
| h | Height of droplet (m) |
| I | Moment of inertia ($kg.m^2$) |
| L | Length of the steel bar (m) |
| m | Mass of droplet (kg) |
| $n_A$ | Number of revolutions of the air metering screw from bottom |
| P’ | Pressure in bar ($N/m^2$) |
| P | Projected diameter (m) |
| R | Radius of tool (m) |
| t | Time (sec.) |
| $T_i$ | Tool life at cutting speed $V_i$(s) |
| $\Delta t_i$ | Machining time at cutting speed Vi (s) |
| v | Linear velocity of tool (m/sec) |
| V | Drop volume ($mm^3$) |
| $V_c$ | Cutting speed at the circumference (m/min) |
| $V_0$ | Magnitude of initial velocity (m/sec) |
| $V_f$ | Velocity of the fluid (m/sec) |
| $V_{pn}$ | Velocity of the particle with respect to needle (m/sec) |

| | |
|---|---|
| $V_{pf,x}$ | Velocity of the particle with respect to the fluid in x-direction (m/s) |
| $V_{pf,y}$ | Velocity of the particle with respect to the fluid in y- direction (m/s) |
| $x_{pn}$ | X co-ordinate of the particle with respect to the nozzle tip (m) |
| $y_{pn}$ | Y co-ordinate of the particle with respect to the nozzle tip (m) |
| $\theta$ | Contact angle (degrees) |
| $\theta_0$ | Angle of entry (degrees) |
| $\Delta\sigma$ | Work done per unit area in separating the liquid from the surface (N/m) |
| $\sigma_1$ | Surface energy of solid (N/m) |
| $\sigma_2$ | Surface tension of liquid (N/m) |
| $\sigma_{12}$ | Interfacial energy (N/m) |
| $\sigma_{ij}$ | Surface tension between two phases i and j (N/m) |
| $\Delta_{max}$ | Deflection of the steel bar (m) |
| $\rho$ | Density ($kg/m^3$) |
| $\mu$ | Absolute viscosity (Pa.s) |
| $\theta_0$ | Angle of entry (degrees) |

# 1. INTRODUCTION

The continuous push towards product miniaturization has created a growing interest in academia to develop new micro-manufacturing technologies. This trend in the market has been suitably responded to by industries by development of tools and machinery for the improvement of micro-machining processes. The data suggested by most machining handbooks are developed for macro-machining and there are currently no standards to select micro-tools and machining parameters to effectively produce micro-components. This research focuses on analysis and modeling of tool life and lubricating mist for a cost effective and standard solution to micro-machining.

A quantitative definition of micro-machining is machining of miniature mechanical devices and components having features < 0.1 mm. Methods followed in the industry for development of micro-components either for micro-machinery or micro electro-mechanical systems (MEMS) related devices is typically surface micro-machining or bulk micro-machining. In surface micro-machining, a substrate is chosen and layers are deposited and etched on top of it, whereas in bulk micro-machining, the structure is etched selectively in the substrate. As products have grown in complexities of shape and material, development of alternate methods that are more conventional yet reliable like micro-milling has gained interest. With the use of advanced technology, it has become possible to achieve the extreme accuracy required for producing micro-components.

---

This thesis follows the style of Machining Science and Technology.

Tools having diameter less than 0.1 mm are developed for such applications. The usage of these tools cannot be assumed as a mere scaling of the macro tools. Such assumptions have caused high unpredictability and inaccuracy of the process.

The interest in minimum quantity lubrication (MQL) is due to problems of waste disposal and ineffectiveness in conventional flood cooling. In this method, extremely small quantity of lubricant is mixed with sufficient quantity of air. This breaks up the coolant into submicron particles before spraying on to a tool. Although micro-milling has the capability to fabricate 3D miniature parts, it comes at the cost of unpredictable tool life and premature tool failure (Tansel et al 1998). A possible solution to this problem is suggested in the form of MQL. It is found that MQL reduces the friction co-efficient in micro-milling (1mm diameter) of pure copper by reducing the tool-chip contact length (Prakash et al. 2001).

According to Masuzawa and Tönshoff (1997), micro-machining is a form of precision machining. In precision machining, the final shape of the part is very important and is directly dependent on a certain element used in the manufacturing process. They call this important element as the Shape Specification Element (SSE) (Figure 1). We can very easily justify from the information available here that mask SSE's have a limitation in producing complex three dimensional shapes. Whereas controlled solid tools as SSE's provide much more flexibility and dexterity due to the sharp nature of the tool geometry and the precise control of the tool path.

| SSE | Tool | | Mask |
|---|---|---|---|
| | Fixed tool | Controlled tool | |
| Method | Injection Molding<br>Coining<br>Electro-forming | EDM<br>Turning<br>Milling<br>Punching<br>Grinding<br>LBM<br>IBM | Etching<br>Electro-forming |

Figure1: Main micro-machining methods grouped by the shape specification element (Masuzawa and Toenshoff 1997).

The applications of micro-manufacturing range from automobiles, biotechnology, health sciences to aeronautical sciences. Conventional machining requires removal of material using mechanical force due to contact between cutting edge and material. Surface integrity of the component at micro level is thus an important consideration.

In lieu of the above considerations, a conscious effort is made to make sure that the best machine tools that had minimum runout and optimal cutting parameters are chosen.

The benefits of micro-milling compared to conventional lithographic techniques are:

1) Less setup costs

2) Flexibility in material selection

3) Consistent availability of precision tools and machinery

There is a lack of consistency in data published on MQL by different researchers due to:

1) Differences in MQL techniques

2) Lack of proper mist cooling equipments

3) Non-standard testing procedures. We have used a commercial micro-fluidization system which will allow direct application of results obtained in industrial environment.

The basic process requirements that dictate the failure mode of the tool and the surface integrity of the material are lubrication and cooling.

## 1.1 RESEARCH OBJECTIVES

This work is focused on the modeling of tool life in microend-milling of SS 316L. The lack of reliability in micro-tool performance is reduced by improving tool life with the use of mist cooling/lubrication.

The main objectives of the research would be:

1. Study and model tool wear for micro-tools.
2. Characterize a micro-fluidization system to ensure effective micro-machining.
3. Suggest optimal lubricating conditions for effective micro-machining of stainless steel.

## 1.2 RESEARCH SCOPE

The scopes of this research include:

1. Application of cumulative tool wear model for micro-milling cutters.
2. Use of 316L stainless steel for all tests.
3. Utilization of a micro-fluidization system for cooling and lubrication.
4. Identification of physical properties of various cutting fluids for effective micro-machining.

# 2. LITERATURE REVIEW

The evolution of micro or nano technology as we know today owes its inception to the most fundamental devices of micro-electronics. The invention of the first point contact transistor by Bardeen, Brattain and Shockley in 1947 at Bell Labs was the trigger for the evolution of micro-technology. This was followed by the invention of the Integrated Circuit by Jack Kilby in 1958. Since then, engineers and scientists have not looked back particularly in the field of miniaturization of components and development of silicon based monolithic structures. Micro-fabrication was generally limited to silicon till a few years ago with optical lithography widely accepted as the most viable means of manufacturing. One reason of this could be the fact the field of silicon fabrication is now completely matured and proven.

The advances in application demand more sophisticated materials for development of micro-components. This has created a need for a generic micro-machining methodology involving non silicon materials. Micro-machining is the most basic technology for production of micro-components and advanced miniaturization of parts (Taniguchi 1983). The growth of applications of micro-technology is not just limited to the fields of military, automobiles and aeronautics. It has extended further to domains of biotechnology and medical applications. Machining is the one of the key technologies that can enable the realization of such varied requirements of parts (Masuzawa 2000). The main reasons to consider alternative manufacturing techniques can be summarized as (Snoeys et al. 1986):

1) Machinability of workpiece material

2) Workpiece shape complexity

3) Surface integrity and precision requirements

4) Automation of data communication

5) Miniaturization requirements

The distinctive feature for miniaturized parts is the ability of micro-machines to handle tasks and move freely in small spaces. Small machines can further co-operate and hence integrate their tasks to perform large operations. Flextures, cantilevers, membranes, nozzles, other symmetric or non symmetric products for MEMS devices are particularly made by LIGA (lithography, electroforming and molding), other various etching techniques like wet etching, dry etching and plasma etching. These 3D mechanical structures maybe static or dynamic in their use and hence require sustainability (Lee and Dornfeld 2004). Deep ultraviolet lithography is used to machine bevel gears and implants at micron level. Thermal energy is used in the form of laser beam machining and electron beam machining primarily as a non conventional form of machining. Only bulk machining can justify the high initial cost and low productivity of such non conventional fabrication techniques (Masuzawa and Toenshoff 1997).

Although machining is the most conventional technique of manufacturing, there are various challenges in ultra precision machining in the form of the large number of process features to be controlled. These control features can only be justified by means of high speed computers that control the machine feedback. The important control parameters are:

1) Tool to workpiece position

2) Velocity and acceleration

3) Tool workpiece 3 D error compensation while machining

4) Vibration and tool runout

The objective is to design machines that are totally predictable in their work zone accuracies (McKeown 1987). Continuous improvement has permitted used of micro-machining for production of micro-components. Ultra-precision cutting machines that are numerically controlled can achieve high level of position accuracy. Hence permitting use for fabrication of micro-components. Apart from machinery, adequate tooling is essential for achieving desired cutting condition. Small radius of tool cutting edge and strength of tool for cutting small thickness and hard material respectively are important considerations. Micro-drilling, micro-milling, micro-turning, micro-grinding and micro-punching are few types of machining techniques commonly used for machining micro-holes, complex 3D profiles and micro-pins (Masuzawa 2000).

## 2.1 MICRO-MACHINING

A useful form of micro-machining for producing features such as grooves, cavities and 3D convex shapes is micro-milling. In this case, the tool force has a major influence on accuracy, as cutting force acts perpendicular to the tool axis (Masuzawa 2000). Due to extremely small and thin parts and tools, mechanical deformation is a major challenge. Thermal deformation is not so pronounced because in the process of miniaturization, the amount heat produced is also scaled down. This may however be untrue for large machines, as precision can be affected by thermal deformation of parts. Micro-machining requires high accuracy and greater control of machining path. Also, surface integrity of micro-components cannot be scaled down from their counterpart requirements of macro product. The process is greatly dependent on the quality of tools available. The interfacial condition between the tool and the workpiece are important as the principle of cutting is the reproduction of the shape of the tool (Masuzawa and Toenshoff 1997). These problems are resolved as the quality of machine tools and cutting tools is improved. State of the art micro-machining tools and equipments like miniature end mills having diameter of the range 100-500 μm are developed that provide accuracy within $\pm$ 1μm along.

The dimensional accuracy of a miniaturized part in a micro-actuator is important to its functionality. Spindle runout (lateral movement of its rotation axis) is identified as one of the major causes for lack of accuracy. Due to runout, tools have a dominant

cutting edge and a non dominant cutting edge. Cutting marks from non dominant cutting edge are observed on microend-milled parts. Typically, controlling tool runout will have a considerable effect in improving the surface integrity of micro-machined components (Bao and Tansel 2000[a]). The 3D parts produced by microend-milling have further scope of material, geometry specifications than those produced by lithography. Microend-milling is suggested as a companion to lithography for MEMS fabrication techniques (Lee and Dornfeld 2004). It can also be used for fabrication over a large range of materials including stainless steel, aluminum, copper and brass. Fabrication of part that is too small for conventional machining (features less than 0.1mm) can be done only by microend-milling on a precision machine with high speed spindle capability. To control the surface integrity of parts under such considerations, a chip load (1-6μm) should be determined very conservatively and cutting speed (0.05-0.5m/s) should be monitored (Lee and Dornfeld 2004).

The overall quality of parts is affected easily by undue forces and vibrations in the tool while micro-milling. In a bid to improve the quality of the parts and the performance of micro-machining in general, several tool monitoring systems are developed (Malekian et al. 2009). These monitoring systems are responsible for providing feedback on the tool performance. Several systems using accelerometers, force sensors, acoustic emissions and multiple fused sensors are developed to maintain part quality and monitor machining at extremely low tolerances. Up to 27% inaccuracy in prediction of tool wear is reported.

An attempt is made by Rusnaldy et al. (2007) to machine single crystal silicon wafers using microend-milling. It is very difficult to machine single crystal silicon structures using microend-milling as it is very brittle. Ductile machining of silicon is done under high hydrostatic pressure with diamond coated tools using very small feed rates (2-20μm/s). Lai et al. (2008) suggest that the undeformed chip thickness should be comparable to the cutting edge radius in micro-milling of oxygen-free high thermal conductivity (OFHC) copper using a 0.1mm end-mill. If the chip thickness is less than the minimum thickness, the shear energy and the cutting force increase greatly. Hence in order to remove extremely small amount of material, a very sharp cutting edge is required. The sharpness of cutting edge is limited by the fabrication techniques and by grain size of the carbides. While machining hard materials, the cutting edge deteriorates very fast. This limits the tool life for micro-machining. Aramcharoen et al. (2008) suggest that tools coatings should be deposited on tungsten carbide microend-mills to improve tool life and tool performance. Flank wear and edge chipping of TiN coated micro-tools is found to be lesser than TiAln, TiCN, CrN and CrTiAlN coated tools. The application of coatings to micro-tools especially around the cutting edge is a huge technological challenge. It is found that most coated tools fail due to de-lamination of the coated layer from the base material due to inadequate adhesion between the two (Aramcharoen et al. 2008).

A study on micro-milling of copper is done by Rahman et al. (2001)[a]. They have created a model to compare tool life for micro-tools (1mm diameter). The tool life criteria are not defined categorically. Comparison is made between different cutting

parameters like axial depth of cut (0.15-0.25mm), cutting speed (25-75m/min) and helix angle ($25^0$ and $30^0$) of tool by comparing flank wear after a fixed number of passes. Since the tools are extremely small, cutting forces are also found to be considerably less compared to conventional machining. Grooves are cut on a copper block under different conditions and the tool performance is studied. A tool maker's microscope is used to measure flank wear. Wear is found to be non-uniform on both edges, hence increasing the cutting force and probability of failure. For an axial depth of cut 25% of tool diameter, the tool life increases considerably when compared to an axial depth of cut 15% of tool diameter. Tool wear on a $25^0$ helix tool is found to be better than the $30^0$ helix. They conclude that tool life increases with increase in depth of cut and reduction in cutting speed.

The flank wear criteria for macro-machining (0.3mm) cannot be used for micro-machining since this is larger than most of the tools themselves. This makes it difficult to define a common base line for measurement of tool life.

## 2.2 MICRO-TOOLS

The design of end mills can be a miniaturized version of the macro sized tool but process of tool fabrication is much more complex and challenging. Custom fabricated tools (smaller than 100 micrometer) can be made with the help of focused ion beam (FIB) machining followed by machining on custom built ultra precision micro-milling centers. Repair of masks, junctions and sectioning of metallization layers in the semiconductor industry is carried out successfully with FIB. The main advantage is the controlled removal of metals in the range of atoms/ion. Complete control of the beam intensity and its movement allows the user to remove metal very precisely, providing extensive flexibility in design. The material used for the tool is typically a cylindrical piece of very hard material like tungsten carbide or tool steel. Cutting edge is machined using FIB first on one side, followed by $180^{o}$ rotation of the pin (Friedrich et al. 1997).

The conventional micro-milling process is more desirable from an economical standpoint. Vasile et al. (1996) has used custom built 22 microns end-mills to machine trenches in PMMA (Poly[methyl methacrylate]) with features in the 1-2 micron range.

The geometry of the cutting edge is important in micro-machining. In micro-machining, edge radius and chip thickness ratio is more significant. A rounded cutting edge is found to be more favorable in generating better surface finish (Aramcharoen and Mativenga 2009). Fang et al. (2003) have proposed various tool geometries:

1) ‘Δ’ cross section with tapered body;

2) Two flute end mills;

3) ‘Δ’ cross section end mills;

4) ‘D’ cross section end mills;

5) ‘D’ cross section with tapered body.

The two-flute end mills have the least rigidity compared to other geometries. Tool geometries no (3) and (4) are not suitable for micro-machining. Tools with tapered bodies can be used to form tapered features and other complex 3D structures. Two flute end mills below 0.1 mm diameter are very weak and not suitable for machining. Eelectrical discharge machining (EDM), grinding, wire electro-discharge grinding (WEDG), FIB are the different processes used to fabricate micro-tools (Dornfeld et al. 2006).

The micro-tools for milling, drilling and grinding can be coated with single layer or multilayer coatings combining titanium carbo-nirtide (Ti-CN); titanium aluminum-nitride (Ti-AlN) or titanium nitride (Ti-N). Chemical vapor deposition (CVD) and physical vapor deposition (PVD) are methods of depositing these coatings on carbide cutting tools (Prengel et al. 2001). Of these, PVD coatings offer performance advantages over CVD. These coatings can be monolayer or multilayer. Hard multilayer coatings are found to de-bond easily due to high compressive residual stresses.

The un-deformed chip thickness is comparable to the cutting edge radius in micro-machining. To keep the material removal at its minimum, a very sharp edge is required in micro-tools. A wide selection of coatings is tested in micro-milling of steel by Aramcharoen et al. (2008). A very thin coating of 1.50±0.15 μm thickness is applied on micro-tools compared to 2-3μm on a macro-tool to keep the cutting edge sharp. These

coated tools are found to facilitate MQL type cooling and lubrication. The failure model is based on flank wear and coating chip off. Cutting edge chipping is found to be the major failure mode in most cases. Of all coatings, TiN is found to be the best coating while improving tool life and surface quality of machined surface while machining hardened tool steel.

The models used for micro-machining are an extension of Taylor's tool life equation in most cases. The basic equation is modified by design of experiments by various researchers to develop a model for micro-machining. There is no published model developed for machining using mist cooling/micro-milling.

The modeling of tool life in end milling stainless steel is done by Alauddin and El Baradie (1997). The model is developed for macro-machining and the failure criteria are defined as a 0.3mm flank wear or 0.5mm localized wear. A tool life model based on Taylor's tool life equation is used in this process and a large number of experiments are carried out based on a mathematical model involving changes in cutting speed, feed per tooth, and axial depth of cut. A first order model and a second order model are developed and both of them are valid under different cutting conditions. A single model cannot be used to generalize the tool life calculations. Tool wear is measured using a tool maker's microscope after slots are cut on a steel block.

The requirement for any tool wear/tool life model is the fact that it should be suitable to a wide range of machining parameters. The model should also be easily adaptable to industry applications and should be easy to use. The model developed for near dry machining or MQL by Marksberry and Jawahir (2008) is based on the some of

the above requirements. Their model is based on the Taylor's equation and incorporates mist spray parameters in the basic equation. The calculation of this exponent is based on a torque test of the tool while using different metal working fluids.

To reduce the number of tests and the material usage, design of experiments is used to frame a series of experiments having reduced number of trials. Random design of experiments is found to reduce the number of experiments by more than 50% (Kuljanić and Šolaja 1980). This involves randomly selecting values of depth of cut, feed per tooth, cutting speed. It also requires knowledge of maximum and minimum cutting speed, depth of cut, feed for a given material on a given machine and specific tool. Although reliable, this makes the technique very complex and unsuitable for generic usage. The most common method for solution of Taylor's equation is regression analysis using the method of least squares.

The cutting forces in micro-machining are the same in nature as in macro-machining. The wear and failure mechanisms are different in micro-milling. Failure of tools depends on the process parameters in micro-milling. Characteristic failure conditions in mist, dry and flood conditions while macro end milling Titanium is flank wear, crater wear, chipping, flaking and catastrophic tool failure (Sun et al. 2006). Tansel et al. (1998) found out that while slot milling during micro-machining, failure took place due to a static component of cutting force in the direction of the feed. They developed a model using wavelet transformations and average values of cutting direction force measurements. Tool failure is defined as breakage of the tool shaft and its prediction is done by monitoring the static part of the force in the cutting direction.

A limitation for using a microscope for measuring flank wear on micro-tool is the resolution of the device. Filiz et al (2007) use an SEM to measure wear on a 254μm tungsten carbide (WC) end mill after performing wear tests using a 3 different RPM's and 4 different feed rates. Wear is measured using the reduction in tool diameter. The width of the micro-milled channel is compared to the diameter measurement. Diameter is measured from the end view of the tool under an SEM. The wear is a form of attrition where individual WC particles get extricated from the cobalt matrix, which is softer.

Hung and Zhong (1996) suggest a cumulative tool wear model for machining metal matrix composites, which involves much fewer steps in tool life testing. The principle of this technique is to machine either at high then low speeds or low then high speeds with constant feed rate and depth of cut until failure of the tool. The data shows no difference for either cases of low to high or high to low speed variation. They suggest that their model can be used in all machining cases having abrasive wear. This technique is experimentally verified for turning, milling and facing operations, making it a generic approach. The equations presented by them are:

The model for side milling is derived:

$$\frac{1}{\lambda} QC = \sum_{i=1}^{k} \Delta t_i V_{ci}^{\frac{1}{n}} \quad ; \; Q = 1.00 \tag{1}$$

$$\lambda = \frac{\text{tool - chip interaction time}}{\text{milling time}} = \frac{M.Arc\cos(1-\frac{2a}{D})}{360°} \tag{2}$$

where:

$\Delta t_i$ : machining time at cutting speed Vi.

i, j: discrete steps;

$T_i$: tool life at cutting speed $V_i$

$V_c$: cutting speed at the circumference

Q: total accumulative damage

K: number of machining passes

C, n: constants

a: width of cut (radial depth) in side milling

D: diameter of a milling cutter

M: number of teeth on a milling cutter

Equivalent tool life $T_e$: $$T_e = \sum_{i=1}^{k} \Delta t_j \quad (3)$$

Equivalent speed $V_e$: $$V_e^{\frac{1}{n}} = \frac{\sum_{i=1}^{k} \Delta t_i V_{ci}^{\frac{1}{n}}}{Q \sum_{i=1}^{k} \Delta t_i} \quad (4)$$

This model is utilized with tool wear/tool life data obtained for micro-milling in this research.

## 2.3 TOOL WEAR

The research on end mill tools has enabled constant progress in the development of end mill design that can perform better, with less wear and longer life. The optimum conditions have to be justified for the type of tool being used, especially for microend-mills. The technique used for fabrication of these tools make them extremely expensive compared to ordinary end mills. To make the process more cost effective, researchers have showed a lot of interest in improving cutting conditions and reducing tool wear. A worn out tool can cause a lot of burrs and affect the surface finish. Due to unpredictable performance of microtools, the accuracy of machining gets affected. It thus becomes necessary to predict the tool performance and life for effective micromachining. Dolinek et al. (2001) have suggested that tool wear in high speed cutting is caused by:

1) Oxidation of tool protective layer;
2) Tool flank and chip adhesion;
3) Abrasion due to workpiece inclusions.

These processes are thermally assisted and the rate of wear increases with increase in temperature.

The estimation of tool wear can be done by tool wear monitoring systems that do not require disengagement of tool from the machine. These methods do not require physical measurement of wear using an optical microscope. Wear can be monitored using various sensors like accelerometers, force and acoustic emission sensors (Malekian

et al. 2009). The signals are used to determine whether the tool is worn out. The methods used for monitoring tool wear in micro-machining are:

1) Use of motor current and power (Salgado and Alonso 2007) for detecting breakage and tool wear
2) Acoustic emissions using coolant as transmission medium (Dolinek and Kopa 1999)
3) Cutting force signals for detecting tool breakage, fracture and wear (Tansel et al. 2000)
4) Force signals for detecting tool wear
5) Multiple fused signals (cutting force, acoustic signals, spindle vibration, spindle current) are used to estimate wear in micro-milling (Jemielniak et al. 2008).

All of these are highly complex, expensive systems and of all these, accurate cutting force measurement provides most effective monitoring results. At micron level, impracticality of dynamometer limits scope of application (Huang et al. 2007).

The cutting force increases with tool wear and this in turn affects the surface finish. Analytical models are developed to estimate the cutting force knowing the amount of tool wear (Bao and Tansel 2000[b]) as shown in Figure 2. It is concluded that 1) both feed and normal direction cutting forces increases with the increase of tool wear, 2) the ratio of feed and normal direction cutting forces remains the same for a new tool and an old tool. It is suggested that as wear of a tool increases slowly in the beginning and then has an exponential rise until failure, the progress in increase of cutting forces is also

slow in the beginning and then increases fast as the cutting edge becomes blunt and built up edges start forming. In Figure 2, the tool life is measured in inches of work travel.

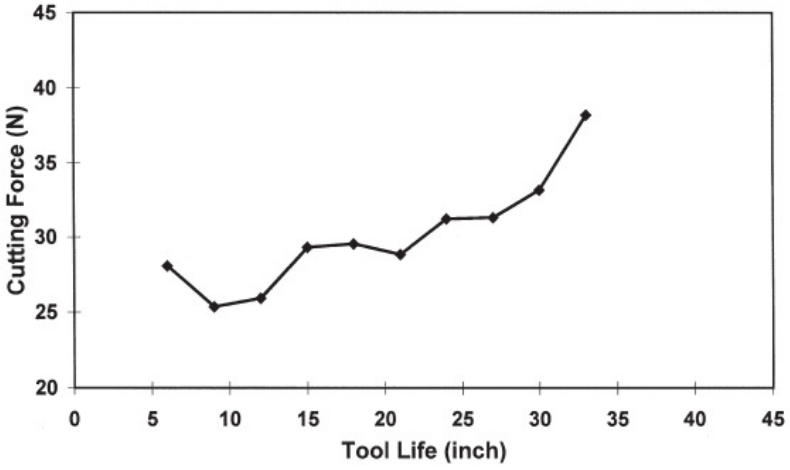


Figure 2: Relationship of maximum cutting force and tool usage for machining of a NAK-55 steel workpiece with a carbide tool (Bao and Tansel 2000 [b]).

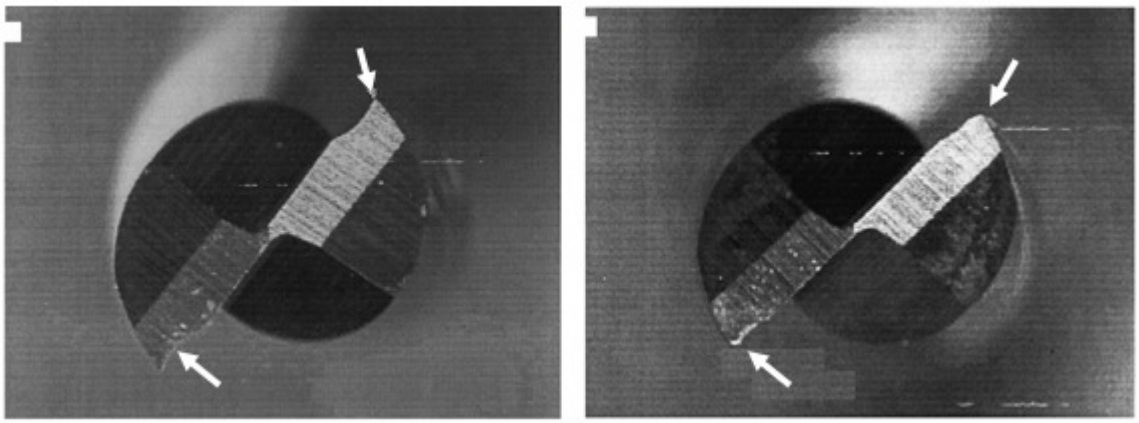

(a) (b)

Figure 3: a) Arrows point to cutting edges of a new tool b) arrows point to cutting edges of a worn out tool (diameter 0.762mm) (Bao and Tansel 2000 [b]).

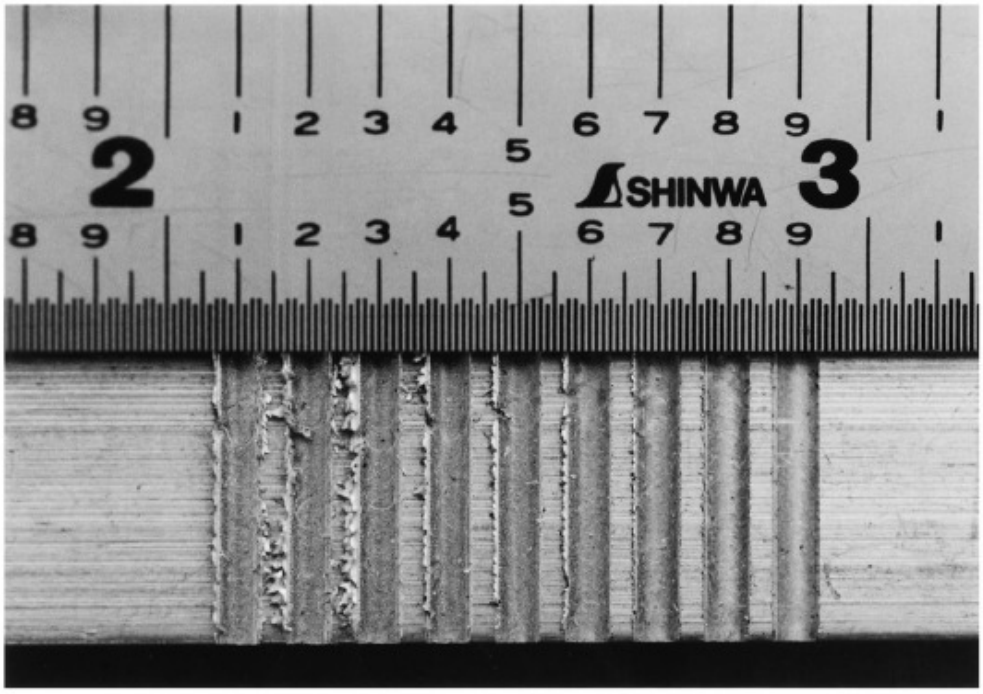


Figure 4: The burr free (right) and the burr (left) slots on an aluminum workpiece after machining with a new to worn out microend-mill (Bao and Tansel 2000 [b]).

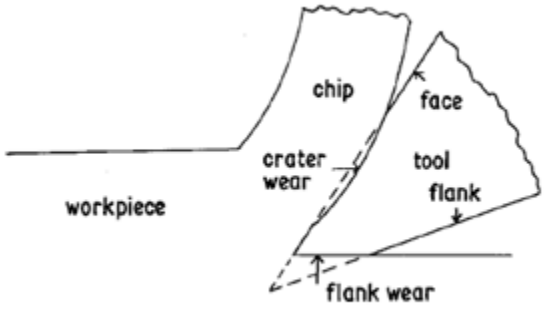


Figure 5: Regions of wear on a cutting tool (Kim and Chun 1985).

Tool wear is a gradual phenomenon by which material is removed from the cutting edge and the nose of the tool due to the abrasion and frictional contact between the workpiece material and the tool (Figure 3). As the tool wears out, the machined

surface becomes rough and has a lot of burrs sticking to it as shown in Figure 4. Figure 5 represents the regions of wear on a tool. The cause of wear can be abrasion, diffusion, oxidation and adhesion. Since cutting edge is also miniaturized, none of these forms of wear can be completely neglected as the tools are very small (Kim and Chun 1985).

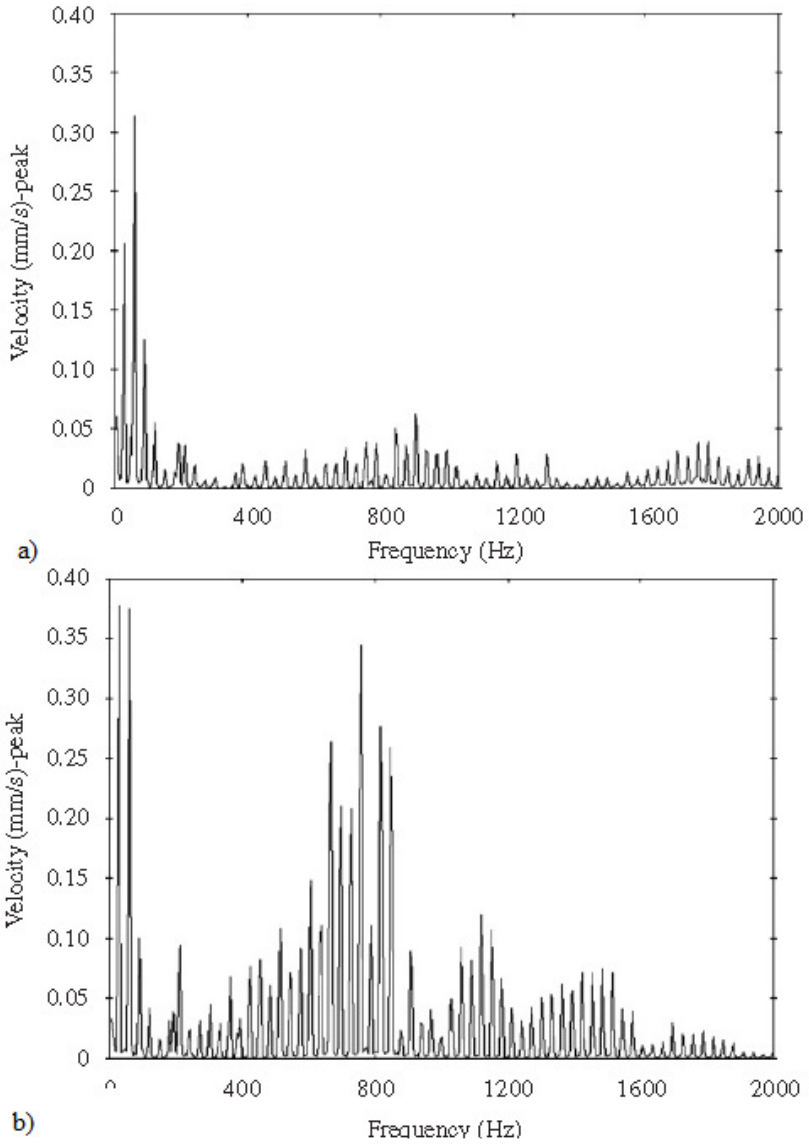


Figure 6: Sample comparison between tool vibrations a) new tool; b) worn out tool (Orhan et al. 2007).

A model to study tool wear in end milling using vibration analysis of the tool (35mm diameter) is done by Orhan et al. (2007). They use an acceleration sensor to measure vibration of the tool in the direction of cutting. The tool wear is measured continuously until failure using a tool maker's microscope. The vibration amplitude is found to increase considerably when the tool is worn out. A sample comparison between vibration amplitude on a new tool and a worn out tool is shown in Figure 6. A variation in the tool monitoring methods is suggested using online/offline systems in micro-milling.

1) A laser system is mounted on the machine spindle. The laser spot is focused on the cutting edge of the tool while machining (online).
2) A potential is applied between the tool and workpiece. Voltage is measured and abrupt changes in voltage are measured (online).
3) Standard laser systems used to monitor tool positioning in machining centre's are used to measure the cutters at specified intervals. An error is displayed on the machining screen (on the CNC machining centre) if the tool fails (Gandarias et al. 2006).

The small geometry of micro-tool can make it very difficult to measure wear using an optical microscope. Weinert and Petzoldt (2007) use SEM for measuring wear on a microend-mill having a diameter of 0.4mm. Similarly, Filiz et al. (2007) measure the width of the micro-milled groove as an assessment of tool wear. The final groove width is compared to the SEM measured diameter on a 254μm end-mill after micro-milling copper.

The methods suggested for tool life measurement are expensive and time consuming. To save on time and material, short methods are suggested by Dos Santos et al (1999), Alauddin and El Baradie (1997) including methods of continuously increasing cutting speed. Most of these methods are only established for a specific type of material. The methods of Dos Santos et al. (1999) show a mean percentage error in tool life from 10% to 46% between stainless steel and medium carbon steel. Figure 7 discusses different factors influencing tool life in micro-milling. Tool life is influenced by machine, workpiece and tool characteristics as input by the machinist. The type of end milling operation finally defines the characteristics of wear.

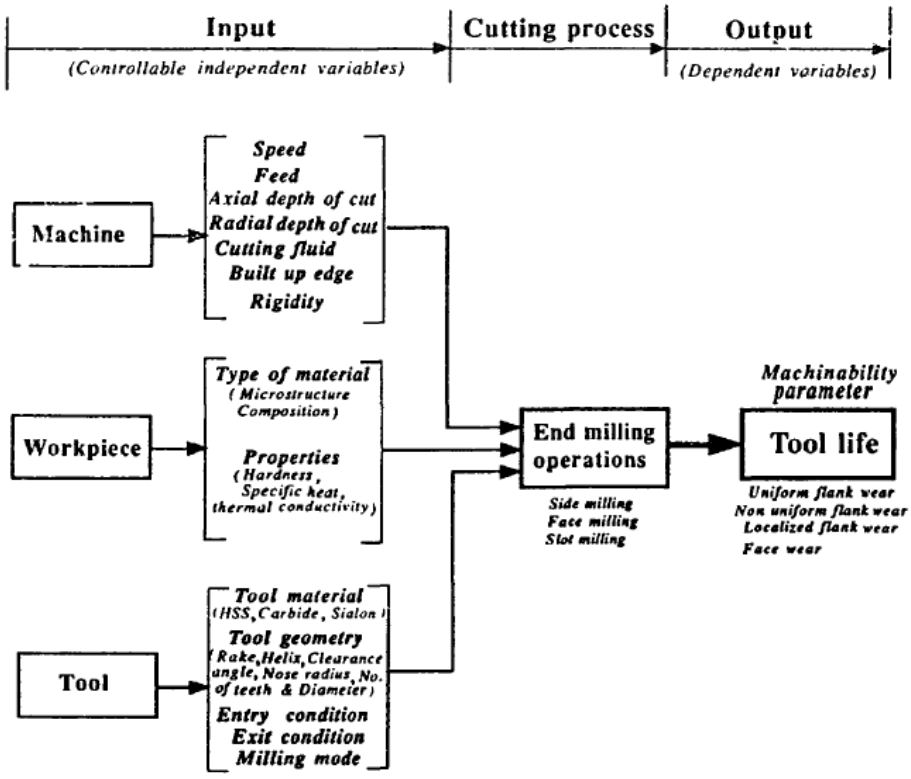


Figure 7: Factors influencing tool life in micro-milling (Alauddin and El Baradie 1997).

The most common method of evaluating micro-tool performance is using tool wear/tool life model. Various models are created for measuring tool wear/tool life and most common model applied for evaluating tool life is using Taylor's tool life equation. Most models are based on an extension of Taylor's elementary equation primarily because although it is a lengthy process, it provides a direct and easy way to correlate cutting speed and tool life. Following Taylor's tool life based models are widely used:

1) Taylors tool life equation- This is the most elementary form for tool life measurement. Expressed as $VT^n = C$; T represents tool life (minutes); V represents cutting speed (m $min^{-1}$); C is a constant; n is an exponent. To determine the value of n, tool life at different cutting speed needs to be experimentally determined, which is a very laborious and lengthy exercise.

2) Wu's tool life equation: This is another form of the Taylor's tool life equation. $TV^{\alpha}f^{\beta}d^{\gamma} = C$, where T is tool life (minutes), V is the cutting speed (mm $min^{-1}$), f is the feed rate (mm $rev^{-1}$), d is the depth of cut (mm), C is a constant, $\alpha$, $\beta$, $\gamma$ are exponents determined by curve fitting tool life testing data. In Taylor's tool life equation, the feed rate and the depth of cut are kept as constant whereas in Wu's equation, feed rate and depth of cut can vary. Hence for arbitrary conditions, Wu's equation would be preferred over Taylor's equation (Kim and Chun 1985). The exponent of depth of cut as expressed in Wu's equation is found negative in many cases. Negative exponents are not acceptable in Taylor's equation or Wu's equation. It is suggested that depth of cut is not a significant factor in determining tool life (Kuljanić and Šolaja 1980).

## 2.4 MINIMUM QUANTITY LUBRICATION AND COOLING

The demands of Occupational Safety and Health Administration (OSHA), National Institute for Occupational Safety and Health (NIOSH) and International Organization for Standardization (ISO) to reduce coolant costs, provide effective maintenance, reduce disposal, maintain emission standards has made near dry machining attractive to metal working industries not just in the USA but around the world (Chakraborty et al. 2008). The utilization of metal working fluids is around 100 million gallons in USA alone, around 640 million gallons all over the world. The primary role of these metal working fluids is to cool the tool and the chips, provide lubrication at the tool chip interface, wash the chips, residual metal, improve surface finish of the workpiece, reduce adhesion between tool and workpiece, balance the distribution of heat generated. Although these effects are beneficial, the harmful effects outweigh the benefits forcing us to relook at the means by which we fulfill these objectives. The cost of cutting fluids is around 17% of the machining costs of automotive components and there are 1.2 million workers that are affected by the chronic effects produced by these cutting fluids (Marksberry and Jawahir 2008).

The conventional cooling techniques practiced in most metal working industries is complete flooding of a water based coolant over the tool workpiece interface. Apart from the composition of the coolant, most other factors regarding the technique are randomly chosen. Amount of fluid, exact application of the fluid are unknown. Also, most shops use the same kind of fluid for all their applications. Different metals react

differently to the type of cutting fluid chosen. This causes lot of uncertainty over the usage of cutting fluids for sophisticated operations; especially while micromachining using expensive tools and a wide range of materials from polymer to exotic metals. Ying-lin et al. (2009) use nitrogen gas for cooling and lubrication while machining titanium alloys. This avoids burning of chips and reduces tool abrasion.

There are three basic types of machining conditions:

1) Flood cooling: This involves flooding of the tool and workpiece using a cooling fluid that maybe like an emulsion of oil and water. Multiple nozzles can be used and the fluid is filtered and re-circulated.

2) Mist cooling: This is an alternate form of cooling that requires a spray nozzle, which mixes a small quantity of cutting fluid with a high pressure jet of air. This breaks down the oil of coolant into extremely fine particles that flow within the high pressure jet of air. This is aimed directly at the cutting edge and cannot be re-circulated. This method allows a significant reduction in the amount of cutting fluid being used. Instead of flooding the tool, with gallons of fluid per minute, few ounces of cutting fluid is used per hour. This is also known as MQL.

3) Dry machining: This is the crudest operating condition that involves machining without the application of any cutting fluid.

The MQL type is beneficial to tool life in both coated and uncoated tools (Kang et al. 2008; Liao and Lin 2007; Liao et al. 2007). High speed end milling performance with hardened steels is found to improve under MQL, whereas flood cooling resulted in lesser tool life due to large number of thermal cracks. The welding of chips to the tool is

delayed by MQL. Liao and Lin (2007) also suggest that in high speed milling (150 - 250 m/min) of hardened steel, MQL provides extra oxygen to the tool which facilitates formation of a protective oxide layer on the cutting edge. This oxide layer is formed at an optimal machining speed and is not helpful in extreme high speed machining. Less viscous oil should be used so that the cooling effect can be effective. Most of the research is focused on drilling (connecting the MQL directly to the spindle- Tasdelen et al. 2008) and turning operations. Published info of using MQL in micro-milling is yet to be found.

The aspect of health and safety under near dry machining or mist cooling is covered by many authors and they have commented that due to the aerosol formation during mist flow at high pressure, an air suction unit should be installed to prevent breathing of the aerosol particles by the operator. If the pressure is low and the quantity of metal working fluid that is being vaporized is also limited, the process is much more safe. Regarding the effectiveness of the process, it is suggested that obstruction from workpiece and chip flow greatly affects the performance of the process (Marksberry and Jawahir 2008). Rahman et al. (2001)[b] have also suggested that tool life does not improve over flood cooling while milling at low speed and low feed rates and surface finish in most cases is equivalent for near dry machining and flood cooling as shown in Figure 8 and Figure 9.

The application of MQL to micro-milling is studied by Prakash et al. (2001). The mode of failure is defined as 0.08mm of flank wear or catastrophic failure of tool due to chipping. It is found that lower the cutting speed higher the tool life since the mist can

penetrate the tool-chip interface at low speeds. They also predict that tool life increases with feed rate. Since wear is primarily due to abrasion, slower the feed rate, more is the abrasion. They predict that the tool life will keep increasing with feed rate after which it will fail by tool fracture/chipping. Depth of cut also affects the rate of wear similarly.

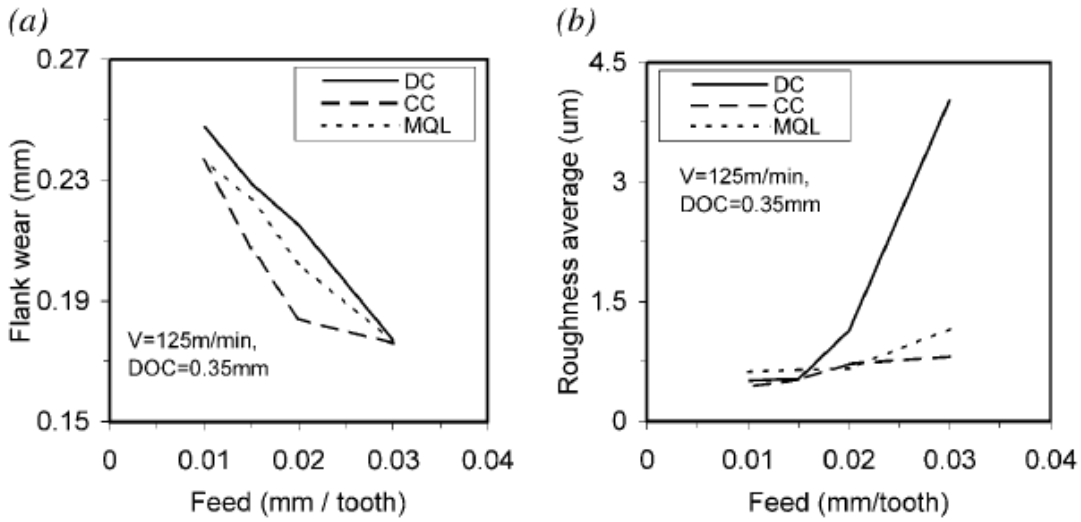


Figure 8: Effect of feed on a) flank wear b) surface finish. DC: dry cutting; CC: flood cooling; MQL: minimum quantity lubrication, DOC: depth of cut; V: cutting velocity (Rahman et al. 2001) [b].

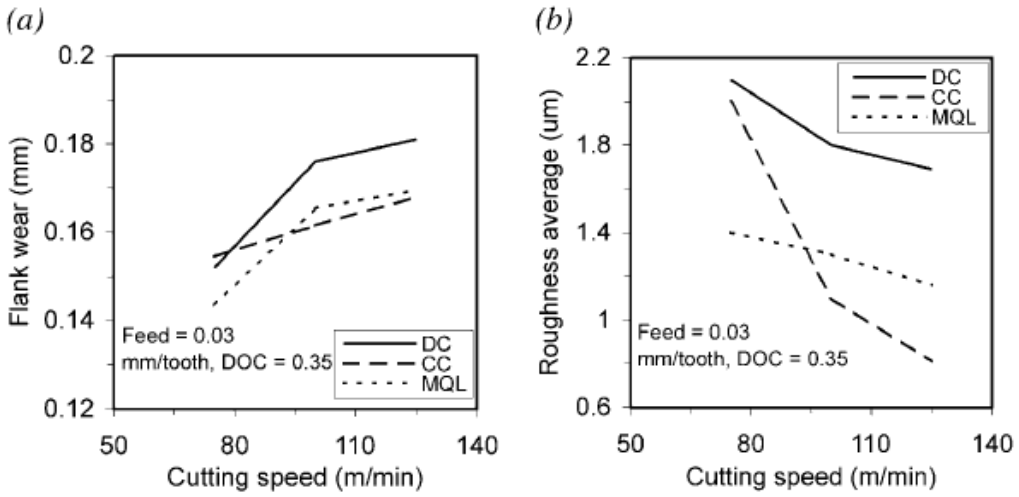


Figure 9: Effect of cutting speed on a) flank wear b) surface finish. DC: dry cutting; CC: flood cooling; MQL: minimum quantity lubrication, DOC: depth of cut; V: cutting velocity (Rahman et al. 2001 [b]).

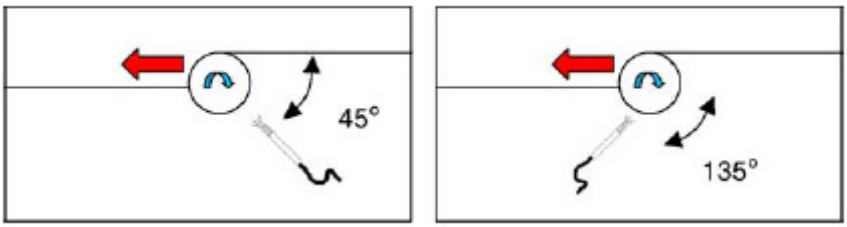


Figure 10: Recommendations for nozzle positioning in down-milling [Sic] (L´opez de Lacalle 2005).

A series of experiments conducted by Rahman at al. (2001) [b] shows that MQL has best performance over dry machining or compressed air blast machining. Among these, MQL produced least flank wear when the coolant rate is as low as 6ml/h. At higher feed rates, larger shear stresses would be produced causing deterioration of tool. It also clearly states that the oil droplets have difficulty reaching the tool tip and wetting the cutting edge if the tool is rotating at a high speed (95-125m/min). Figure 10 shows the recommendation for nozzle positioning with respect to the tool and workpiece in down milling. The nozzle is placed at an angle with the direction of cutting, facing the workpiece. There is no justification provided by the author (L´opez de Lacalle 2005) regarding this suggestion. The effect of distance between nozzle tip and workpiece is pronounced in case of mist cooling. Closer nozzle tip is found to provide more effective lubrication. In spite of the interest shown in micro-milling, no work is done so far on microend-milling of stainless steel using mist cooling/lubrication.

## 2.5 APPLICATIONS OF 316L STAINLESS STEEL

The application of MEMS devices in more complex mechanical, electrical, thermal, fluidic and medical devices has increased the demand for material flexibility in MEMS products. The conventional materials used for MEMS devices include mostly silicon and semiconducting materials. The reason for choosing silicon for most applications is because the technology for silicon fabrication is completely matured and this makes industry more comfortable in its development efforts. The fact that MEMS can be used in more sophisticated applications like biomedical, surgical, biotechnological rather than just electronics opens up a whole new spectrum of opportunity to develop techniques for fabrication of other interesting materials. Major chemical ingredients in weight percentage of SS 316L including Mn, Cr, Ni and Mo are as shown in Table 1. Stainless steel 316L is a suitable candidate for medical application particularly because it is extremely low in carbon (less than 0.03 %) content and this improves its corrosion resistance. Due to low carbon content, the chromium carbides do not precipitate over the grain boundaries of the microstructure. In cases where the chromium carbides precipitate over the grain boundaries, the amount of chromium at the boundary depletes, making it susceptible to corrosion, also known as sensitization (Han et al. 2009). Stainless steel 316L has excellent creep properties and stress to rupture is very high. It is already in use for many medical implants like screws and pins for joint replacements and other orthopedic uses.

Table 1. Composition of stainless steel 316L alloy in weight percentage (ASTM A 240, 2007).

| ELEMENT | PERCENTAGE (%) |
|---|---|
| Manganese (Mn) | 2 |
| Chromium (Cr) | 16.00-18.00 |
| Nickel (Ni) | 10.00-14.00 |
| Molybdenum (Mo) | 2.00-3.00 |
| Iron (Fe) | Balance |

The properties of 316L stainless steel makes it highly resistant in extremely corrosive environments such as chloride. Stainless steel has high hardness (Table 2) compared to some types of carbon steel, making it a preferred choice in applications involving abrasive contact. Physical properties are as shown in Table 2. Stainless steel 316L is medically qualified to be used for making coronary stents because of better formability, affordability and weldability. Wires coated with special amorphous oxide layers are made for medicinal applications, which are found to reduce thrombosis when used as a stent (Lo et al. 2009). Considering the broad applicability of stainless steel in multiple applications due to favorable cost effectiveness, compatibility to various environments, ease of availability, it is a preferred choice for further technological development.

Table 2. Mechanical properties of stainless steel 316L (Azom 2009).

| Grade | Tensile Strength (MPa) | Yield Strength 0.2% Offset (MPa) | Elongation % in 50 mm | Hardness (Max.) | |
|---|---|---|---|---|---|
| | | | | Brinell (HB) | Rockwell B (HR B) |
| 316L | 485 | 170 | 40 | 95 | 217 |

# 3. EXPERIMENTS

The proper selection of experimental conditions is important while optimizing process performance. The basic objective of our experiments is to predict micro-tool life and optimizing of mist performance. The basic milling parameters for a material are cutting speed, chip load and cutting depth. These parameters are easily available through the Machinery's Handbook for macro-tools and materials. For micro-tools, these are neither supplied by the manufacturer nor is it available from any machining reference book. The focus of this research is modeling of the micro-tool life and evaluating the performance of mist systems in machining.

The cutting fluid parameters are studied to determine the best characteristics for a fluid to work for a fast rotating micro-tool. Failure of micro-tools is studied by performing a wide variety of experiments. Several cutting conditions are experimented and the tool performance is studied for determining the best process parameters. Intensive groundwork is done on the HAAS milling machine including testing for vibration and runout to prepare for machining experiments. We also study the accuracy of conventional tool positioning methods and developed alternate ways to position tool with respect to workpiece repetitively with the same accuracy.

A short list of experiments carried out to achieve the research objectives:

1. The spindle supplied with OM2 for micro-machining purposes are supported by air bearings to allow maximum performance at high RPM- up to 50,000. Runout is measured with the tool rotating at different speeds without coolant. Various

combinations of tool motion are studied to determine the nature of vibration and runout. Tool deflection is also measured while cutting 316L stainless steel.

2. Tool wear is studied while cutting at various different speeds in dry and mist conditions. Materials of tooling involved tungsten carbide (WC), as well as some coated tools with WC as base. A laser displacement system is used to set the Z direction tool position with respect to the workpiece. End mills are used to cut slots on SS 316L. These tools are then studied under an optical microscope to measure different types of wear. Cutting conditions involved dry cutting as well as mist conditions using the micro-fluidization system supplied by UNIST.
3. Several experiments are performed to study cutting fluids. To prove that the mist completely wets a tool at high RPM, a boundary layer penetration test is carried out. To check for the minimum particle size required for particles to wet the tool surface when it is rotating at high RPM, we measure the surface tension of the liquid, average particle size of the droplets that are being sprayed. The viscosity of fluids is measured to provide a comparison between different fluids.
4. A basic computational analysis is done to study the nature of coolant mist flow over a rotating cylinder. The purpose of such an investigation is to understand how the cutting fluid (mist) would flow over the tool and whether it will touch the tool or not.

This research studies the use of mist cooling, suggests the best use of mist coolants, proper testing methods for reducing setup inaccuracies and models tool life of microend-mills.

## 3.1 EQUIPMENT

### 3.1.1 M.A. FORD END MILL

The tools used for these experiments are provided by M.A. Ford. The basic size selected is 1.016 mm in diameter. The tooling material involved a tuff-cut tungsten carbide (WC) end mill, as well as 3 types of coated end mills coated with 1) Titanium carbo-nitride (Ti-CN) 2) titanium aluminum-nitride (Ti-AlN) 3) titanium nitride (Ti-N). The flute length of the cutting tool is 0.08" or 2.032mm and the shank diameter is equal to 1/8" or 3.175mm. The helix angle of the cutting flutes is $30^0$. Figure 11 shows the part drawing of the tool. Tool, material specifications are shown in Table 3, Table 4 respectively.

Table 3. Specifications of the tungsten carbide cutting tool (M.A.Ford 1998)

| Tool Material | Cutter diameter | Cutter length | Number of flutes | Shank diameter |
|---|---|---|---|---|
| Tungsten carbide | 1.016mm | 2.032mm | 2 | 3.175mm |

Table 4. Properties of the tungsten carbide material (M.A.Ford 1998) (MEMSnet 2009)

| Density | Vickeres Hardness (VH) | Knoop Hardness (KH) |
|---|---|---|
| 14500 kg $m^{-3}$ | 1730 | 1870 |

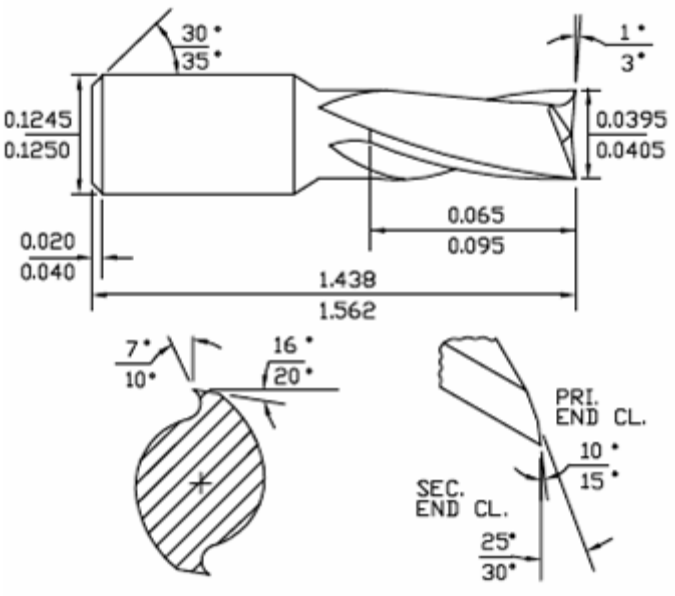


Figure 11: Dimensions of the microend-mill (Tool # 1640400 – 0.04x.080x1-1/2) (M.A.Ford 1998).

### 3.1.2 316L STAINLESS STEEL

The workpiece material is chosen as stainless steel 316L due to its wide variety of application in industry and its unique material properties. Another version of the 316 stainless steel is 316L having less carbon content. Tables 1 and 2 show the composition and mechanical properties of SS 316L. It is an austenitic stainless steel with iron, chromium, nickel, molybdenum and manganese. The physical properties and grade specification comparison of 316L stainless steel are shown in Tables 5 and 6 respectively.

The blocks chosen for the experiments are stainless steel 316L bars having a rectangular cross section:

1) 16.25mm x 12.7mm (0.64in x 0.5 in)

2) 20.53mm x 25.4 mm (0.808in x 1.0in)

These bar stocks are mounted on OM2 as shown in Figure 12 and face milled at extremely slow speeds (to avoid work hardening) using a 3.175mm (0.125 in.) two-flute end mill. Mist cooling and lubrication is used while milling the top surfaces. The objective of face milling is to remove the unevenness, work hardened layers.

Table 5. Physical properties of 316L stainless steel (Azom, 2009)

| Grade | Density ($kg/m^3$) | Elastic Modulus (GPa) | Mean coefficient of Thermal Expansion (µm/m/°C) | | | Thermal Conductivity (W/m.K) | | Specific Heat 0-100°C (J/kg.K) | Elec Resistivity (nΩ.m) |
|---|---|---|---|---|---|---|---|---|---|
| | | | 0-100°C | 0-315°C | 0-538°C | At 100°C | At 500°C | | |
| 316/L | 8,000 | 193 | 15.9 | 16.2 | 17.5 | 16.3 | 21.5 | 500 | 740 |

Table 6. Grade specification comparison of 316L stainless steel (Azom, 2009)

| Grade | UNS No | Old British | | Euronorm | | Swedish SS | Japanese JIS |
|---|---|---|---|---|---|---|---|
| | | BS | En | No. | Name | | |
| 316L | S31603 | 316S11 | - | 1.4404 | X2CrNiMo17-12-2 | 2348 | SUS 316L |

### 3.1.3 HAAS OFFICE MILLING MACHINE

The machine used for performing micro-machining is HAAS office mill OM2. The spindle is calibrated and measurements are made for the runout of the spindle under different conditions of operation. A basic requirement of micro-machining is the accuracy of the machine, according to HAAS, OM2 can achieve a positioning accuracy of $\pm$5µm ($\pm$0.0002") and repeatability of $\pm$3µm ($\pm$0.0001"). These numbers show a highly stable system. For high spindle speeds which maybe more than 10,000 RPM, the machine has a high positional accuracy which makes it an ideal choice for our micro-machining experiments. The OM2 micro-machining system is capable to run upto 50,000 rpm. The stainless steel workpiece is mounted on a 3 axis trunnion and tool is mounted on the spindle using a special collet. Most NC codes for machining are developed using FeatureCAM software as well as manual coding for attaining desired machining conditions.

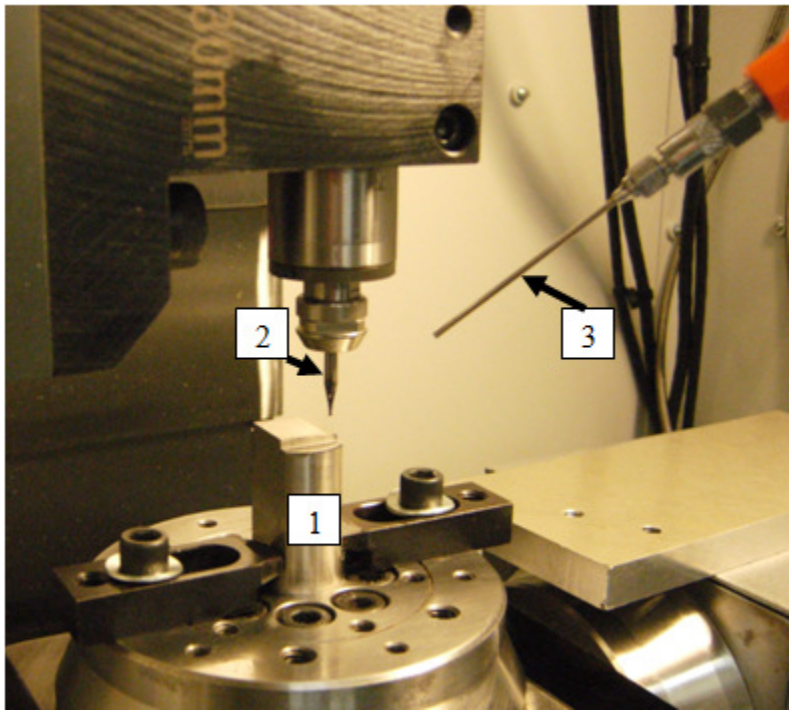


Figure 12: Setup during machining SS316L using a two-flute WC end-mill. 1) Workpiece; 2) 1.016mm two flute microend-mill; 3) mist nozzle.

### 3.1.4 SESILE DROP APPARATUS

The apparatus used for measurement of surface tension is known as Sesile drop apparatus (Figure 13). The FTA 188 video tensiometer is manufactured by First Ten Angstroms Inc. The sesile drop apparatus can measure surface tension upto an accuracy of 0.01 milli-newton/meter. We can use different types of fluids which maybe water based or oil based. Depending on the shape of the drop, the apparatus uses an inbuilt software to calculate surface tension from the projected surface area or volume of drop.

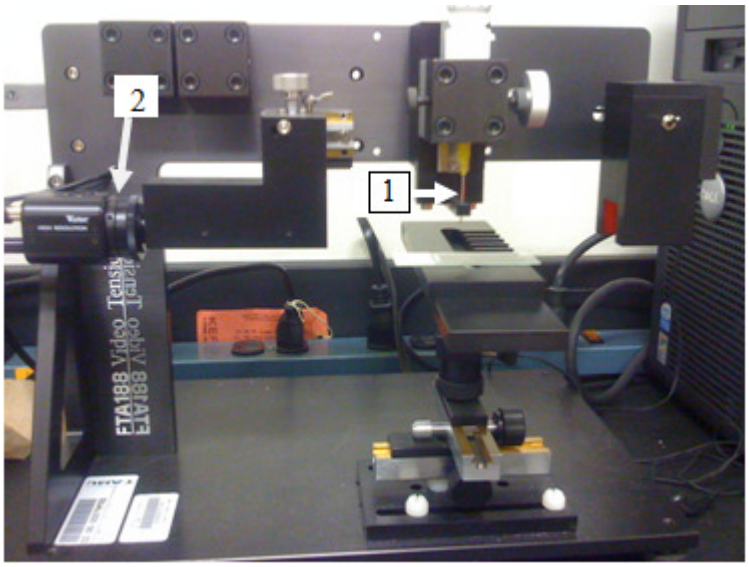


Figure 13: Setup of a sessile drop apparatus for measurement of surface tension.
1) Stainless steel needle; 2) camera.

### 3.1.5 AR G2 RHEOMETER

The measurement of viscosity involved the use of a TA Instruments AR G2 rheometer. It comes with a magnetic thrust bearing spindle that provides accurate torque control in measurement of viscosity. This is a very temperature sensitive device, capable of getting accurate measurements. It has a torque resolution of 0.1 nN.m. Figure 14 shows the measurement setup. The parameters selected for viscosity measurement are as follows:

- Model no of viscosity measurement equipment: AR G2
- Manufacturer: TA Instruments
- Name of viscosity measurement equipment: Rheometer
- Geometry notes: standard steel cone - default AR measurement geometry
- Geometry name: 40mm 1° steel cone
- Geometry material: Steel
- Angle: 1:00:36 deg:min:sec
- Diameter: 40.0 mm
- Truncation gap: 29.00 µm
- Temperature: 25.0 °C
- Method: variation of shear rate
- Volume: 1 mL

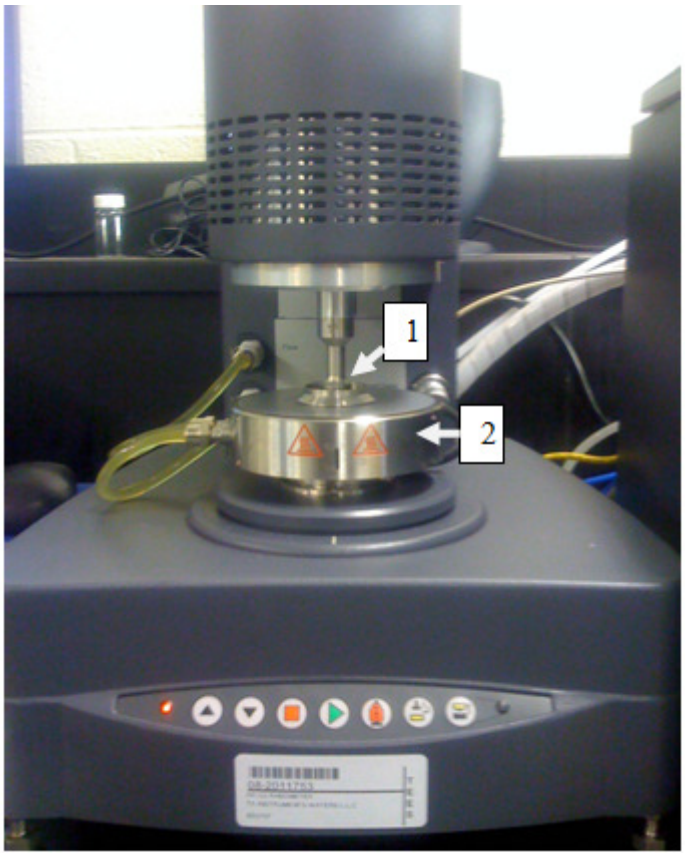


Figure 14: Setup of AR G2 rheometer for measurement of viscosity.
1) Standard steel cone; 2) base plate.

### 3.1.6 KEYENCE LK-G157 LASER

The measurement accuracies required for micro-machining is in the range of microns. This requires the use of ultra precision measuring instruments that are stable and reliable. The Keyence laser systems allow the user to measure differentially over various surfaces ranging from glass like to highly dull metals. It is a 2D displacement system that has an emitter and a receptor, which are calibrated to measure with an accuracy of ±0.5% and resolution of 0.5µm. The laser system is used to investigate the stability of the spindle as well as measurement of distance between tool and workpiece. The latter information is used to position the tool with respect to the workpiece. Keyence uses software known as LK navigator to calibrate the laser intensity for different types of surfaces. The setup for tool setup in z–direction is shown in the figure on page 52.

### 3.1.7 UNIST MIST COOLUBRICATOR SYSTEM

The challenge of generating and delivering a constant mist supply is overcome with the help of uni-max coolubricator system (Figure 15). This is a one of a kind micro-fluidization system that uses air pressure to power a variable rate pulse generator that produces infinite repetitive cycles of the metering pump. It can be adjusted to deliver 0.1 to 3.0 drops of lubricant per cycle and the number of cycles can vary between 4 and 200 per minute. This allows the user extreme flexibility of adjusting the amount of cutting fluid to be used for a given purpose.

This system is compatible with all types of fluids. We used fluids supplied by UNIST namely 2210 EP, 2210, 2200, 2300. Coolube 2210EP coolant is used for the tool wear experiments. It is an environmentally acceptable vegetable based lubricant for use with the UNIST mist systems[4]. This system has a flexible metal hose that allows user to position the nozzle in any orientation. There is a coaxial nozzle for air and lubricant mixing which maintains constant rate of atomization. Amount of air and liquid can be varied easily to achieve the desired volume flow rate of mist. The nozzle is positioned as shown in Figure 12. The different components are shown in Figure 16.

The features of the mist system are:

1) Co-axial nozzle that keeps air and fluid separate till they reach the tip.
2) Continuous external lubrication through automatic cycles of metering pump.
3) Air-pressure powered pulse generator.
4) Semi-rigid nozzle providing flexibility in positioning.


Figure 15: UNIST mist system.

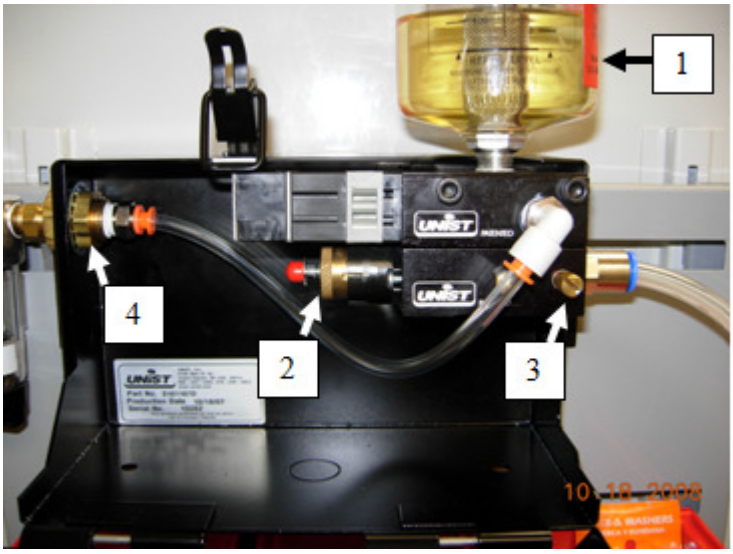


Figure 16: Components of mist system. 1) Coolant reservoir; 2) coolant volume regulator; 3) air volume regulator; 4) air intake

### 3.1.8 LUBRICANTS

The lubricants used in this research are UNIST supplied Coolube 2210, 2210EP, 2200, 2300HD. 2210 EP is used while modeling tool life of microend-mills. These are specially formulated for ferrous and non-ferrous materials. These coolants/lubricants are non polluting, non hazardous, non toxic and non-staining. They are designed for heavy duty cutting operations as well as longer tool life. The features of Coolube lubricants are:

1) Low surface tension and high heat capacity.
2) Designed to eliminate burrs, oversized holes and rough finishes
3) Does not require pumps, high pressure systems for application
4) Viscosity index does not change much with temperature. This makes it easier for it to penetrate heat zones and provide effective lubrication.

### 3.1.9 MICROSCOPE

The microscope used for measurement of tool wear is an Olympus STM6 3D measuring microscope with DP70 12.5 Mp camera. This is an optical microscope having a resolution of 0.1μm. It is a 3-axis measuring microscope having objective lens from 1.25x to 50x. Measurements can be taken in both bright-field mode and dark-field mode. Co-axial knobs are provided for movement of the 3-axis stage. Different stages on these knobs provide coarse and fine movement.

The tools tested for wear are placed under the objective lens after going through an ultrasonic cleaner. Wear is measured by aligning the cutting edge with the horizontal and taking measurements over it.

### 3.1.10 SEM

The study of tool failure mode requires the use of a Scanning Electron Microscope (SEM). A JEOL JSM-6400 SEM is used for studying failed micro-tools. This is a tungsten source SEM having secondary electrons (SE), backscattered electrons (BSE) and x ray imaging modes. The magnification range is from 10x to 300,000 xs with a resolution of 3.5nm and the accelerating voltage can be varied from 0.2 to 40kV. The sample to be studied is placed in the SEM chamber after being cleaned in an ultrasonic cleaner. As electrons are accelerated from the tungsten filament to the anode, it leads to interaction of the electron beam with the sample. At this, various signals are produced which can be collected using the detectors mounted in the column for SE, BSE or x ray imaging.

## 3.2 TOOL/ WORKPIECE POSITIONING

Micro-tools have cutting edges so small that cannot be defined clearly by naked eye. This requires the use of novel methods of positioning tools. The relative position of the tool with respect to the workpiece is the first definitive step in setting up the machining process. This information is used by the machine to calculate offset in the X, Y, Z direction. This is incorporated in the NC code to define the origin of the Cartesian co-ordinate system within which the tool moves on geometrically defined paths. Errors in tool positioning with respect to the workpiece add on as machining progresses. The requirement of setup methodology is to position the tool with repetitive accuracy that is within permissible limits.

The conventional methods of positioning tools with respect to workpiece involve the use of human eye by eyeballing the tool's cutting edge. This method is very primitive and cannot be used in micro-machining due to limitations in reproducing accurate measurements. Alternatively, people have used mechanical devices like edge finders. These devices also have a lot of error in measurements and upon repeated trials are found less accurate than laser positioning methods. The procedure for determining the z height as shown in Figure 17 is as follows:

1) Mark a central point on the surface of the foam block with a pencil, and measure the height of the block at that marked location. Repeat this process multiple times, each time moving the block to a slightly different location. Average these heights.

2) Clean the work surface of the CNC machine and tip of the tool with rubbing alcohol and place the foam block on top.

3) Place the foam block on the work surface, and adjust it so that the tip of the tool is directly above the central marked point on the foam block surface.

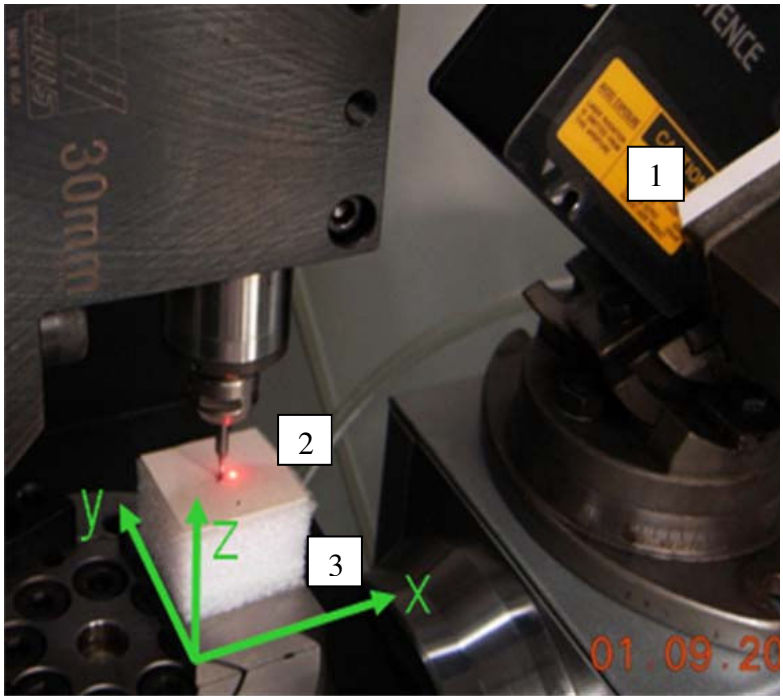


Figure 17: Setup showing the Keyence laser and cutting tool for tool positioning in z-direction. 1: Keyence laser, 2: Cutting tool and 3: Workpiece.

4) Mount the laser on the vice clamp at an angle so that the laser spot is 1-2 mm away from the marked point.

5) Slowly lower the tool until it contacts the foam block. This is indicated by a sudden change in laser values. When the tool contacts the foam block, the value

on the laser will jump suddenly. (Notice that the values themselves are not important; the sudden change in values is the necessary indicator).

6) The z coordinate displayed on the CNC work co-ordinate display screen combined with the average height of the foam block indicates the height of the tool above the work surface.

## 3.3 EXPERIMENTS

### 3.3.1 TOOL WEAR MEASUREMENT

The objective of this research is to model life of micro-tool under mist cooling and predict improvement in performance due to better cooling and lubrication. The calculation of tool life requires measurement of tool wear at regular intervals. Tool life is defined as the length of time for which the cutting tool machines properly before starting to fail. To define it more quantitatively, we have to set a standard for the failure of the tool being studied for wear. As mentioned in the literature review, the tool wear criteria for macro-tools cannot be used for micro-tools. Although a lot of work is done on micro-tool life, there is no agreement on a standard for failure (Bao and Tansel 2000 [b] and Rahman et al. 2001 [b]). Allowable wear decreases with the size of the tool. Since there is no standard available from the literature, multiple failure criterions are more suitable. Failure modes in micro-milling are due to abrasion or tool/cutting edge breakage. For a 1.016 mm diameter end mill, the tool failure criteria are set at: 1) 50μm of flank wear; 2) 50μm of nose wear; 3) chipping or breaking of cutting edge; whichever happens earlier.

Failure criterion is chosen at 50μm (for 1.016mm end mill) because the rate of wear increases drastically leading to catastrophic failure after flank/nose wear reaches 50μm. Till the wear reaches the above mentioned limits, it is considered good for use. Other important parameters important while measuring tool wear are:

1) Chip load: Chip load is set at 10μm/tooth (0.000394 in/tooth). Chip load is the lateral distance an end mill advances per cutting edge as it cuts into the material.
2) Depth of cut: Radial depth of cut is set at 0.558 mm (0.022in). Axial depth of cut is set at 0.348mm (0.0137 in).
3) Material is standardized as 316L stainless steel.
4) Mist position is fixed with respect to the tip of the tool (origin) at a spherical co-ordinate of (r, θ, φ) = (30mm, $60^0$, $55^0$). Where 'r' is the radial distance; 'θ' is the angle between the tool axis and the mist nozzle direction; 'φ' is the angle between the y axis on the machine co-ordinate system and the mist nozzle direction. The orientation of 'θ' and 'φ' is chosen to position the mist nozzle towards the cutting edge of the tool as it comes out of the workpiece material.

   The cutting conditions in dry cutting are:

   - Chip load: 10μ (0.000394 in)/tooth
   - Coolant: dry
   - Material: 316L
   - Tool: 1.0.16mm (0.04in) dia
   - Axial depth: 0.348mm (0.0137 in)
   - Radial depth: 0.558mm (0.022 in)

The cutting conditions in mist cutting are:

- Chip load: 10μ (0.000394 in)/tooth
- Coolant: 0.022cc/min 2210EP
- Material: 316L
- Tool: 1.016mm (0.04in) dia
- Axial depth: 0.348mm (0.0137 in)
- Radial depth: 0.558mm (0.022 in)
- Mist angle: (r, θ, φ)= (30mm, $60^0$, $55^0$)

The cutting conditions in flood cutting are:

- Chip load: 10μ (0.000394 in)/tooth
- Coolant: Blasercut 2000 universal, 5: 1 mixture
- Material: 316L
- Tool: 1.016mm (0.04in) dia
- Axial depth: 0.348mm (0.0137 in)
- Radial depth: 0.558mm (0.022 in)

The cutting conditions in spray (Blasercut mist) cutting are:

- Chip load: 10μ (0.000394 in)/tooth
- Coolant: Blasercut 2000 universal; 14cc/min, 0.8Mpa
- Material: 316L
- Tool: 1.016mm (0.04in) dia
- Axial depth: 0.348mm (0.0137 in)
- Radial depth: 0.558mm (0.022 in)

- Spray distance: 30 mm
- Spray position: 60° from z-axis, 45° in x-y plane

The tool is mounted in the machine carefully to make sure there is no damage to the cutting edge. The tool position is set with respect to the block using a laser system in the z direction as explained earlier. The x, y position of the tool is set by using an ocular lens. The positioning in x, y direction is not detrimental to the testing procedure as the NC code is written for multiple passes in the x-direction and provides clearance in y-direction. Slots are machined on the SS 316L block and after every few passes, the tool is dismounted from the machining center. The tool is then immersed in isopropyl alcohol and cleaned ultrasonically to remove any chips that might be stuck on it. It is mounted on a v-block and placed in an Olympus STM6 3D measuring microscope to measure tool wear. Both flank wear and nose wear are measured and any formation of burrs/ chipping of cutting edge are reported. Measurement of flank wear is shown in Figure 18. The top of the original cutting edge is aligned with the reference box on the screen and the position of the microscope stage is reset. The stage is then moved till the reference box is aligned with the bottom of the worn out cutting edge. The movement of the stage in microns gives the value of flank wear. Nose wear is also measured in a similar way as shown in Figure 19. This is repeated till either of the failure criteria listed above is achieved.

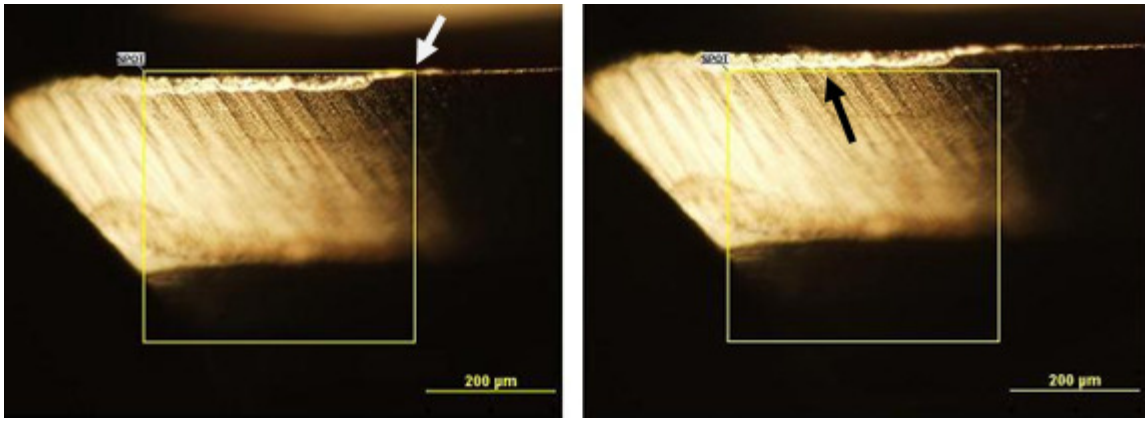


(a) (b)

Figure 18: Sample measurement of flank wear using optical microscope. (a) Reference box is aligned with the top of the original cutting edge (shown by arrow). (b) Reference box is aligned with the bottom of the worn-out cutting edge (shown by arrow).

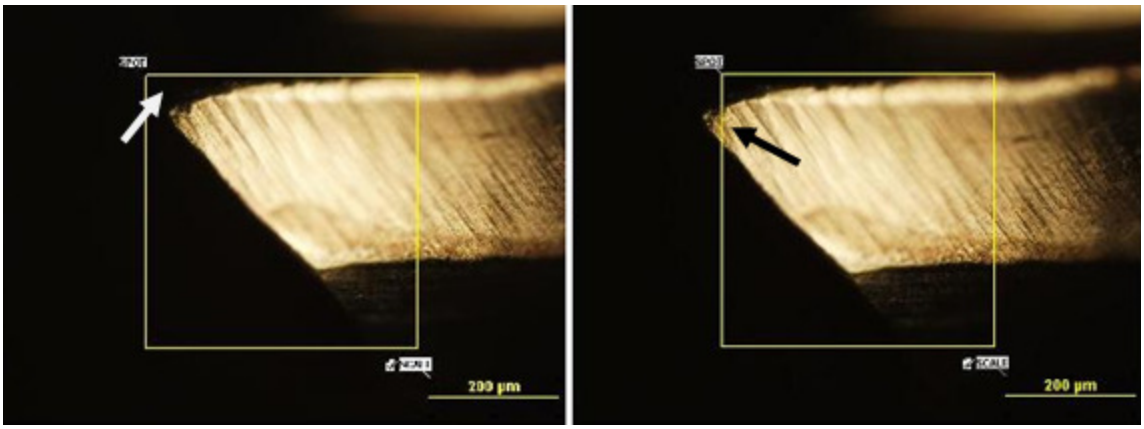


(a) (b)

Figure 19: Sample measurement of nose wear using optical microscope. (a) Reference box is aligned with the position of the original nose (shown by arrow). (b) Reference box is aligned with the bottom of the worn-out nose (shown by arrow).

### 3.3.2 VERIFICATION OF TOOL WETTING AT HIGH SPEED

The validity of mist droplets wetting the tool surface is a major concern for mist flow researchers. At high RPM, the concern of mist particle's inability to penetrate the boundary layer and wetting of the tool is raised by Rahman et al. (2001) [b]. To validate this, a series of experiments are carried out to investigate wetting of tool surface.

1. Surface Tension Measurement: The ability of a liquid to wet a surface is determined by its surface tension. Surface tension acts against the centrifugal force of a rotating tool and prevents the droplet from falling off. Surface tension is defined as the attractive property of the surface of the liquid. This force is developed due to the cohesive force between molecules that holds the surface of the liquid drop in shape. For the measurement of surface tension, we used a video tensiometer type sessile drop apparatus (Figure 20). The apparatus consists of a micrometer type syringe having a 2 milliliter glass burette with a Teflon plunger. The temperature is kept constant at $25^0$ C. The syringe is flushed with alcohol to clean any trace of previous fluid. It is then flushed and filled with the fluid to be tested. The Teflon plunger is engaged to the glass burette using the threads on both of them. As the micrometer is rotated, it pushes the Teflon plunger into the glass burette and forms a drop of fluid at the tip of the needle. The volume of the droplet is increased till it reached maximum size just before dropping from the needle. The camera captures the projected image of the drop and calculates the

pendant area. Inbuilt software then calculates the surface tension from the projected pendant area.

The parameters in surface tension measurement are as follows:

- Material of needle: stainless steel-20 gage, length:25.4mm needle; ID: 0.635mm (0.025 in); OD: 0.9144mm (0.036 in)
- Syringe details: micrometer syringe, 2mL glass burette with Teflon plunger
- Model no. of surface tension measurement equipment: FTA 188 video tensiometer
- Manufacturer: First Ten Angstroms Inc.
- Method: Pendant area calculation
- Temperature: 25.0 °C

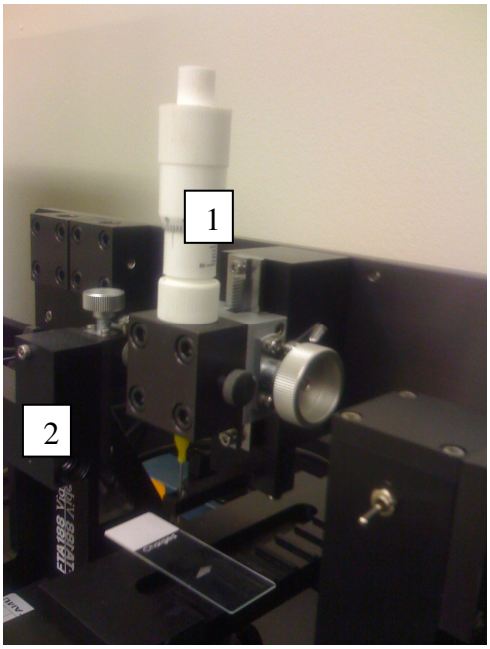


Figure 20: Apparatus for surface tension measurement.
1) Needle for delivering liquid droplets 2) Camera

2. Validation of boundary layer penetration: Rahman et al. (2001) [b] suggest that the oil droplets may have trouble reaching the tool surface when it is rotating at high RPM. To validate the fact that mist droplets do touch the tool and stick to it even at high RPM, a series of experiments is conducted to verify tool wetting. Two tools are chosen, a 12.7mm (0.5in) 2 flute end-mill and a 3.175mm (0.125in) two flute end-mill. The centrifugal force acting on a droplet is a function of the surface speed of the tool (Equation 9). At the same RPM, surface speed is much more on a macro tool compared to a micro-tool. On an OM2, maximum spindle speed is 50,000 RPM for a tool shank diameter of 3.175mm. 1 mm holes are drilled in radial and axial direction on the tool surface using electrical discharge machining (EDM) to capture mist droplets that touch the tool (Figures 21 (b) and 22(b)). The mist nozzle is placed at a distance at 25.4 mm (1in.) from the tool horizontally aiming towards the drilled hole (Figures 21 and 22). To run a trial, the following steps are carried out:

   a) Tool is first cleaned with alcohol and dried to make sure there is no trace of oil on it. It is then run at the desired surface speed.

   b) Mist spray is switched on at this moment. The mist flow does not start immediately with the air flow. Hence it is important to visibly notice if the mist flow has started. Once the mist flow starts, it is run for a short duration to ensure proper wetting of the tool (approximately 5 seconds).

   c) The mist flow is stopped completely followed by the rotation of the tool. A piece of dry absorbent tissue is then used to wipe the exterior of the tool as well

as the inside of the hole on the surface. If mist penetrates the boundary layer, touches the tool and sticks to it, small traces of the fluid will be observed on the dry absorbent tissue. The tool must be cleaned of the entire oil residue using alcohol before the next trial is run.

Parameters of tool wetting experiments:

- Tool diameter: 3.175mm (0.125 in)
- Air pressure: 3.197 to 3.39 bar
- Stroke length: 2.7 mm
- Stroke frequency: 12 strokes/min
- Volume flow rate of coolant: 3.33 x $10^{-9}$ $mm^3$/sec

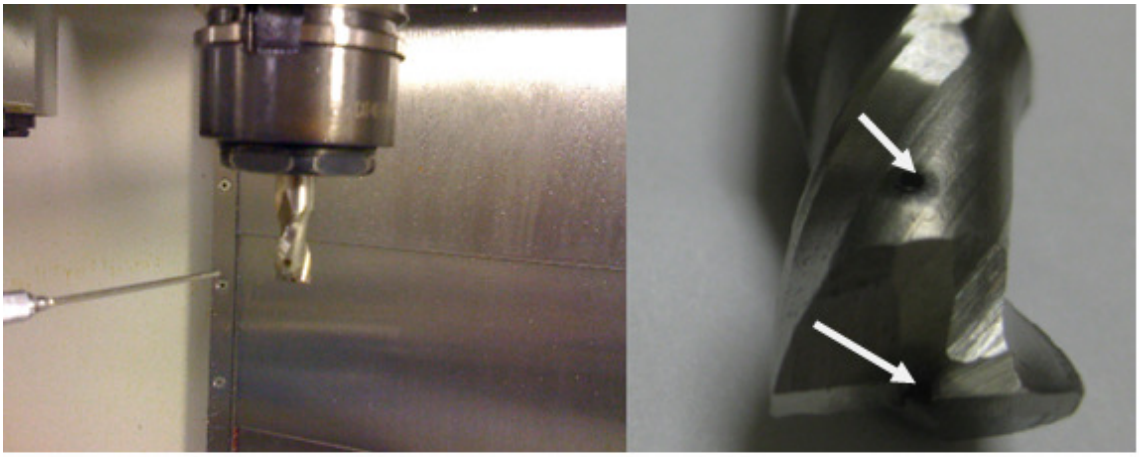


Figure 21: (a)Mist spray on a 12.7mm 2 flute end-mill. Nozzle is horizontally positioned at a radial distance of 25.4mm from the tool surface pointing towards the center of the tool. (b) Arrows pointing at the holes drilled on the tool.

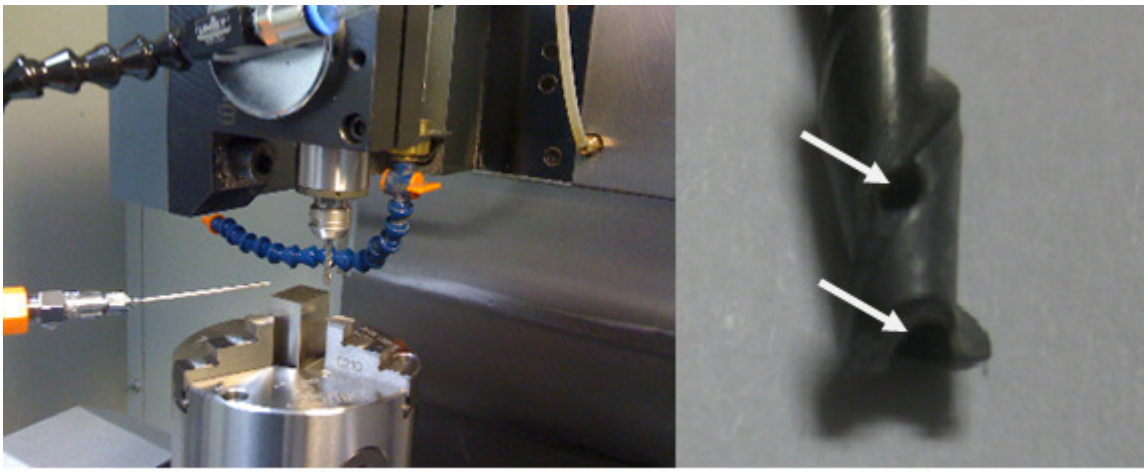

(a) (b)

Figure 22: (a)Mist spray on a 3.175mm 2 flute end-mill. Nozzle is horizontally positioned at a radial distance of 25.4mm from the tool surface pointing towards the center of the tool. (b) Arrows pointing at the holes drilled on the tool.

### 3.3.3 CONTACT ANGLE AND PARTICLE SIZE MEASUREMENT

The characterization of mist flow equipment and the cutting fluid characteristics for improved performance is necessary to predict the optimum cutting conditions accurately.

1. Contact angle: Consider a drop of liquid on a flat surface, neglecting the effect of gravity; the drop will form a portion of a sphere to minimize its Gibb's free energy. Contact angle is defined as the angle at which the liquid interface meets the solid interface. Contact angle measurement is carried out using a novel technique. This method employs the use of a micro-pipette to drop a known volume of liquid on a clean, flat metal surface. The preparation of the surface involves washing it with alcohol and drying it completely. Careful considerations must be made to make sure that the environment is dust free. Immediately after dropping the liquid, the drop is placed under an optical microscope to measure its mean diameter. This data is then used to calculate the contact angle between 316L stainless steel, which is the material of the flat plate and the cutting fluid in question.

The characteristics of micro-pipette used for dropping a known volume of coolant on a stainless steel 316L sheet are the following:

- Micro-pipette: Eppendorf Reference
- Volume range: 0.1-2.5μL

2. Particle size: To determine whether the drop of liquid sticks to the tool surface or not, the size of the droplet is an important criterion. It is also interesting to know the level of atomization of liquid droplets when passed through the mist system. To measure the particle size, a very simple experiment is carried out. Mist droplets are sprayed on a flat, clean 316L stainless steel sheet vertically from a distance of 304.8mm (12 in). The drop is spherical before hitting the plate. After touching, it becomes a part of a sphere. The diameter and height of the drop on the steel sheet is measured under an optical microscope. This data is then used for calculating the mean particle size. It is very important to make sure that the plates are cleaned with alcohol and dried before spraying with mist droplets.

   The parameters chosen for particle size measurement are as follows:

   - Stroke frequency: 32/ min
   - Air pressure: 3.1 bar
   - Stroke length : 2.7 mm

### 3.3.4 AIR/MIST PRESSURE

The pressure of mist jet is a characteristic of the machining condition. Calibration of mist pressure enables user to find out exact pressure of mist jet required for effective mist cooling. Air/ mist pressure in the micro-mist system is adjusted using air metering screw as shown in Figure 23. However, there is no pressure gauge to measure the pressure of the air/mist mixture at the needle tip. This situation calls to calibrate pressure and relate the exit pressure at the needle tip with the number of rotations of the air metering screw. To do this the set up shown in Figure 24 is required. In this set up the deflection of a steel plate is measured and that deflection is converted to the exit pressure by using beam deflection formula.

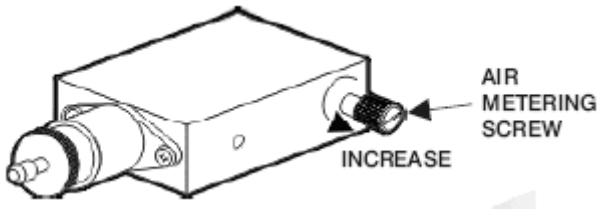


Figure 23: Air/mist pressure control system on mist generator.

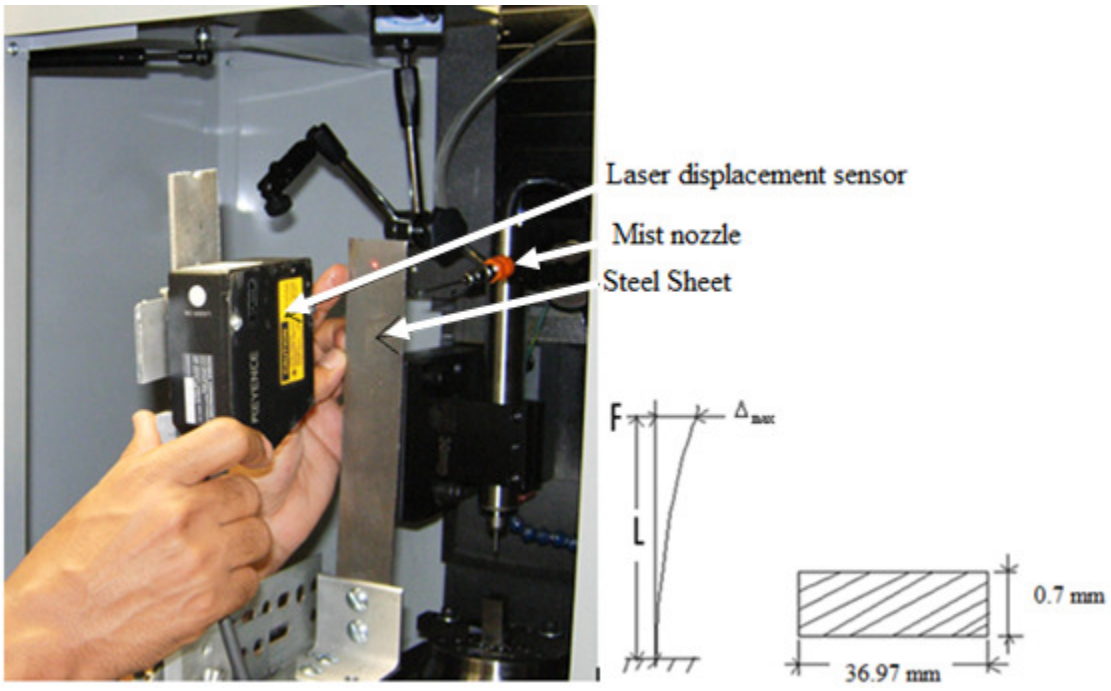


(a) (b) (c)

Figure 24: (a) Exit pressure measurement setup (b) steel sheet deflection analogy (c) cross section of the steel sheet.

# 4. MODELING OF CUTTING FLUID CHARACTERISTICS

The modeling of cutting fluid characteristics requires measurement of various cutting fluid characteristics like surface tension, viscosity and contact angle. Mathematical models are developed to evaluate these characteristics as well as compare them with one another to evaluate coolant performance. Some mathematical models are also developed to further the scope of this research with different tools and cutting fluids.

## 4.1 MODELING OF SURFACE TENSION AND CENTRIFUGAL FORCE

The conditions in which adhesive force produced by surface tension would exceed centrifugal force can be studies with the help of a model that compares forces acting on a liquid drop resting on a rotating tool. Let us consider a liquid droplet that comes to rest on a rotating tool. The drop would be spherical shape before hitting the tool surface. After it comes to rest, its shape will change depending on the interaction energy between the two surfaces. The shape that it attains at rest will correspond to minimum energy levels.

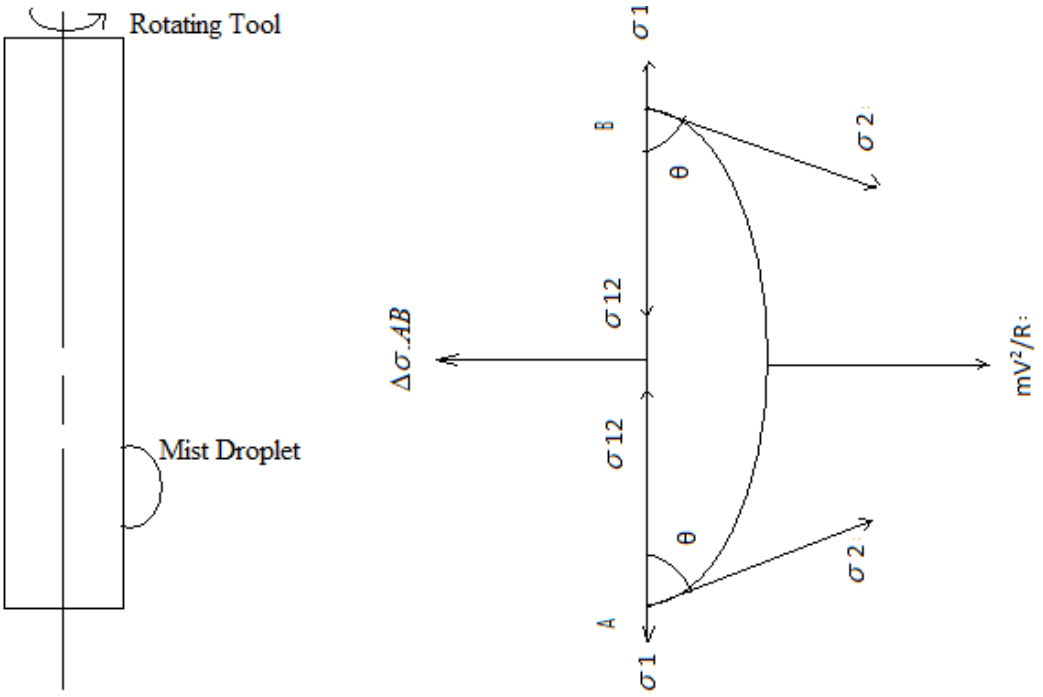


a) b)

Figure 25: (a) Micro-droplet on a rotating tool (b) free body diagram of forces acting on the micro-droplet.

The particles of mist that come in contact with the tool are really small compared to the size of the tool. Although the geometry of the tool is a complicated curved surface, we can assume that the line of contact is linear and the 2 dimensional picture of the droplet looks as shown in Figure 25 (a) and (b).

At equilibrium, the work done in separating unit area of liquid from a surface is (Macdougall and Ockrent 1942):

$$\Delta\sigma = \sigma_1 + \sigma_2 - \sigma_{12} \quad (5)$$

Where:

$\Delta\sigma$ = work done per unit area in separating the liquid from the surface

AB= Drop diameter ‘D’

$\sigma_1$ = Surface energy of solid

$\sigma_2$ = Surface energy of liquid

$\sigma_{12}$ = Interfacial energy

$\frac{mv^2}{R}$ = centrifugal force on the droplet

Equating moment at point A to zero,

$$\sum M_A = -(\frac{D}{2})(\frac{mv^2}{R} + 2\,\sigma_2 \sin\theta - \Delta\sigma\, D) = 0 \quad (6)$$

For complete wetting: $\theta = 0$

Hence, $$\frac{mv^2}{R} = \Delta\,\sigma\, D \quad (7)$$

If $\theta$ is not equal to 0,

$$\frac{mv^2}{R} + 2\,\sigma_2 \sin\theta = \Delta\,\sigma\, D \quad (8)$$

At $\theta = 0$, the drop leaves the tool surface, hence Equation (5) becomes:

$\Delta\sigma = \sigma_2 + \sigma_2 - 0 = 2\,\sigma_2$

Hence, $$\frac{mv^2}{R} = 2\,\sigma_2\, D \quad (9)$$

This happens when drop is about to leave the surface. Adhesion force becomes zero. The parameter in equations (9) that need to be experimentally determined is $\sigma_2$, which is the surface energy or surface tension of the liquid in air. From drop size calculations, we can determine the mass of the droplet (m). Linear velocity of the tool (v) is calculated from its diameter and RPM. Equation (9) signifies the point at which the

droplet has just left the tool surface as a result of centrifugal force increasing beyond adhesion force. This provides us with the minimum diameter of droplet that sticks to the tool. A plot of surface speed and 'D' from equation (9) will provide the drop diameter for adhesive force equaling centrifugal force.

## 4.2 CONTACT ANGLE MEASUREMENT

The measurement of contact angle is important in a quantitative comparison between different cutting fluids. The measurement of contact angle can be done using different techniques including use of a contact angle goniometer.

Consider a drop of liquid on a flat surface (Figure 26). Neglecting the effect of gravity, the drop will form a portion of a sphere to minimize its Gibb's free energy. Surface tension is the line tension between liquid and solid surfaces.

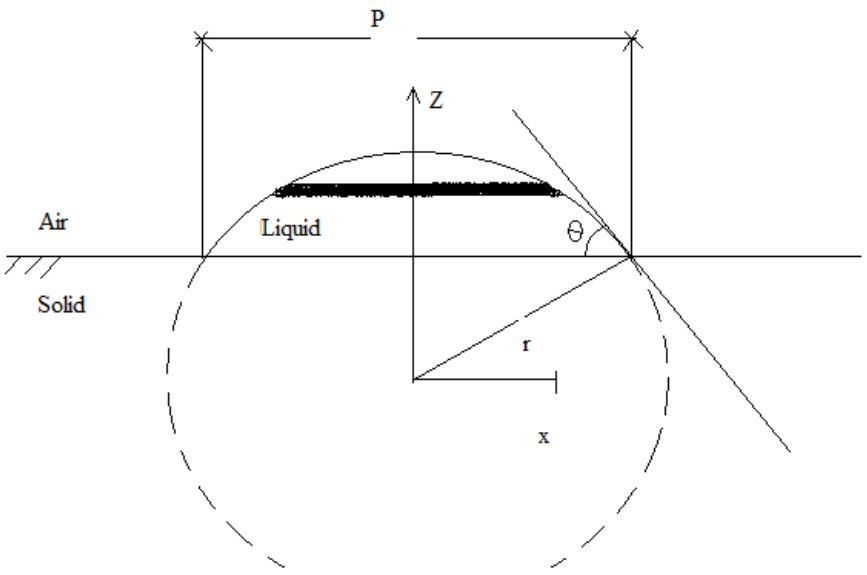


Figure 26: Contact angle measurement technique using micro-pipette.

To find the volume of the droplet, section the part of the sphere above the solid into extremely small elements of thickness ‘dz’ perpendicular to the ‘Z’ axis as shown by the shaded black lines. Differential volume (dV) of an element at a height ‘z’ is given by:

$dV = \pi x^2 dz$

x: Radius of the section.

Use $x^2 + z^2 = r^2$ and integrate the above result to obtain an equation for contact angle θ (Appendix B1):

$$\frac{P}{V^{1/3}}(\theta) = \left[\frac{24}{\pi} \cdot \frac{(1 - K\cos^2\theta)^{3/2}}{2 - 3\cos\theta + \cos^3\theta}\right]^{1/3} \quad (10)$$

Where:

P : Projected diameter

V: Drop volume

θ: Contact angle

K = 0 ; θ lying between [90, 180]

K = 1 ; θ lying between [0,90]

Clearly, the dimensionless parameter $\frac{P}{V^{1/3}}$ is a function of 'θ'. To find out the contact angle between any liquid and solid surface:

1) Deposit a known volume of liquid (V) on any surface using a micro-pipette and measure its diameter (P).

2) Use equation (10) to plot $\frac{P}{V^{1/3}}$ versus 'θ'.

3) As shown in Figure 27, knowing the values of 'P' and 'V', we can calculate the contact angle 'θ'.

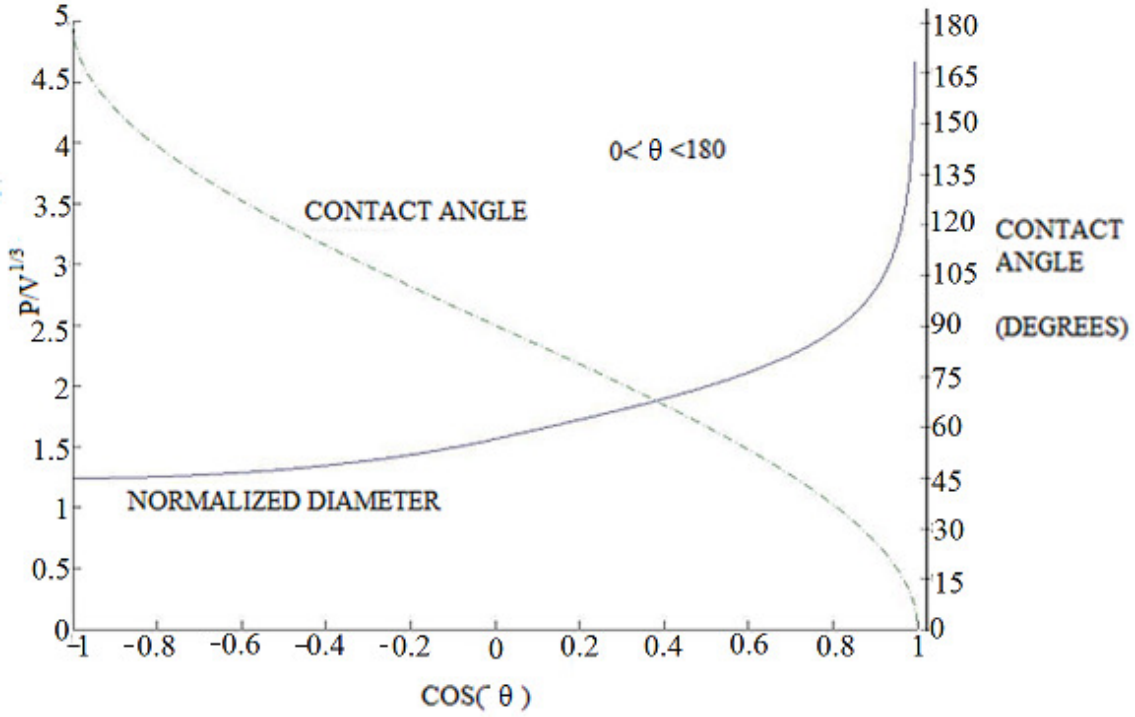


Figure 27: Contact angle plot.

## 4.3 EVALUATION OF AIR PRESSURE AND DROPLET SIZE

### 4.3.1 AIR PRESSURE MEASUREMENT

The evaluation of velocity of mist particles and their droplet size allows us to compare theoretical results with experimental values. Using this data, we can change the settings on the mist generator for maximum performance. The measurement of air pressure is done using the principle of cantilever deflection. The deflection is measured using the Keyence laser displacement sensor.

Beam deflection formula:

$$\Delta_{max} = \frac{FL^3}{3EI} \tag{11}$$

Where:

$\Delta_{max}$ = Deflection of the steel plate

F = Force

E = Modulus of elasticity (E steel = 2.8*107 psi = 1.931*1011 N/ $m^2$)

I = Area moment of inertia

L = Length of the steel bar

Using derivation shown in Appendix B2,

$$P' = 408\Delta_{max} \tag{12}$$

P’ = pressure in bar, $\Delta_{max}$ = deflection in m

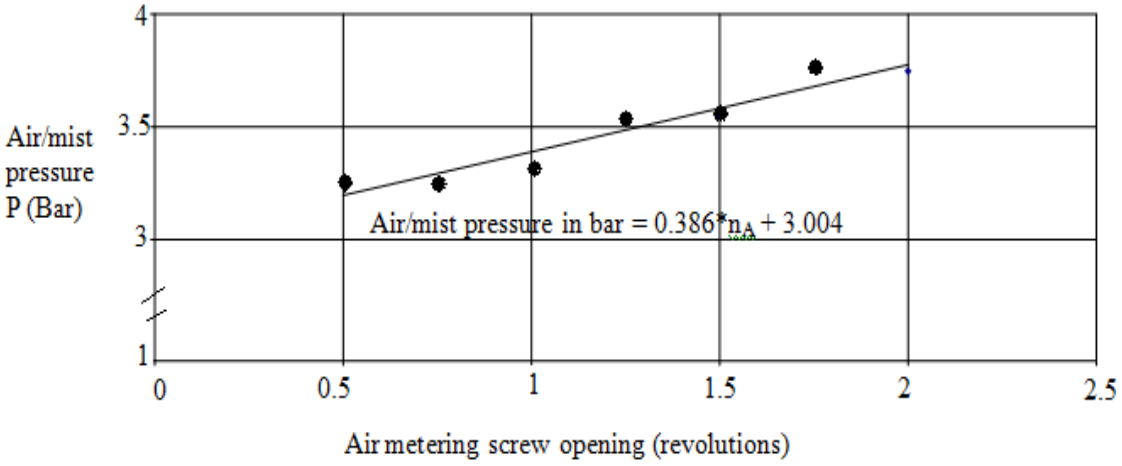


Figure 28: Air/mist pressure versus air metering screw opening.

The values of air pressure P' obtained at different air metering screw openings are plotted in Figure 28. A straight line can be fit through the data points to obtain an empirical formula for air/mist pressure:

$$P' = (0.386) * n_A + 3.004 \quad (13)$$

Where:

P' = air/mist pressure in bar

$n_A$ = number of revolutions of the air metering screw from bottom

### 4.3.2 DROPLET SIZE MEASUREMENT

The calculation of drop size can be done by collecting mist droplets on a flat metal plate. Since the droplet is a part of a sphere as shown in Figure 29, we can measure the volume of the droplet from its average diameter and height. Assuming that the drop is a sphere before hitting any surface, we can equate the volume of the droplet with the volume of the partial sphere as measured with a microscope.

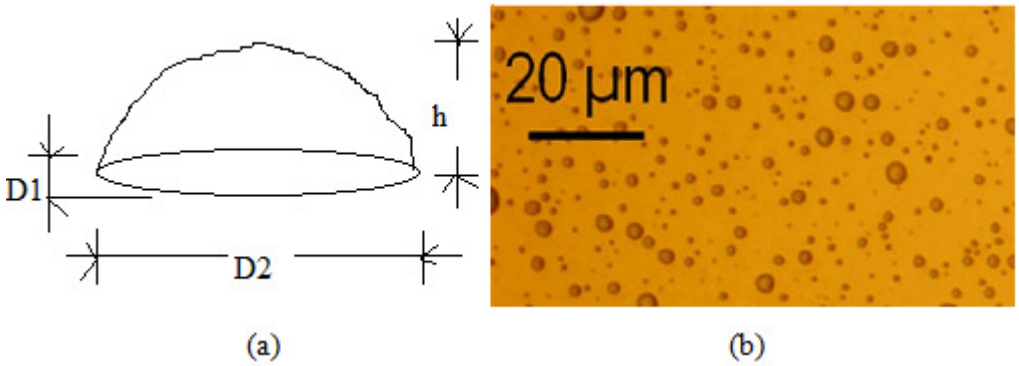


Figure 29: (a) Actual shape of droplet after hitting the metal plate (b) sample 2D image of the surface.

After hitting the surface of the steel plate, some droplets coalesce and form larger droplets as can be seen in Figure 29 (b). These are neglected during measurements and small diameter sizes are measured while assuming no evaporation takes place in oil based cutting fluids. The volume of the droplet is calculated as shown in Appendix B3 and is represented by equation (14).

$$V = \pi h^2 \left[ \frac{h}{6} + \frac{r^2}{2h} \right] \tag{14}$$

Where:

Radius $r = \frac{D_{avg}}{2}$ (15)

Average diameter of droplet:

$$D_{avg} = \frac{D_1 + D_2}{2}$$

Droplets are full sphere before hitting tool tip, therefore:

$$V = \frac{4}{3} \pi R^3 \tag{16}$$

Hence radius of the droplet in air ‘R’ can be calculated.

## 4.4 MODELING OF PARTICLE TRAJECTORY

The modeling of particle trajectory requires knowledge of the flow field in which the particle is introduced. If there is a boundary layer around the tool that needs to be penetrated in order for the tool to be wet by the cutting fluid, it is important to describe the motion on the mist particle in the boundary layer. Since the particle size is very small compared to the cylinder, we can assume the tool surface where the droplet comes in contact as a flat surface (Figure 30). For the purpose of this model, assume the tool to be stationary and the boundary layer flowing over it with a velocity $V_f$ that varies with respect to 'y'. To determine the trajectory of the particle in a 2-D flow-field, let us assume the flow field shown in Figure 30. The origin of this flow field is at the tip of the nozzle. Knowing $V_0$ and angle of entry $\theta_0$, the trajectory of the particle can be calculated.

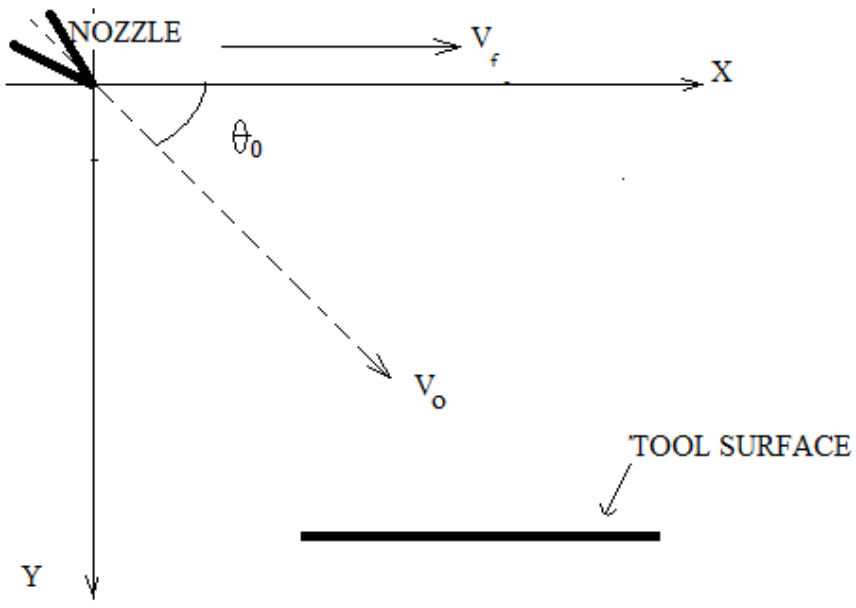


Figure 30: Trajectory of a particle upon entering a flow field.

The mist particle enters the flow-field as shown in Figure 30. The flow is one directional in positive x-direction with a velocity $V_f$. At the point of entry, the particle has an initial velocity $V_0$ at an angle $\theta_0$ with the x-axis. The particle size is very small compared to the flow field and it has a spherical shape, hence, the force acting on the particle is as expressed by Stokes' law:

$$F = -3\mu \pi D V_0 \quad (17)$$

Where,

$\mu$ = Absolute viscosity of air = 18.2075 kg/ms at $20^0$ C.

D = Diameter of micro-mist particle.

$V_0$ = Magnitude of initial particle velocity.

Let $F = -\alpha . V_0$

Where $\alpha = 3\mu \pi D$

The forces acting on the particle in 'X' and 'Y' direction can be resolved and simplified to obtain the trajectory of the particle with respect to the nozzle as $x_{pn}$ and $y_{pn}$ respectively. Complete derivation is shown in Appendix B4.

$$x_{pn} = V_f t + \frac{\alpha}{M} ( V_0 \cos\theta_0 - V_f ) [1 - e^{-(\alpha/M) t}] \quad (18)$$

$$y_{pn} = \frac{\alpha}{M} V_0 \sin\theta_0 [1 - e^{-(\alpha/M) t}] \quad (19)$$

$x_{pn}, y_{pn}$ : X, Y co-ordinate of the particle with respect to the nozzle tip.

M = Mass of particle.

$\theta_0$ = Angle of entry.

t = Time.

$V_f$ = Velocity of the fluid.

The trajectory is exponential as expected with $x_{pn}$ approaching infinity at time infinity and $y_{pn}$ approaching a constant at time infinity. Knowing tool diameter and boundary layer velocity, we can plot the x and y position of the particle and predict wetting of the tool. The change in direction of rotation will only influence the sign of $V_f$. Equations (18) and (19) can be used in clockwise or anticlockwise rotation of the tool.

# 5. RESULTS AND DISCUSSION

## 5.1 TOOL LIFE TEST RESULTS

The most exhaustive way of quantitatively judging improvement in process performance is by measuring tool life and comparing the same while changing various process parameters. Tungsten carbide end mills are selected as standard for testing tool life improvement. Changes in tool life are observed by changing the cooling conditions while cutting. The tool wear data is recorded for dry and mist cutting conditions using 2210 EP. Additional study using Blasercut flood coolant and Blasercut mist coolant are performed for comparison. Most WC tools tested in dry conditions failed by breaking the cutting edge caused by inter-granular shearing. Whereas under mist conditions, failure is due to ideal abrasive wear. This is a better option as it prevents sudden damage of the part being machined as well as formation of unnecessary burrs.

The same cutting conditions are also employed to test coated tools including TiN, Ti-AlN, Ti-CN. All of these cutting tools failed under both cutting conditions mainly by coating peel off and chipping of the cutting edge. Lots of burrs are also observed on the machined side after the tool failed, suggesting failure due to tool breakage. The cutting direction chosen for tool wear test is down-milling, since it provides a better surface finish. In order to reduce the load on the coated tool, up-milling is performed as it starts cutting at the thin side of the chip and ends at the thick side. This did not help as the

coating continued to peel off as earlier. Ideal abrasive wear is not observed in any of these cases primarily due to inadequate adhesion of the coating.

The results obtained from tool wear data are shown in Appendix D. Table D2 contain figures obtained for wear testing of WC tools in mist conditions. Tools are run at constantly increasing cutting speed till failure conditions are reached. The machining time for failure is calculated. Using Equations (3) and (4), the equivalent tool life and equivalent cutting speed can be calculated. This is plotted in Figure 31 showing machining time versus machining speed. The data points are slightly scattered because of the unpredictable tool performance, instability of micro-tools and possible inclusions in workpiece material. Equation (1) is a straight line in a log-log plot. The slope 'n' of the lines in Figure 31 is constant. Hence, once the value of 'n' is established in initial experiments, subsequent testing requires only few data points to obtain tool life plot. The data shows that mist cooling with 2210EP prolongs tool life better than flood cooling, or dry cutting. Cumulative wear model reduces the experimental time by 70% by reducing the time for a tool to reach failure. Tool life is 300s at 10,000RPM (1.016mm end mill, mist cutting, 10μm chip load) compared to a tool life of 100s running at a continuously increasing speed under same cutting conditions. Sample calculation for cumulative tool life ($T_e$) and equivalent cutting speed ($V_e$) is illustrated below :

Using machining time data from Table D2 (Appendix D) in Equation (3):

$$T_e = \sum_{i=1}^{k} \Delta t_j = 0.92+0.82= 1.74\text{m/min}$$

Using Q=1; n= 1.818 in Equation (4). The equivalent speed $V_e$ can be calculated:

$$V_e^{\frac{1}{n}} = \frac{\sum_{i=1}^{k} \Delta t_i V_{ci}^{\frac{1}{n}}}{Q\sum_{i=1}^{k} \Delta t_i} = \frac{0.92 * 31.92^{\frac{1}{1.818}} + 0.82 * 47.87^{\frac{1}{1.818}}}{1.74}$$

$V_e = 40.53$ m/min

The effectiveness of mist cutting while using oil based cutting fluid is observed and proved at different cutting speeds. These results prove that mist is a better cooling method compared to flooding or dry cutting at all cutting speeds when compared to observations made by Rahman et al (2001) [b] while machining ASSAB 718HH steel (diameter 20mm end mill, cutting speed 80-125 m/min). The improvement in tool life with 2210EP is up to 1500% compared to dry cutting at low speeds (10m/min) and 300% compared to flood cooling at higher speeds (30-60m/min). It can be seen that failure is due to chipping and plastic deformation while dry cutting compared to abrasive wear in mist cutting. Chipping and plastic deformation occurs primarily due to thermal fatigue. In mist cooling, abrasive wear is found due to better cooling and low friction between chips and tool. This corresponds to the work done by Su et al. (2006). They conclude that tool life of carbide tools in macro-milling of Ti-6Al-4V using mist cooling/lubrication improves by over 400-800% compared to dry and flood cooling/lubrication conditions. The cutting forces are also reduced due to penetration of mist particles in the cutting zone providing sufficient cooling/lubrication. Figures 32 and 33 show the comparison between failure modes in dry cutting and mist cutting.

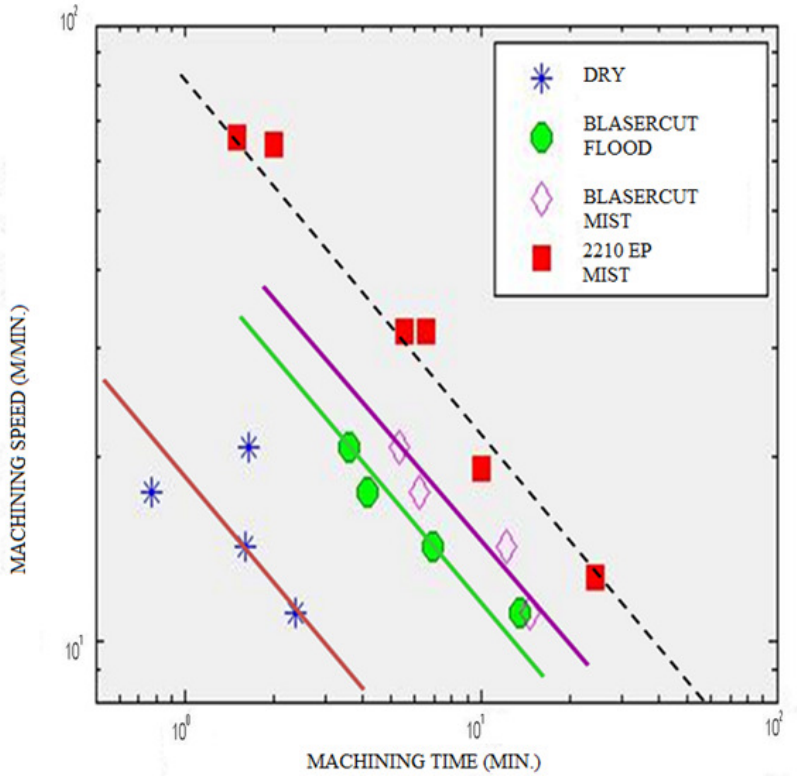


Figure 31: Tool life plotting for micro-milling of 316L stainless steel using WC endmill.

While macro-milling (10mm inserts) of P20 tool steel and NAK 80 steel using mist conditions, MQL is found to reduce cutting forces and temperature (Wu and Chien 2007). In high speed milling of hardened steel (300-500 m/min) using carbide inserts (16mm diameter), mist cooling is found to increase tool life by 80-200% over dry machining (Liao and Lin 2007) by promoting protective oxide layer formation. Prakash et al. (2001) report a decrease in friction co-efficient and smaller chips compared to dry cutting while microend-milling pure copper. The mode of failure in coated tools while using mist cooling/lubrication is: 1) chipping of flank; 2) de-bonding of coating. This failure is observed at an early machining time compared to WC tools under the same

cutting conditions. Coated tools are expensive and are expected to last longer under the same cutting conditions compared to carbide tools.

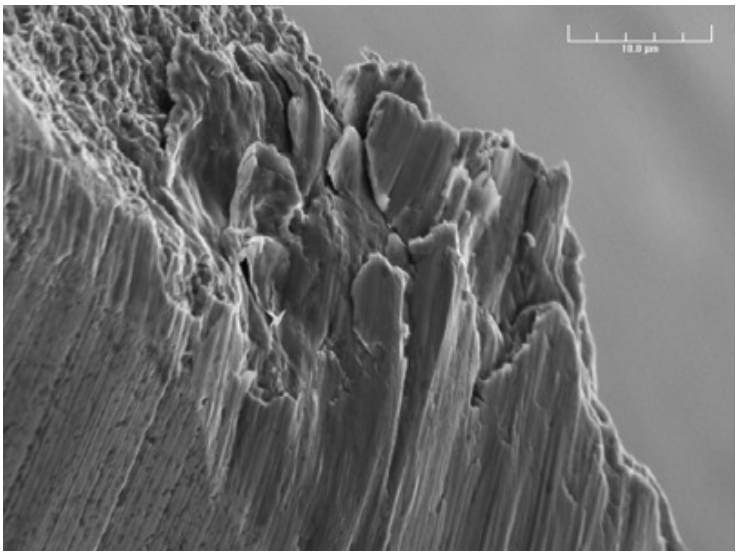

Figure 32: Scanning electron pictures of chipping and plastic deformation of a cutting tool (dry machining, machining time: 83s, cutting speed: 0.30 m/s).

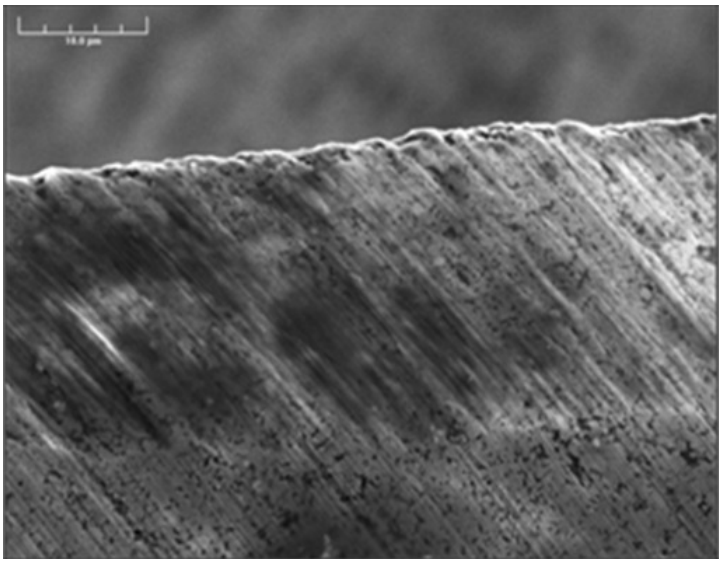

Figure 33: Scanning electron pictures of abrasive wear (mist cooling/lubrication, machining time: 1300s, cutting speed: 0.25 m/s).

Figures 34 and 35 shows a picture of tool failure due to chipping of coating. Figure 36 shows a chipped flank in a TiN coated end-mill. The coated tools are approximately 5μm (0.0002") larger in diameter compared to carbide tools due to coating thickness. Hence, we can assume coating thickness to be of the order of 2.5μm (0.0001”). Since wear is primarily due to abrasion in mist cooling, coatings needs to bond strongly to the base material. Inadequate bonding results in early peel off. This is in contrast with the observations made by Kang et al. (2008) while macroend-milling die steel under mist conditions. The coated tools are found to have chipping free edges compared to failure due to chipping and thermal fatigue in dry and flood conditions. Aramcharoen et al. (2008) report de-bonding and de-lamination of coatings as a major cause of failure in micro-milling of hardened tool steel (dry cutting, 2 flute end mill φ 0.5mm).

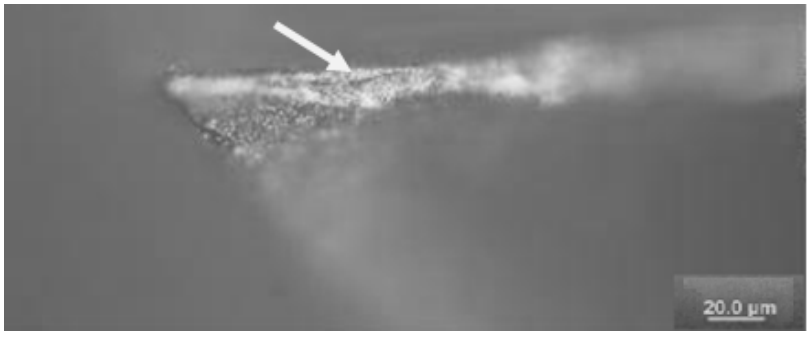


Figure 34: Optical microscope generated image of coating chip off (shown by arrow) on a TiN coated end-mill (mist cooling/lubrication, machining time: 246s; cutting speed: 0.08m/min).

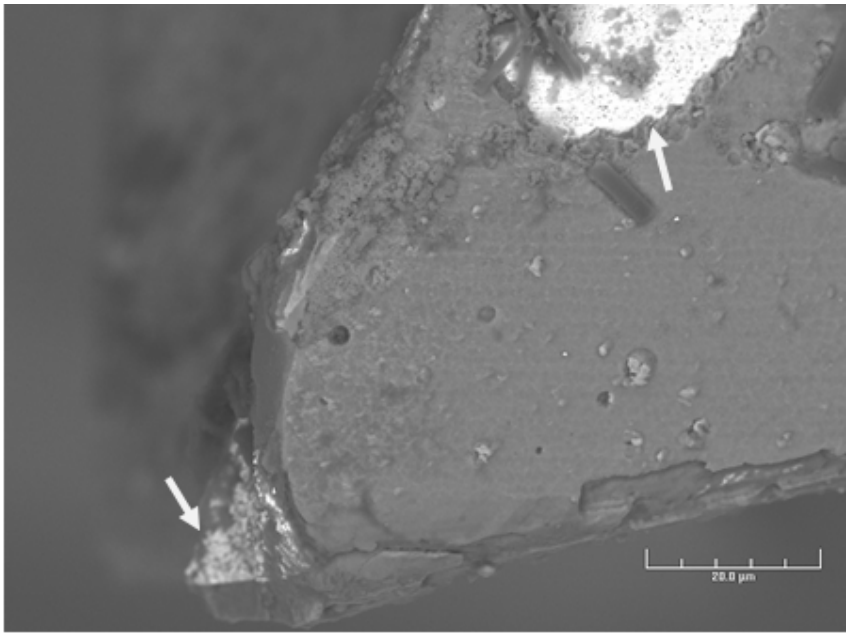

Figure 35: SEM image (BSE) of a chipped nose and de-laminated coating (shown by arrows) in a TiN coated end-mill (mist cooling/lubrication, machining time: 246s; cutting speed: 0.08m/min).

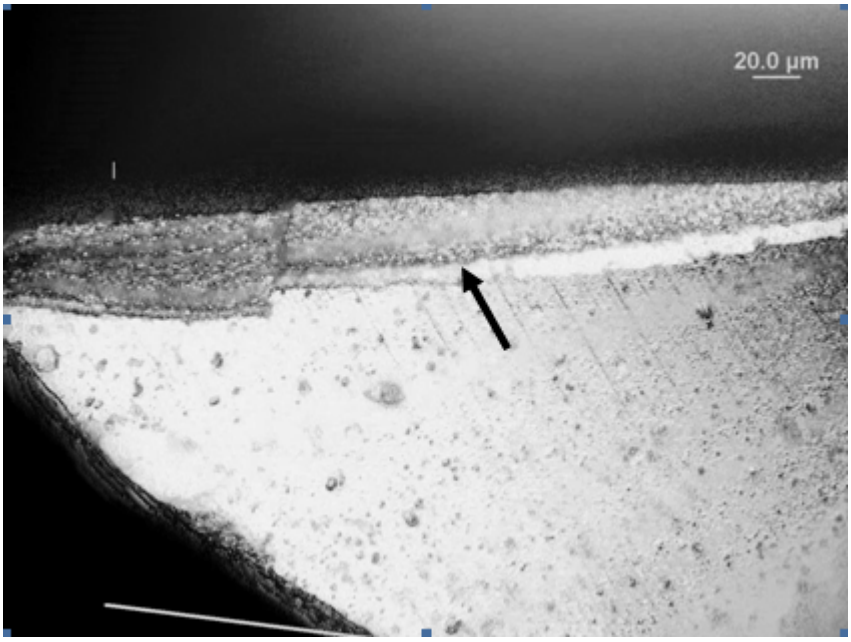


Figure 36: Optical microscope generated image of a chipped flank (shown by arrow) in a TiN coated end-mill (mist cooling/lubrication, machining time: 82s; cutting speed: 0.06m/min).

## 5.2 TOOL WETTING AND SURFACE TENSION COMPARISON

A measure of coolant surface tension is used to compare the effectiveness of the coolant in wetting a rotating tool. When the mist droplet comes in contact with the tool, a low surface tension of the droplet would result in spreading of the coolant over the tool. When a drop of 2210EP is poured over a WC microend-mill, it spreads over the tool immediately, whereas, a water based coolant beads up on the tool surface. Surface tension is lowest in 2210EP when compared to other oil based cooling fluids. Cutting fluids having high surface tension will tend to bead up easily and will not spread on the surface of the tool. Equations (8) and (9) show that lower surface tension will increase the wetting area of the tool hence helping the liquid drop to stick to the tool surface. Substituting following values in to Equation (9):

$$\frac{mv^2}{R} = 2\,\sigma_2.\,D$$

m = mass of droplet = $2.98 \times 10^{-17}$ Kg;

R= radius of tool = 0.508mm

$\sigma_2$ = surface tension from Table 7

After simplification,

$$v^2 = 8.83 * 10^{11} D \qquad (20)$$

Diameter of the droplet ‘D’ can be plotted against surface speed ‘v’ to compare minimum droplet size at a given surface speed.

Coolants tested for surface tension are 2210EP, 2210, 2200, 2300HD (Table 7). These are vegetable oil based lubricants and hence have much lower surface tension in air compared to water. This allows them to split into extremely small particles when introduced in pressurized air making them suitable for mist application.

Table 7. Surface tension measurements

| # | Surface Tension (mN/m) | | | | |
|---|---|---|---|---|---|
| | Water | 2210 EP | 2210 | 2200 | 2300HD |
| 1 | 72.8 | 25.9 | 28.98 | 34.15 | 33.57 |
| 2 | 72.8 | 25.85 | 29.33 | 34.1 | 34.22 |
| 3 | 72.8 | 25.88 | 29.68 | 34.2 | 34.15 |

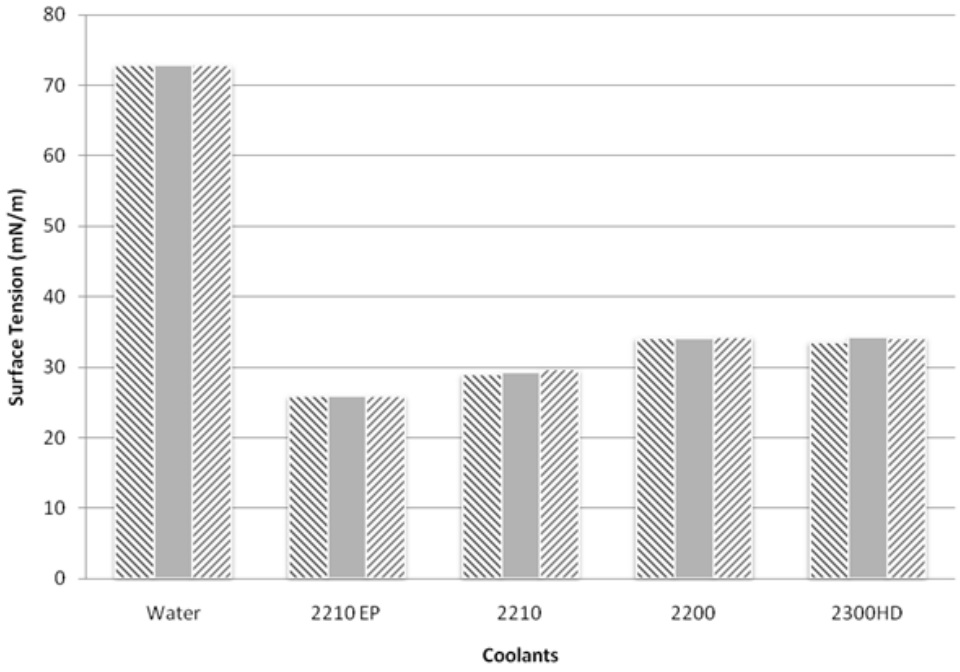


Figure 37: Surface tension comparison.

The low surface tension values of 2210 EP compared to 2210, 2200, 2300HD as shown in Figure 37 make it the preferred choice for machining stainless steel 316L using tungsten carbide end mills.

The boundary layer penetration experiment also proves that mist system used for machining is capable of wetting the tool rotating at high speed. Although 2210 EP has the best surface tension characteristic, it is observed that 2210, 2200, 2300 HD also wet the tool. These mist droplets continuously wet to the tool surface as the tool continued to rotate. This proves that the mist coolant provides lubrication by wetting the cutting edge of the tool as it penetrates in to the workpiece material to form a chip. Equation (9) provides the threshold limit for micro-mist droplet size that can wet a rotating tool. The centrifugal force acting on the droplet is balanced by the adhesion force between the droplet and the tool. The adhesion force ($\Delta\ \sigma$) is dependent on surface tension of the liquid in air and the size of the mist droplet 'D' (Equation 7). Sample calculation is shown below:

$$\frac{mv^2}{R} = \Delta\ \sigma\ D \tag{7}$$

With $m=2.98*10^{-17}$kg, R= 0.508mm, v= 31.93m/min.

Equation (7) becomes:

$$\Delta\ \sigma = \frac{5.98*10^{-11}}{D} \tag{21}$$

Knowing the particle size and fluid characteristics of any mist system, we can analyze whether the droplet will wet the tool at the given speed. Figure 38 marks the

zones of adhesion force versus centrifugal force for wetting of a 1.016mm end mill using 2210EP mist.

Similar work done by Rahman et al (2001) [b] concludes that mist droplets will be ineffective at high surface speed (100m/min to 140 m./min). Mist droplets are found to successfully penetrate any boundary layer on a micro-tool and wet the tool surface from a range of 0-500 m/min. Droplets of 2210 EP are also found to wet a 12.7mm tool moving at 0-279 m/min and a 3.175mm tool moving at 50-498 m/min.

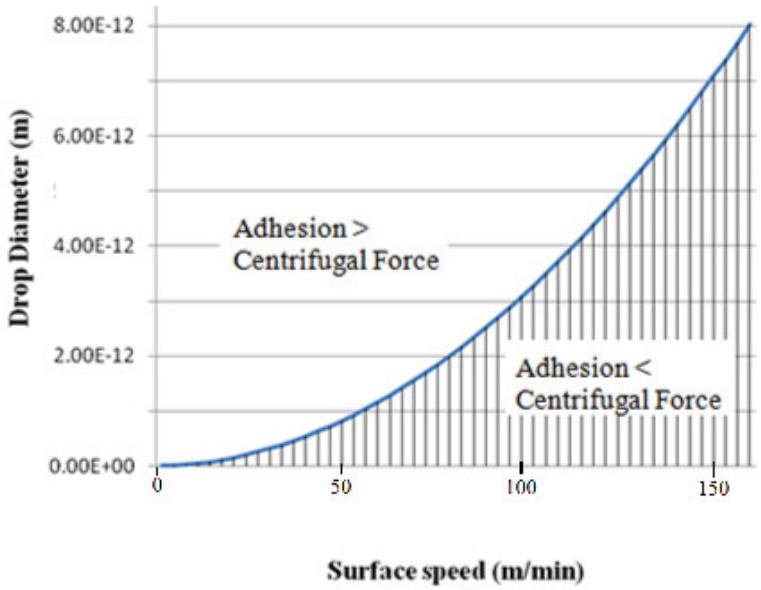


Figure 38: Balance of adhesion and centrifugal force on a 2210EP micro-droplet.

## 5.3 CONTACT ANGLE COMPARISON

The contact angle measurement technique used for comparing contact angle between various different types of fluids has given us repetitive results for the same fluid hence making it a reliable method of comparison (Table 8).

The pH of water is as expected at 7.0, Coolube is found to be highly alkaline at 9.0. 2210 EP and 2210 are found to be very slightly acidic close to neutral pH (6.59 and 6.34 respectively). Micro-machining has a wide scope of materials. Use of 2210/2210 EP with materials that maybe sensitive to alkaline fluids will prevent any staining that may occur due to unexpected chemical interaction between the cutting fluids and workpiece materials.

A comparison between same volumes of different cutting fluids on SS 316L is seen in Figure 39. While water and Coolube make a nice round droplet on the base sheet, 2210 and 2210 EP being oil based, spread around immediately. This provides more effective wetting of the workpiece material. While it is important to have proper wetting of the tool, it is also imperative to choose a cutting fluid that does not stain the material being machined. Figures 39 and 40 clearly establish that 2210 EP has the least contact angle compared to water, Coolube 1:30, 2210, 2300 HD and 2200. With 316L stainless steel, 2210 EP forms a contact angle around $10^0$ compared to $70^0$ of water. This makes 2210 EP the preferred choice for machining stainless steel 316L.

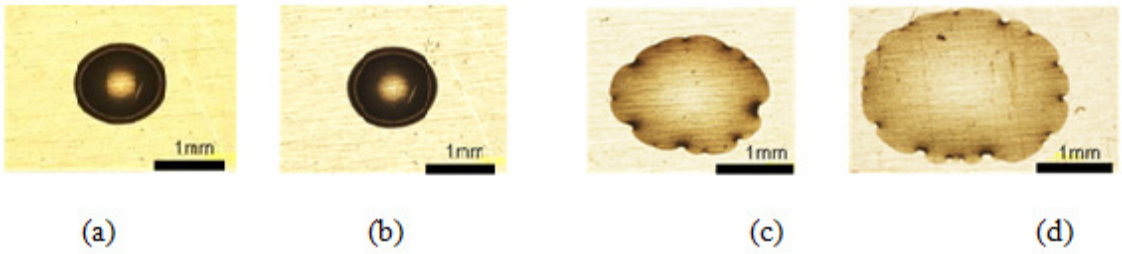


Figure 39: Drop shape of drop of coolant on 316L stainless steel plate for contact angle measurement. (a) Water (b) Coolube 1:30 (c) 2210 (d) 2210 EP. Droplet Volume: .25µl.

Table 8. Results of contact angle comparison

| Coolant | Water | CL 1:30 | 2210 | 2210EP | 2300 HD | 2200 |
|---|---|---|---|---|---|---|
| Contact | 70 | 60 | 17.5 | 12 | 25 | 15 |
| Angle | 70 | 65 | 22.5 | 5 | 25 | 15 |
| (Degrees) | 69 | 65.5 | 27.5 | 10 | 25 | 15 |
| | 64 | 67.5 | 22.5 | 2.5 | 25 | 15 |

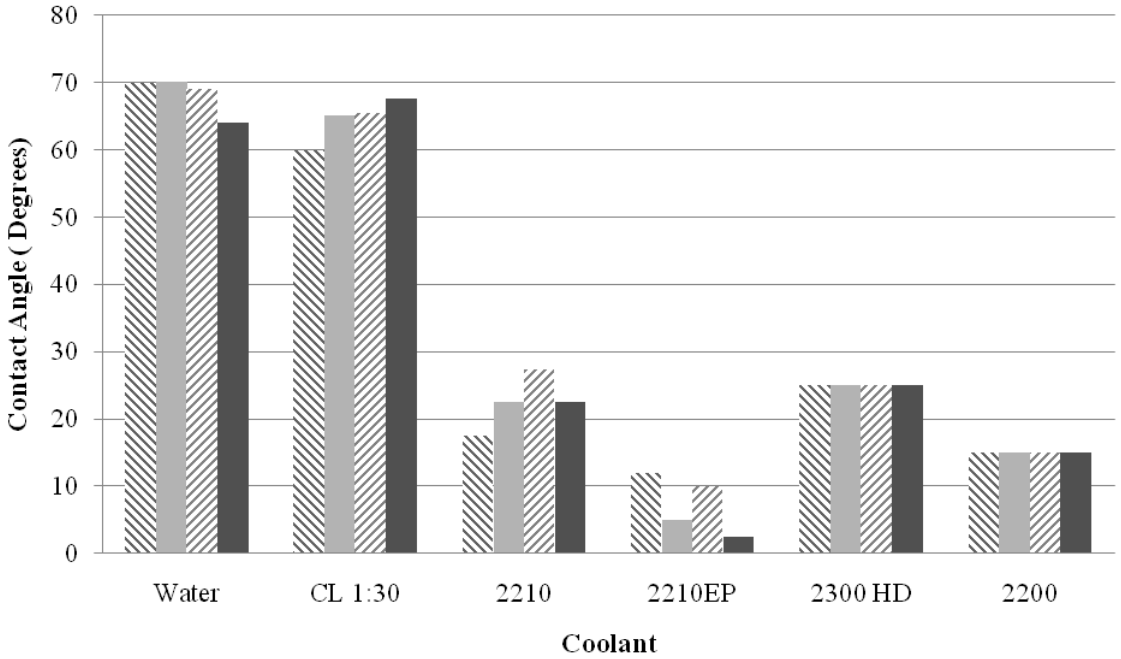


Figure 40: Contact angle comparison.

Sample calculation for contact angle measurement for Equation (10):

$$\frac{P}{V^{1/3}}(\theta) = [\frac{24}{\pi} . \frac{(1 - K\cos^2\theta)^{3/2}}{2 - 3\cos\theta + \cos^3\theta}]^{1/3} \quad (10)$$

Appendix (D5) provides values for volume V and projected diameter P for all cutting fluids. For water use the following values in the above equation:

P = 1.18mm

V= 0.25μL

Hence, $\frac{P}{V^{1/3}}(\theta) = \frac{1.18}{0.25^{\frac{1}{3}}} = 1.866$ (22)

In Figure 27, corresponding to a normalized diameter of 1.866, contact angle 'θ' equals $70^0$.

This is a novel method of comparison of contact angle between different liquids. An attempt is also made to compare contact angle between different fluids on the tool material. The droplets are found to immediately spread all around the tool due to extremely low surface tension.

## 5.4 PARTICLE SIZE COMPARISON OF CUTTING FLUIDS

The mist particles are sprayed on a flat stainless steel 316L plate from a point 12 inches vertically above. It can be seen that the droplets are very small- diameter in the order of a few microns. Our assumption that the droplets are part of a sphere when they touch the material base is valid.

The data from Appendix (D6) is used in Equation (14) and Equation (16) to calculate the average volume of 2210, 2210EP, 2200, 2300 HD droplets. The average particle size of these droplets is compared in Figure 41. It can be seen that 2210 EP has the least particle size followed by 2210, 2200, 2300 HD. We can clearly see that the lowest particle size is of 2210 EP (average radius 0.26 microns). This data when compared to the adhesion versus centrifugal force data shown in Figure 38 proves that the droplet size is definitely in the region where it wets the tool surface. A surface speed of 156.4 m/min corresponds to an RPM of 50,000 using a 1.016mm end-mill. At this speed, the smallest particle that sticks to the tool surface is $8 \times 10^{-12}$ m in diameter. The average particle size of micro-mist is between 0.5µm ($5 \times 10^{-7}$m) and 10µm ($1 \times 10^{-5}$m) in diameter. This clearly falls in the zone: ‘adhesion>centrifugal force’.

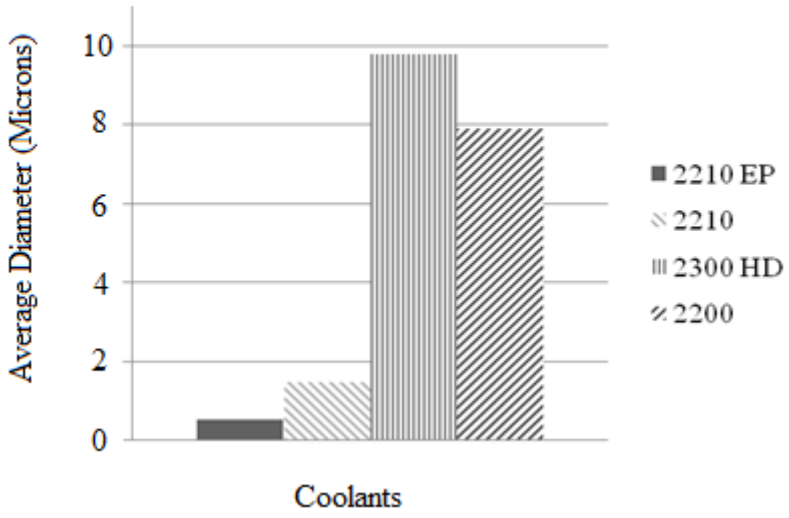


Figure 41: Droplet size comparison.

Sample calculation of particle size:

As shown in Figure 29, measure D1, D2 and h. From Appendix D5:

$h_{avg}$= 0.4μm

$r_{avg}$ = (D1+D2)/4= 1μm

Average volume of droplet from Equation (14):

$$V_{avg} = \pi h_{avg}^{\ 2}\left(\frac{h_{avg}}{6}+\frac{r_{avg}^2}{2h_{avg}}\right)=\pi(4*10^{-7})^2\left(\frac{4*10^{-7}}{6}+\frac{1*10^{-6}}{2*0.4*10^{-6}}\right)m^3$$

$V_{avg}$ = 3.35*10$^{-20}$ m$^3$

Average mass of droplet from Equation (15):

$m_{avg} = \rho * V_{avg}$ = 890 kg/m$^3$ * 3.35*10$^{-20}$ m$^3$

$m_{avg}$ = 2.98 *10 $^{-17}$kg

The average radius of the full sphere droplet is (Equation 16):

$$V_{avg} = \left(\frac{4}{3}\right)\Pi R_{avg}^{\ 3}$$

$$R_{avg} = \sqrt[3]{\frac{3V_{avg}}{4\Pi}} = \sqrt[3]{\frac{3*3.35*10^{-20}}{4\Pi}}$$

$R_{avg}$= 2.0 *10 $^{-7}$ m = 0.2 μm

Hence average diameter is 2 x $R_{avg}$ = 0.4μm

## 5.5 VISCOSITY COMPARISON OF CUTTING FLUIDS

The prediction of particle trajectory as given by Equation (18) and Equation (19) requires knowledge of cutting fluid viscosity. Table 9 and Figure 42 shows the rheometer data while measuring dynamic viscosity of 2210, 2210 EP, 2200, 2300 HD. All cutting fluids chosen are oil based and are highly viscous compared to water based coolants.

Table 9. Viscosity measurement data of 2210 EP, 2200, 2210, 2300 HD.

| Viscosity (Pa.s) | | | | | |
|---|---|---|---|---|---|
| Coolant | 2210 EP | 2200 | 2210 | 2300HD | Water |
| shear rate (1/s) | | | | | |
| 5.0 | 0.0164 | 0.0238 | 0.0136 | 0.0608 | 0.0009 |
| 93.3 | 0.0162 | 0.0232 | 0.0136 | 0.0620 | 0.0009 |
| 181.7 | 0.0164 | 0.0232 | 0.0135 | 0.0610 | 0.0009 |
| 270.0 | 0.0162 | 0.0231 | 0.0135 | 0.0608 | 0.0009 |
| 358.3 | 0.0163 | 0.0231 | 0.0135 | 0.0607 | 0.0009 |
| 446.7 | 0.0162 | 0.0231 | 0.0135 | 0.0606 | 0.0009 |
| 535.0 | 0.0162 | 0.0232 | 0.0135 | 0.0606 | 0.0009 |
| 623.3 | 0.0162 | 0.0232 | 0.0135 | 0.0604 | 0.0009 |
| 711.7 | 0.0161 | 0.0232 | 0.0135 | 0.0604 | 0.0009 |
| 800.0 | 0.0161 | 0.0232 | 0.0135 | 0.0603 | 0.0009 |

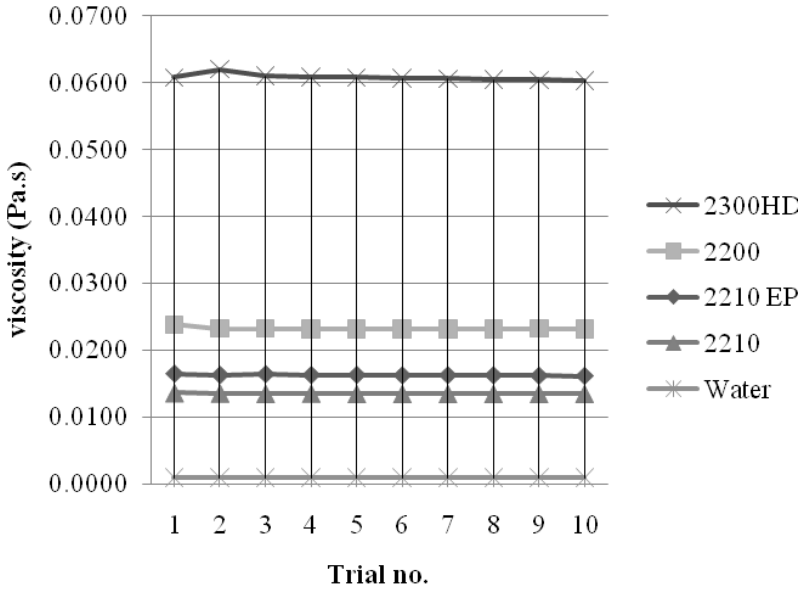


Figure 42: Viscosity of different coolants.

The drag force acting on a particle is directly proportional compared to its viscosity (Equation 17). When mist particles are projected at the rotating tool, higher viscosity will create a higher drag force over the particles preventing it from touching the tool surface. Figure 42 shows the comparison between different mist type cutting fluids. The highest viscosity is of 2300HD, whereas the viscosity of 2210, 2210 EP, 2200 are comparable. This is a high viscosity cutting fluid and should be used for heavier cutting operations. Since it's more viscous, it will not flow in low speed and high friction cutting. A higher viscosity compared to water makes oil based cutting fluids less prone to flowing away when a friction force acts between the chip and the cutting edge of the tool. This provides better lubrication by making a thin film of coolant between the tool and workpiece. All of the above fluids have a particle diameter within 10μm for mist flow with 2300HD having maximum size due to high viscosity.

## 5.6 COMPUTATIONAL ANALYSIS OF FLOW OVER ROTATING CYLINDER

The analysis of air flow over a rotating cylinder is chosen as an analogy for mist flow over a rotating tool. Since mist particles are really small, we can assume that they follow the path of air around the rotating tool. The 2D simulation results in Figures 43 and 44 shows flow from left to right; the cylinder (simplified end mill cutter- diameter 1.016mm) rotates counter-clockwise at 4000 RPM. The magnitude of flow velocity is shown by velocity vectors. It can be seen that flow separates over the rotating tool and forms a wake behind the cylinder.

Problem definition of Fluent calculations:

A cylinder having diameter 0.04 inches is modeled as a wind tunnel test. The cylinder is rotated at 4000 RPM and the air velocity is 0.6495m/s. Reynolds number can be calculated from the data provided. Flow inlet is far away so that flow is fully developed when it reaches the cylinder surface. The temperature and pressure is taken as standard temperature and pressure (STP). The walls of the tunnel are standard no- slip wall. The problem is analyzed in 2 dimensions. The spacing of mesh points can is larger between the circle and the wall. It should have very fine resolution on the circle and very fine resolution of the wall boundaries. Fluid is incompressible at constant temperature.

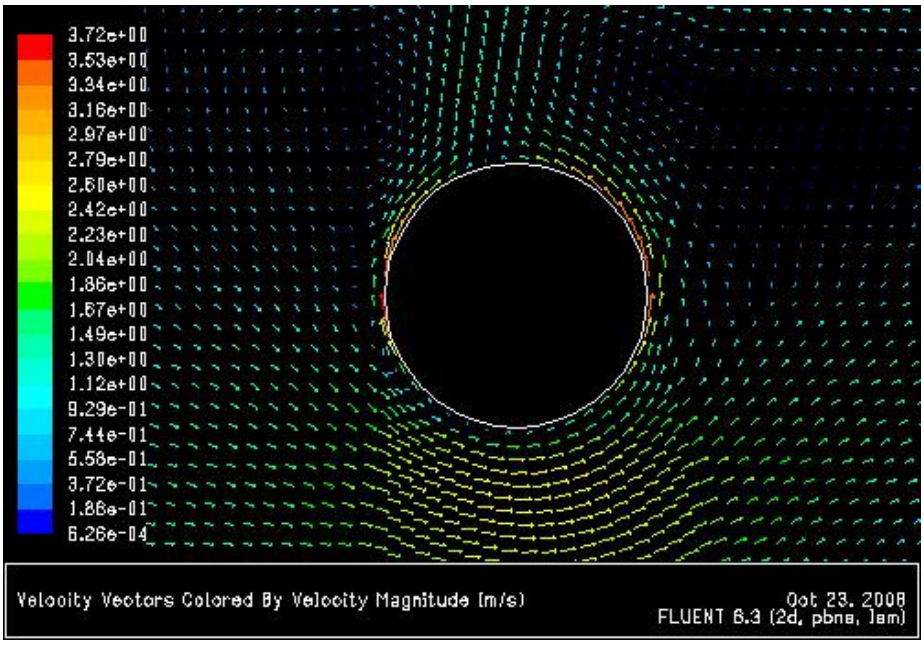


Figure 43: Velocity vectors of fluid around a rotating tool. Ø1 mm (0.04") cylinder @4000 rpm counter-clockwise, flow at 0.65 m/s (25.6 in/s) from left to right.

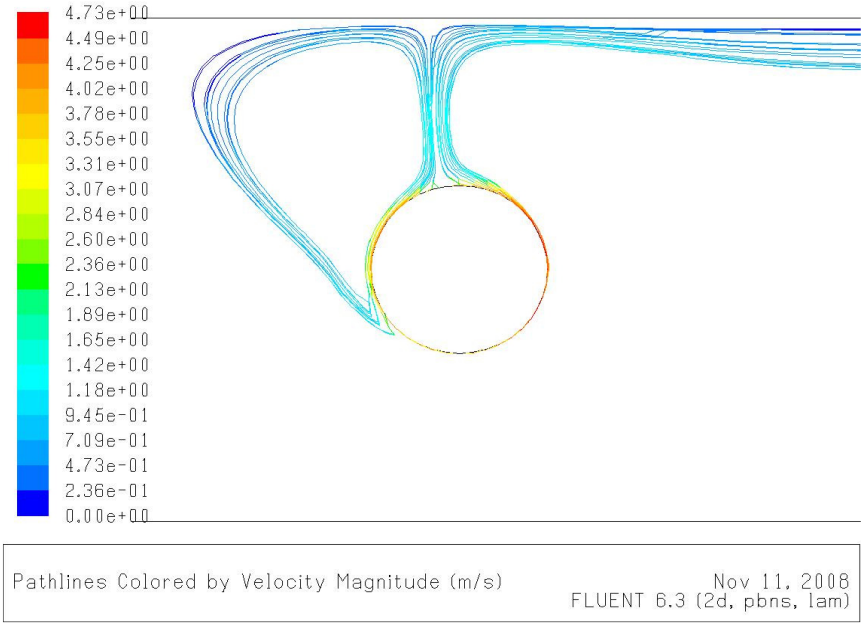


Figure 44: Simulation of flow across a rotating cylinder. Pathlines covered by velocity magnitude(m/s). Ø1 mm (0.04") cylinder @4000 rpm counter-clockwise, flow at 0.65 m/s (25.6 in/s) from left to right.

A stagnation point is observed where the flow line splits. It is concurred that if the mist particles follow the flow of air around the tool, it will touch the tool surface and cause wetting. Experimentally, tool of diameter 1.016 mm rotating up to 50,000 rpm is wet by the mist flow. The workpiece should not be placed in the stagnation zone because the mist droplets do not have enough momentum to penetrate the boundary layer at this point. Further micro-machining analysis is needed to verify this. A similar result is obtained in simulation of mist flow at 120m/s over a rotating tool (12 mm end mill) at 15m/s (Lopez de Lacalle et al.2006). Boundary layer is successfully penetrated by MQL causing wetting of the cutting edge and providing adequate cooling/lubrication.

# 6. CONCLUSIONS

This research studied the micro-milling of SS 316L. It is found that:

1. Micro-tools fail due to ideal abrasive wear in mist cutting conditions. Chipping and attrition may also occur depending on the cutting conditions.
2. Mist improves the tool life performance compared to dry cutting and flood cooling. The improvement in tool life can be up to 1500% compared to dry cutting at low speeds (10m/min).
3. Low surface tension micro-droplets (0.4-10µm diameter) penetrate the tool boundary layer and wet a tool rotating at a surface speed of 500 m/min.
4. Oil based mist droplets has much lower surface tension and hence lower values of contact angle ($10^0$) compared to water ($70^0$) on 316L stainless steel. This improves wetting of workpiece.
5. Mist fluids are highly viscous compared to water based products. This reduces their flow after wetting and allows the mist to form a protective film thus improving lubrication and reducing friction.
6. There is a proper orientation of mist flow with respect to workpiece orientation that will provide most effective cutting. Stagnation zone should be avoided for placement of workpiece.

# 7. RECOMMENDATIONS

1. Coated tools should be tested for bonding strength between coatings and base material. Better bonding will reduce unpredictability in tool performance.
2. The effect of positioning mist nozzle in different 3D positions should be studied. The effect of positioning workpiece in stagnation zone should be verified.
3. Computational fluid flow analysis should be performed using actual conditions of tool geometry and 2-phase mist flow.

# REFERENCES

AK Steel Corporation. (2007). 316L data sheet. http://www.aksteel.com/pdf/markets_products/stainless/austenitic/316_316L_Data_Sheet.pdf. Access date 07/28/2009.

Alauddin, M.; El Baradie, M.A. (1997). Tool life model for end milling steel (190 BHN). Journal of Materials Processing Technology, 68 (1): 50-59.

Aramcharoen, A.; Mativenga, P.T.; Yang, S.; Cooke, K.E.; and Teer, D.G. (2008). Evaluation and selection of hard coatings for micromilling of hardened tool steel. International Journal of Machine Tools and Manufacture, 48 (14): 1578-1584.

Aramcharoen, A. and Mativenga, P.T. (2009). Size effect and tool geometry in micromilling of tool steel. Precision Engineering, 33 (4): 402-407.

AZoM™, Pty.Ltd. (2009). Grade 316L – Properties, fabrication and applications. http://www.azom.com/Details.asp?ArticleID=2382. Access date 07/28/2009.

Bao, W.Y. and Tansel, I.N. (2000)[a]. Modeling microend-milling operations. Part II: tool run-out. International Journal of Machine Tools & Manufacture. 40 (15): 2175–2192.

Bao, W.Y. and Tansel, I.N. (2000)[b]. Modeling microend-milling operations. Part III: influence of tool wear. International Journal of Machine Tools & Manufacture, 40 (15): 2193-2211.

Chakraborty, P.; Asfour, S.; Cho, S.; Onar, A; and Lynn, M (2008). Modeling tool wear progression by using mixed effects modeling technique when end-milling AISI 4340 steel. Journal of Materials Processing Technology, 205(1-3):190-202.

Dolinek, S. and Kopa, J. (1999). Acoustic emission signals for tool wear identification. Wear, 225 (1): 295-303.

Dolinek, S.; Utari, B.; and Kopa, J. (2001). Wear mechanisms of cutting tools in high-speed cutting processes. Wear, 250 (1-12): 349-356.

Dornfeld, D.; Min, S. and Takeuchi, Y. (2006). Recent advances in mechanical micromachining. CIRP Annals - Manufacturing Technology, 55(2): 745-768.

Dos Santos, A. L. B.; Duarte, M. A. V.; Abrão, A. M.and Machado, A. R. (1999). An optimisation procedure to determine the coefficients of the extended Taylor's equation in machining. International Journal of Machine Tools and Manufacture, 39(1): 17-31.

Fang, F.Z.; Wu, H.; Liu X.D.; Liu, Y.C.; and Ng, S.T. (2003). Tool geometry study in micromachining. Journal of Micromechanics and Microengineering, 13(5): 726-731.

Filiz, S; Conley, M.C.; Wasserman, M.B.; and Ozdoganlar, O.B. (2007). An experimental investigation of micro-machinability of copper 101 using tungsten carbide micro-endmills. International Journal of Machine Tools and Manufacture, 47(7-8): 1088-1100.

Ford M.A. (1998). Carbide end mills. http://www.maford.com/taf/catalog.taf?category=a13. Access date 07/20/2009.

Friedrich, C. R.; Coane, P. J.; and Vasile, M. J. (1997). Micromilling development and applications for microfabrication. Microelectronic Engineering, 35(1-4): 367-372.

Groover, M.P. (2004). Fundamentals of Modern Manufacturing. John Wiley & Sons, New York.

Haas Automation, Inc. (2009). Haas VMC - Office mills. http://www.haascnc.com/VMC_MODEL_OM.asp#VMCTreeModel. Access date 07/2/2009.

Haas Automation, Inc. (2009). Haas VMC – 20IN. http://www.haascnc.com/VMC_MODEL_20IN.asp#VMCTreeModel. Access date 06/05/2009.

Han, K.; Xin, Y.; Walsh, R.; Downey II, S.; and Kalu, P.N. (2009). The effects of grain boundary precipitates on cryogenic properties of aged 316-type stainless steels. Materials Science and Engineering. 516 (1-2): 169-179.

Huang, S.N.; Tan, K.K.; Wong, Y.S.; De Silva, C.W.; Goh, H.L.; and Tan, W.W. (2007). Tool wear detection and fault diagnosis based on cutting force monitoring. International Journal of Machine Tools and Manufacture, 47 (3-4): 444-451.

Hung, N.P. and Zhong, C.H. (1996). Cumulative tool wear in machining metal matrix composites: Part I: Modelling. Journal of Materials Processing Technology, 58: 109-113.

Jemielniak, K.; Bombiński, S.; and Aristimuno, P.X. (2008). Tool condition monitoring in micromilling based on hierarchical integration of signal measures . CIRP Annals - Manufacturing Technology, 57 (1): 121-124.

Kang, M.C.; Kim, K.H.; Shin, S.H.; Jang, S.H.; Park, J.H.; and Kim, C. (2008). Effect of the minimum quantity lubrication in high-speed end-milling of AISI D2 cold-worked

die steel (62 HRC) by coated carbide tools. Surface and Coatings Technology, 202 (22-23): 5621-5624.

Keyence Corporation. (2009). LK-G157 laser specification. http://www.keyence.com/products/vision/laser/lkg/lkg_applications_4_1.php. Access date 07/15/2009.

Kim, N. H. and Chun, J. S. (1985). A study of the tool life of TiC and TiC plus Al2O3 chemical vapour deposited tungsten carbide tools. Journal of Materials Science, 20 (4): 1285-1290.

Kuljanić, E.; Šolaja, V. (1980). Random strategy method for determining tool life equations. CIRP Annals - Manufacturing Technology, 29 (1): 351-356.

Lai, X.; Li, H.; Li, C.; Lin, Z.; and Ni, J. (2008). Modelling and analysis of micro scale milling considering size effect, micro cutter edge radius and minimum chip thickness. International Journal of Machine Tools and Manufacture, 48 (1): 1-14.

Lee, K. and Dornfeld, D.A. A Study of Surface Roughness in the Micro-End-Milling Process Laboratory for Manufacturing and Sustainability. Consortium on Deburring and Edge Finishing, 2004. UC Berkeley: Laboratory for Manufacturing and Sustainability.

Liao, Y.S.; Lin, H.M. (2007). Mechanism of minimum quantity lubrication in high-speed milling of hardened steel. International Journal of Machine Tools and Manufacture, 47 (11): 1660-1666.

Liao, Y.S.; Lin, H.M.; and Chen, Y.C. (2007). Feasibility study of the minimum quantity lubrication in high-speed end milling of NAK80 hardened steel by coated carbide tool. International Journal of Machine Tools and Manufacture, 47 (11): 1667-1676.

Lo, K.H.; Shek, C.H.; and Lai, J.K.L. (2009). Recent developments in stainless steels. Materials Science and Engineering, 65 (4-6): 39-104 .

López de Lacalle, L.N.; Angulo, C.; Lamikiz, A.; and Sánchez, J.A. (2006). Experimental and numerical investigation of the effect of spray cutting fluids in high speed milling. Journal of Materials Processing Technology, 172 (1): 11-15.

Macdougall, G. and Ockrent, C. (1942). Surface energy relations in liquid/solid systems. I. The adhesion of liquids to solids and a new method of determining the surface tension of liquids. Proceedings of the Royal Society of London. Series A, Mathematical and Physical Sciences, 180 (981): 151-173.

Malekian, M; Park, S.S.; and Jun, M.B.G. (2009). Tool wear monitoring of micro-illing operations. Journal of Materials Processing Technology, 209 (10): 4903-4914.

Marksberry, P.W. and Jawahir, I.S. (2008). A comprehensive tool-wear/tool-life performance model in the evaluation of NDM (near dry machining) for sustainable manufacturing. International Journal of Machine Tools and Manufacture, 48 (7-8): 878-886.

Masuzawa, T and Toenshoff, H.K. (1997) Three-dimensional micromachining by machine Tools. CIRP Annals - Manufacturing Technology, 46 (2): 621-628.

Masuzawa, T. (2000). State of the art of micromachining. CIRP Annals - Manufacturing Technology, 49 (2): 473-488.

McKeown, P.A. (1987). The role of precision engineering in manufacturing of the future. CIRP Annals - Manufacturing Technology, 36 (2): 495-501.

MEMSnet. (2009). Material: Tungsten Carbide (WC) http://www.memsnet.org/material/tungstencarbidewcbulk/. Access date 07/25/2009.

Orhan, S.; Er, A.O.; Camuşcu, N.; and Aslan, E. (2007). Tool wear evaluation by vibration analysis during end milling of AISI D3 cold work tool steel with 35 HRC hardness. NDT & E International, 40 (2): 121-126.

Prakash, J.R.S.; Rahman, M.; Senthil, A.K; and Lim, S.C. (2001). Effect of minimal quantities of lubricant in micro milling. Initiatives of Precision Engineering at the Beginning of a Millennium. Springer US, New York.

Prengel, H. G.; Jindal, P. C.; Wendt, K. H.; Santhanam, A. T. ; Hegde, P. L.; and Penich, R. M. (2001). A new class of high performance PVD coatings for carbide cutting tools. Surface and Coatings Technology, 139 (1): 25-34.

Rahman, M.; Senthil, A.K.; and Prakash, J.R.S (2001)[a]. Micro milling of pure copper. Journal of Materials Processing Technology, 116 (1): 39-43.

Rahman, M.; Senthil A.K.; and Salam, M. U. (2001)[b]. Experimental evaluation on the effect of minimal quantities of lubricant in milling. International Journal of Machine Tools and Manufacture, 42 (5): 539-547.

Rusnaldy; Ko, T.J; Kim, H.S. (2007). Micro-end-milling of single-crystal silicon. International Journal of Machine Tools and Manufacture, 47(14): 2111-2119.

Salgado, D.R.; Alonso, F.J. (2007). An approach based on current and sound signals for in-process tool wear monitoring. International Journal of Machine Tools and Manufacture, 47 (14): 2140-2152.

Snoeys, R.; Staelens, F.; and Dekeyser, W. (1986) Current trends in non-conventional material removal processes. CIRP Annals - Manufacturing Technology, 35 (2): 467-480.

Su, Y.; He, N.; Li, L.; and Li, X.L. (2006). An experimental investigation of effects of cooling/lubrication conditions on tool wear in high-speed end milling of Ti-6Al-4V. Wear, 261 (7-8): 760-766.

Sun, J.; Wong, Y. S.; Rahman, M.; Wang, Z. G.; Neo, K. S.; Tan, C. H.; and Onozuka, H. (2006). Effects of coolant supply methods and cutting conditions on tool life in end milling Titanium alloy. Machining Science and Technology: An International Journal, 10 (3): 355 – 370.

Taniguchi, N. (1983). Current status in, and future trends of, ultraprecision machining and ultrafine materials processing CIRP Annals - Manufacturing Technology, 32 (2): 573-582.

Tansel, I.; Rodriguez, O.; Trujillo, M.; Paz, E.; and Li, W. (1998). Micro-end-milling-I. Wear and breakage. International Journal of Machine Tools and Manufacture, 38 (12): 1419-1436.

Tansel, I. N.; Arkan, T. T.; Bao, W. Y.; Mahendrakar, N.; Shisler, B.; Smith, D.; and McCool, M.; (2000). Tool wear estimation in micro-machining. Part I: tool usage–cutting force relationship. International Journal of Machine Tools and Manufacture, 40 (4): 599-608.

Tasdelen, B.; Wikblom, T.; and Ekered, S. (2008). Studies on minimum quantity lubrication (MQL) and air cooling at drilling. Journal of Materials Processing Technology, 200 (1): 339-346.

Unist, Inc. (2007). Uni-MAX Coolubricator System. http://www.unist.com/machinecutting/MQL/Continuous_External/uniMAXcoolubricator.htm. Access date 07/28/2009.

Vasile, M.J.; Friedrich, C.R.; Kikkeri, B.; and McElhannon, R. (1996). Micrometer-scale machining: tool fabrication and initial results. Precision Engineering, 19 (2): 180-186.

Weinert, K; Petzoldt, V (2004). Machining of NiTi based shape memory alloys. Materials Science and Engineering A, 378 (1-2): 180-184.

Wu, Cheng-Hsien; Chien, Chih-Hsien (2007). Influence of lubrication type and process conditions on milling performance. Journal Proceedings of the Institution of Mechanical Engineers, Part B: Journal of Engineering Manufacture. 221 (5): 835-843.

Ying-lin, K.E.; Dong, H.; Liu, G.; and Zhang, M. (2009). Use of nitrogen gas in high-speed milling of Ti-6Al-4V. Transactions of Nonferrous Metals Society of China, 19 (3): 530-534.

# APPENDIX A

# PROPERTIES AND SPECIFICATIONS OF MATERIAL AND EQUIPMENT

## A.1.HAAS OM2 SPECIFICATIONS

- The machine is equipped with a 50,000 rpm brushless electric micromotor spindle with 270W power rate.
- The maximum values of feed rate and cutting speed obtained on this micromilling machine are equal to 19.2m/min (757 ipm) and 12.7 m/min (500 ipm).
- The maximum travel distance along X and Z axes are equal to 12” or 305 mm and a travel distance of 10” or 254 mm along Y axis.
- Four-axis machining can be performed using a microrotary table or five-axis machining by installing a microtrunnion table (Haas 2009).

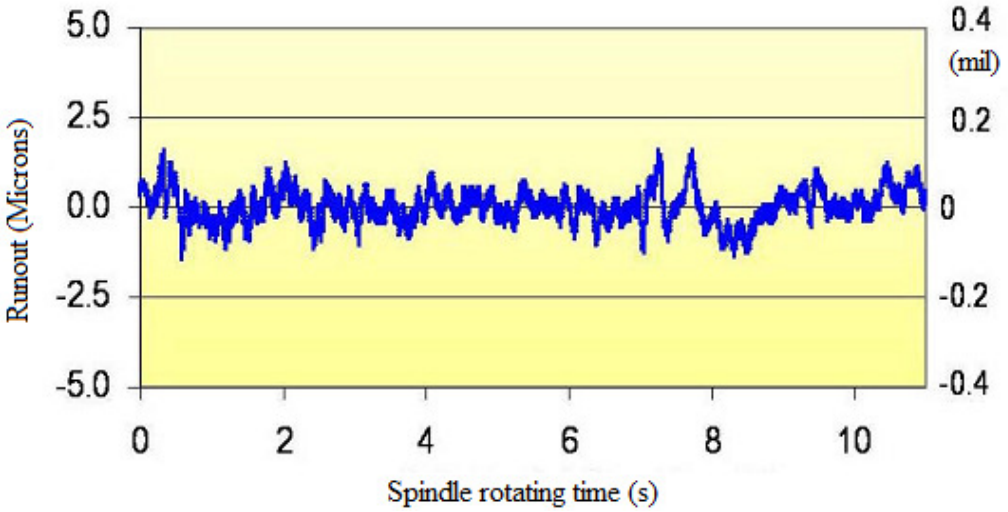


Figure A1: Runout of Haas OM2 air spindle at 10,000 rpm.


Figure A-2. The Haas OM 2 CNC micromachining system (Haas Automation, 2009)

## A.2. HAAS VF1 SPECIFICATIONS

- The machine is equipped with a 40- taper cartridge spindle with maximum speed of 7500 rpm driven by a 14.9kW (20-hp) vector dual-drive (Y-Delta) motor.

- The maximum values of feed rate for rapids and cutting obtained on VF-1 machining system equal to 25.4m/min (1,000 ipm) and 16.5 m/min (650 ipm).
- The tool has 508 x 406 x 508 mm (20" x 16" x 20") XYZ travels and is built utilizing all American-made cast-iron components.
- The system has a 20 tool carousel which can be used for multiple machining operations (Haas 2009).


Figure A-3. The Haas VF 1 CNC machining system (Haas Automation, 2009)

## A.3. KEYENCE LK-G157 LASER SPECIFICATIONS

The main features of this measurement sensor are:

- Sampling speed of 50 KHz
- Measuring range of 150 ±40 mm (5.91 ±1.57" )
- Capable of accurately measuring targets rotating or vibrating at high speed.
- Incorporates state of the art algorithms for measuring plastic, transparent or translucent, and metal targets effectively. The LK- Navigator helps to optimize the laser beam to use it effectively based on the measuring surface (Keyence 2009).

## A.4. UNIST COOLUBRICATOR SYSTEM

- The system is equipped with a 5- 200 pulse/minute pulse generator and a 0.2 drops per cycle to 1.0 drop per cycle liquid metering pump (1 drop equals 0.033cc).
- A brass knurled air metering screw controls the flow of air atomizing out the nozzle which determines the density and distance of the spray.
- The spray output has an included angle of 15-20 degrees depending on the amount of air introduced (Unist 2007).

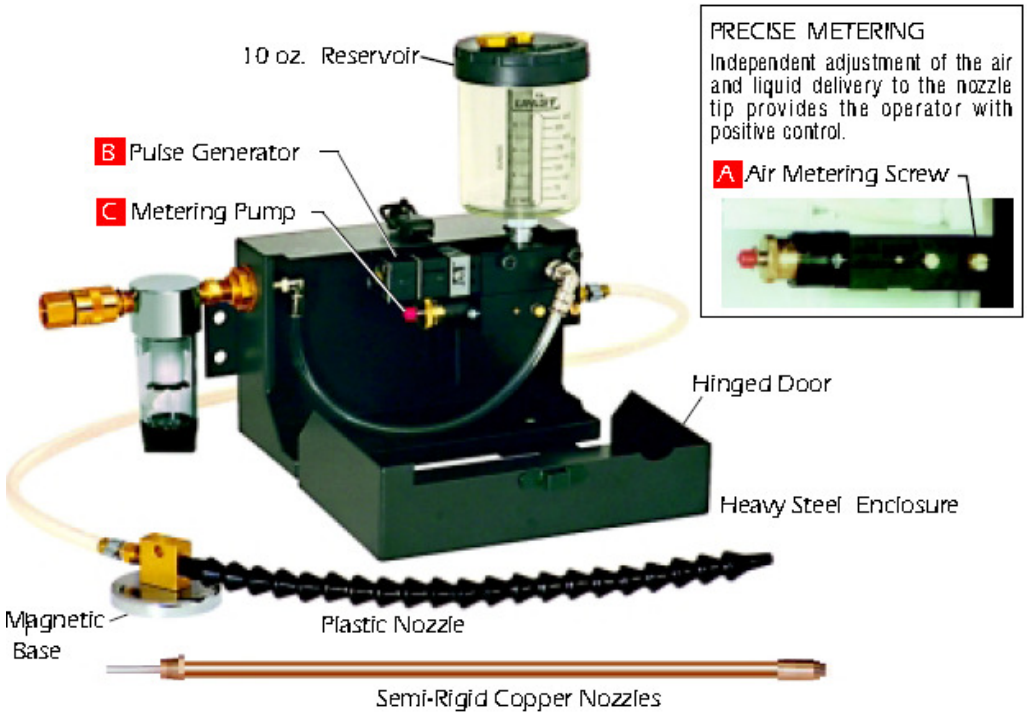


Figure A-5. Unist mist system showing different components (Unist, 2007)

# APPENDIX B

# MATHEMATICAL MODELS

## B.1. DERIVATION OF CONTACT ANGLE

The measurement of contact angle is important in a quantitative comparison between different cutting fluids. The measurement of contact angle can be done using different techniques including use of a contact angle goniometer. This method employs the use of a micro-pippet to drop a known volume of liquid on a clean, flat metal surface. The preparation of the surface involves washing it with alcohol and drying it completely. Careful considerations must be made to make sure that the environment is dust free. Immediately after dropping the liquid, the drop is placed under an optical microscope to measure its mean diameter. This data is then used to calculate the contact angle between 316L stainless steel, which is the material of the flat plate and the cutting fluid in question.

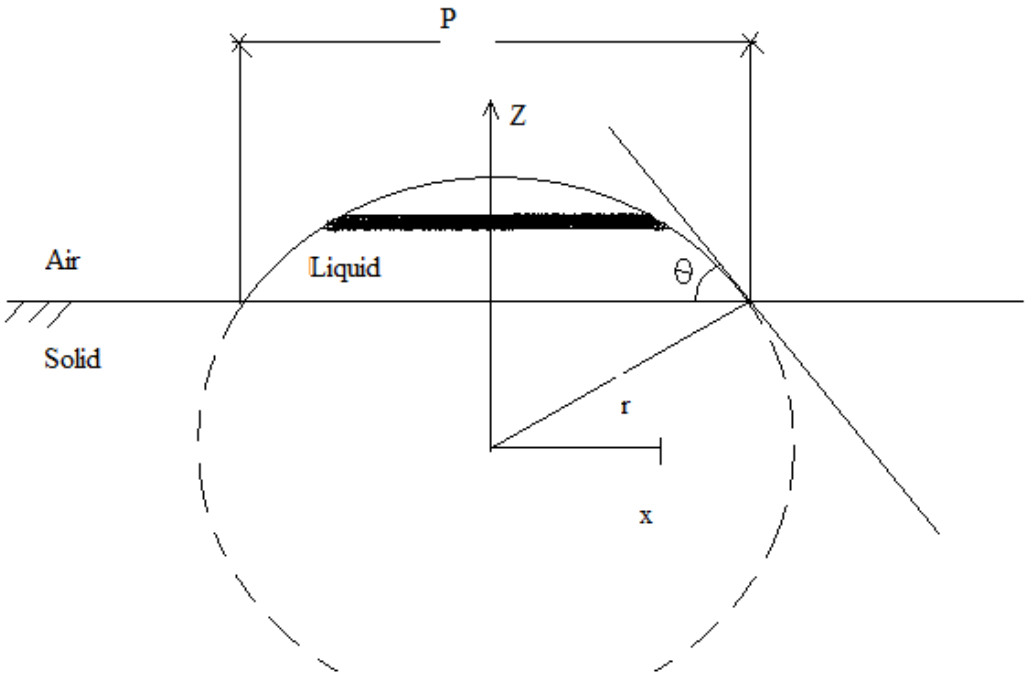


Figure B1: Side view of droplet on a flat solid surface

Consider a drop of liquid on a flat surface, neglecting the effect of gravity, the drop will form a portion of a sphere to minimize its Gibb's free energy. Consider the surface tension as a line tension $\sigma_{ij}$ between liquid and solid surfaces. At equilibrium, the sum of the forces is zero.

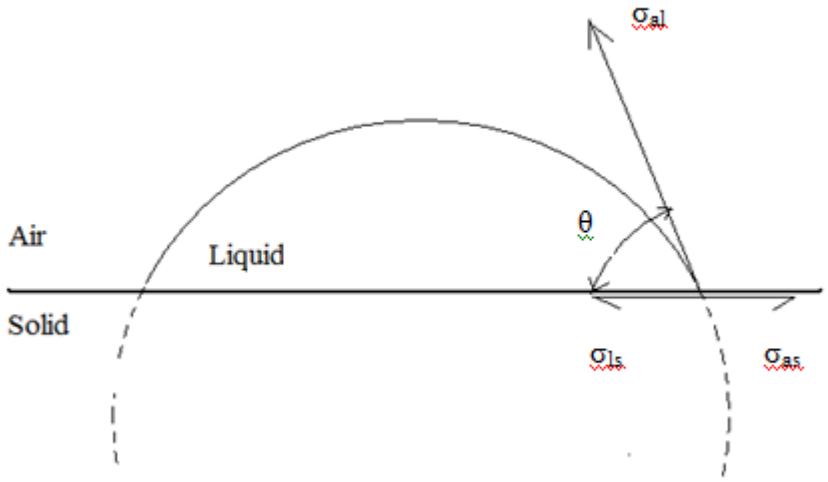


Figure B2 : Surface tension forces on a droplet.

$$\sigma_{ls} = \sigma_{as} - \sigma_{al} \cos\theta \qquad \text{(B1)}$$

Where

$\sigma_{ij}$ = Surface tension between two phases i and j.

a,l,s= air liquid solid

θ= contact angle

Finding the volume of the drop by "cutting" the sphere into small elements perpendicular to Z axis, differential volume is

$$dV = \pi x^2 \, dz \qquad \text{(B2)}$$

Using $x^2 + z^2 = r^2$ and integrating the above result,

$$V = \int_{r\cos\theta}^{r} \Pi x^2 dz = \int_{r\cos\theta}^{r} \Pi(r^2 - z^2) dz = \Pi[r^2 z - \frac{1}{3} z^3]_{r\cos\theta}^{r} \qquad \text{(B3)}$$

$$V = \Pi[\frac{2}{3}r^3 - r^3(\cos\theta - \frac{1}{3}\cos^3\theta)] \tag{B4}$$

$$V = \frac{\Pi r^3}{3}[2 - 3\cos\theta + \cos^3\theta] \tag{B5}$$

Special case: θ= $90^0$, cos θ=0, $V = \frac{2}{3}\Pi r^3$ is the volume of the hemisphere.

Let P= diameter of the projected liquid/solid interface

$$P = 2r * \sin\theta = 2r\sqrt{(1-\cos^2\theta)} \tag{B6}$$

Combining above two equations to get the dimensionless form:

$$\frac{P}{V^{1/3}} = [\frac{24}{\Pi}\frac{(1-x^2)^{3/2}}{2-3x+x^3}]^{1/3} \tag{B7}$$

Where x = cosθ

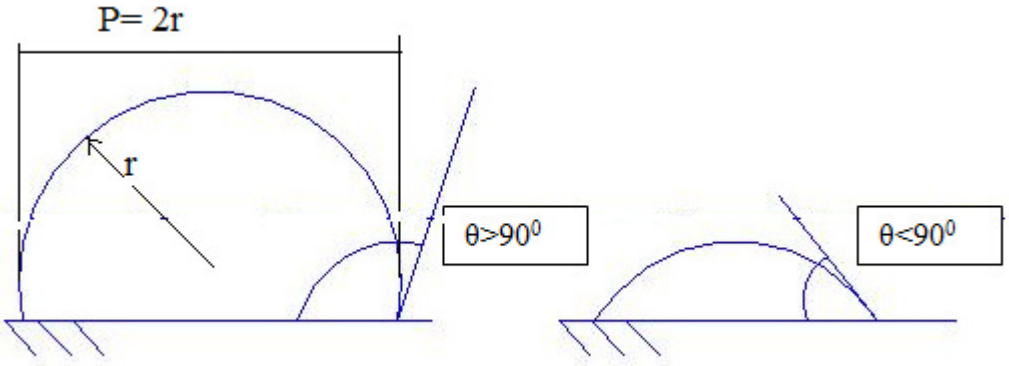


(a) (b)

Figure B3: Two ranges contact angle: a) θ>$90^0$, b) θ<$90^0$

When $\theta > 90^0$, projected image P= 2r. Hence:

$$V = \frac{\Pi}{3}(\frac{P}{2})^3[2 - 3\cos\theta + \cos^3\theta] \quad \text{(B8)}$$

Dimensionless form : $$\frac{P}{V^{1/3}} = [\frac{24}{\Pi}\frac{1}{2 - 3\cos\theta + \cos^3\theta}]^{1/3} \quad \text{(B9)}$$

Combining the 2 dimensionless forms: $$\frac{P}{V^{1/3}} = [\frac{24}{\Pi}\frac{(1 - Kx^2)^{3/2}}{2 - 3x + x^3}]^{1/3} \quad \text{(B10)}$$

Clearly, the dimensionless parameter $\frac{P}{V^{1/3}}$ is a function of ($x = \cos\theta$). Hence, we can calculate the angle $\theta$.

## B.2. DERIVATION OF AIR PRESSURE FOR MIST FLOW

Air/ mist pressure is adjusted using air metering screw (Figure A-5). However, there is no pressure gauge to measure the pressure of the air/mist mixture at the needle tip. This situation calls to calibrate pressure and relate the exit pressure at the needle tip with the number of rotations of the air metering screw. To do this the set up shown in Figure (22) is required. In this set up the deflection of a steel bar is measured and that deflection is converted to the exit pressure by using beam deflection formula.

$$P = \frac{F}{A} \tag{B11}$$

Beam deflection formula:

$$F = \frac{3EI\Delta_{max}}{L^3} \tag{B12}$$

Where:

$\Delta_{max}$ = deflection of the steel plate

F = force

E = modulus of elasticity ($E_{steel} = 2.8*10^7$ psi = $1.931*10^{11}$ N/ $m^2$)

I = area moment of inertia

L = length of the steel bar

Substituting this value of F into Equation (B11) gives:

$$P = \frac{F}{A} = \frac{3EI\Delta_{max}}{\left(\frac{\Pi}{4}\right)d^2L^3} = \frac{12EI}{\Pi d^2}\left(\frac{\Delta_{max}}{L^3}\right) \tag{B13}$$

Where d = Diameter of the needle (d=1.64 mm = .00164 m)

The moment of inertia I of the cross section of the steel bar:

$$I = \frac{1}{12} b_c h_c^3 \tag{B14}$$

where bc = length of the cross-section

hc = height of the cross-section

$$I = \frac{1}{12} bh^3 = \frac{1}{12} * 36.97 * (.70)^3 = 1.06 mm^4 = 1.06 * 10^{-12} m^4$$

$$P = \frac{12 * 1.931 * 10^{11} * 1.06 * 10^{-12}}{\Pi * (.00164)^2} \left( \frac{\Delta_{max}}{L^3} \right) \left( \frac{1 bar}{10^5 Pascals} \right)$$

$$P = 2.9 * \left( \frac{\Delta_{max}}{L^3} \right) \tag{B15}$$

Where L = length of the steel plate 0.1922 m

$$P = 2.9 * \frac{\Delta_{max}}{(0.1922)^3} \tag{B16}$$

$$P = 408 * \Delta_{max} \tag{B17}$$

## B.3. DERIVATION OF MIST DROPLET SIZE

The calculation of drop size can be done by collecting mist droplets on a flat metal plate. Since the droplet is a part of a sphere as shown in Figure B4, we can measure the volume of the droplet from its diameter and height. Assuming that the drop is a sphere before hitting any surface, we can equate the volume of the droplet with the volume of the partial sphere as measured with a microscope.

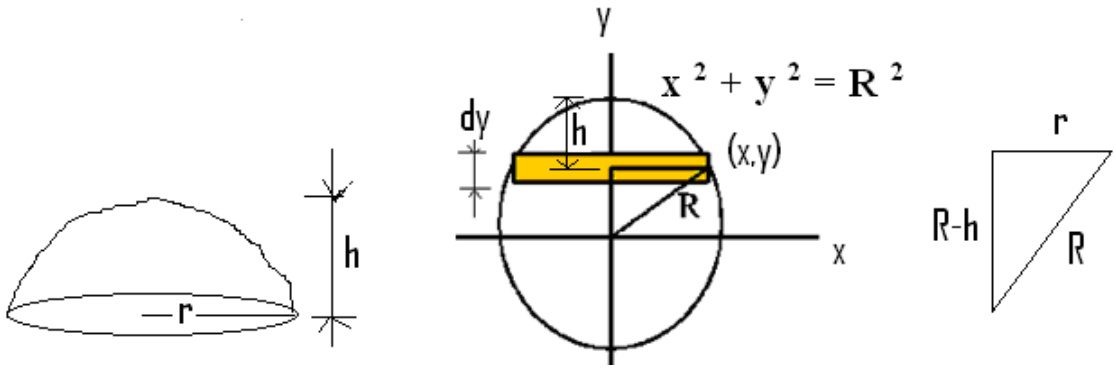


Figure B4: Theoretical shape of droplet

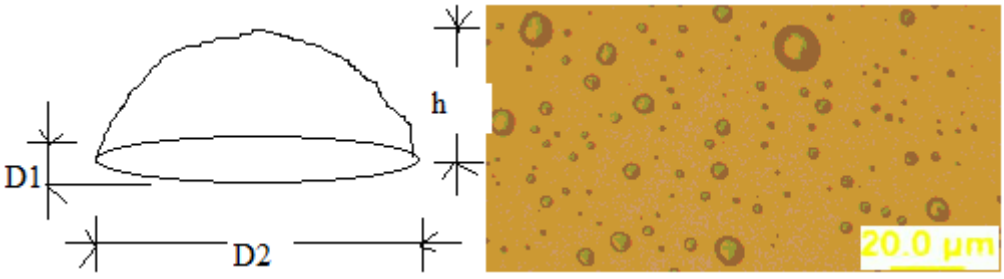


(a) (b)

Figure B5: (a) Actual shape of droplet after hitting the tool tip (b) 2D Image after hitting the surface.

$$V = \Pi h^2 \left[ \left( \frac{h}{6} \right) + \left( \frac{r^2}{2h} \right) \right] \quad \text{(B18)}$$

Assuming the droplet as part of a sphere:

$(R-h)^2 + r^2 = R^2$ (using Pythagorean's theorem for right angle triangle)

Solving for R, $R = \frac{h^2 + r^2}{2h} = \frac{h}{2} + \frac{r^2}{2h}$ (B19)

$dA = \Pi x^2$ (B20)

$dV = dAdy$ (B21)

Volume of the droplet:

$$V = \int dV = \int_{R-h}^{R} \Pi(R^2 - y^2)dy = \Pi \left( R^2 y - \frac{y^3}{3} \right) \Big|_{R-h}^{R} = \Pi h^2 \left( R - \frac{h}{3} \right) \quad \text{(B22)}$$

Substituting $R = \frac{h}{2} + \frac{r^2}{2h}$ in the above equation and simplifying gives:

$$V = \Pi h^2 \left[ \left( \frac{h}{6} \right) + \left( \frac{r^2}{2h} \right) \right] \quad \text{(B23)}$$

By measuring h and r, volume of the droplet can be calculated.

Mass m of the droplet can be calculated as:

$$m = \rho \Pi h^2 \left[ \left( \frac{h}{6} \right) + \left( \frac{r^2}{2h} \right) \right] \quad \text{(B24)}$$

Droplets are full sphere before hitting tool tip, Therefore:

$$V_{avg} = \left( \frac{4}{3} \right) \Pi R_{avg}^{\ 3} \quad \text{(B25)}$$

## B.4. DERIVATION OF PARTICLE TRAJECTORY

The modeling of particle trajectory requires knowledge of the flow field in which the particle is introduced. If there is a boundary layer around the tool that needs to be penetrated in order for the tool to be wet by the cutting fluid, it is important to describe the motion on the mist particle in the boundary layer. Since the particle size is very small compared to the cylinder, we can assume the tool surface where the droplet comes in contact as a flat surface (Figure B6). For the purpose of this model, assume the tool to be stationary and the boundary layer flowing over it with a velocity $V_f$. $V_f$ may vary with respect to 'y' depending on the nature of the boundary layer. To determine the trajectory of the particle in a 2-D flow-field, where Z axis is the axis of the tool, let us assume the flow field shown in figure 30. The origin of this flow field is at the tip of the nozzle.

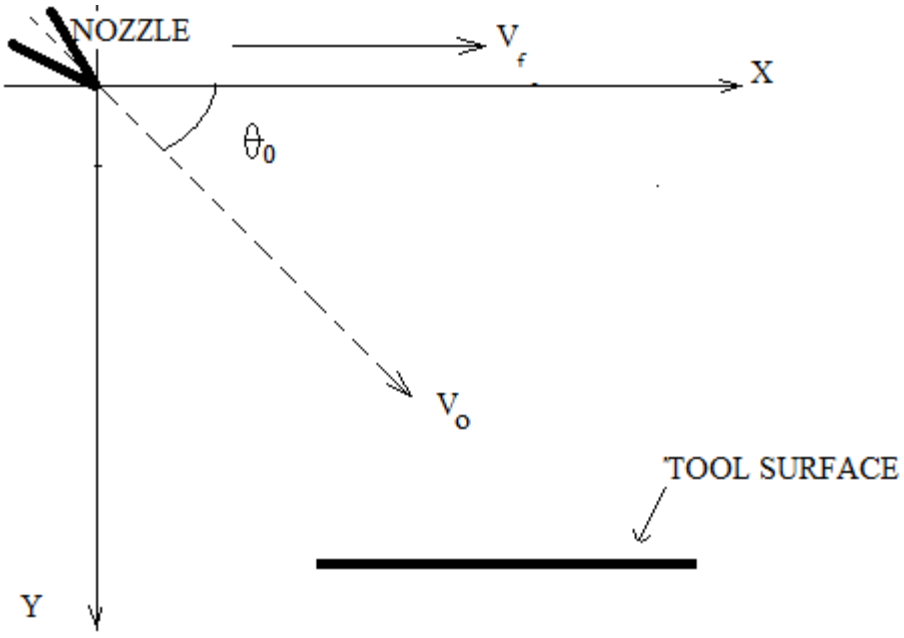


Figure B6: Trajectory of a particle upon entering a flow field

$F = -3\mu \pi D V_0$ (Stoke's Law) (B26)

Where,

$\mu$ = Absolute viscosity = 18.2075 kg/ms at $20^0$C.

D = Diameter of particle

$V_0$ = Magnitude of initial velocity.

M = Mass of particle

$\theta_0$ = Angle of entry

t = Time

$V_f$ = Velocity of the fluid

$V_{pn}$ = Velocity of the particle with respect to the nozzle.

$F = - \alpha . V_0$

$\alpha = 3\mu \pi D$ (B27)

$F_x = - \alpha . V_x$ (B28)

$F_y = - \alpha . V_y$ (B29)

$V_{pn}(0) = V_p \cos\theta \, i + V_p \sin\theta \, j$ (B30)

$V_{pf} = V_{pn} - V_{fn}$ (B31)

$V_x \approx V_{pf,x} = V_{pn,x} + V_{fn,x}$ (B32)

$V_y \approx V_{pf,y} = V_{pn,y} + V_{fn,y}$ (B33)

$V_{pf}$ = Velocity of the particle with respect to the fluid

$V_{pf,x}$= Velocity of the particle with respect to the fluid in x-direction

$V_{pf,y}$ = Velocity of the particle with respect to the fluid in y- direction

Velocity of fluid with respect to nozzle in y direction is zero. $V_{fn,y}=0$

Now,

$$M\, d\frac{V_x}{dt} = -\alpha\,(V_{pn,x} - V_f) = M\, d\,\frac{V_{pn,x}}{dt} \quad \text{(B34)}$$

Since $V_{pf,y} = V_{pn,y}$ (B35)

$$M\, d\,\frac{V_y}{dt} = -\alpha\,(V_{pf,y} + 0) = M\, d\,\frac{V_{pf,y}}{dt} \quad \text{(B36)}$$

$$\text{Or, } d\,\frac{V_{pf,y}}{dt} = -(\frac{\alpha}{M})\,\alpha\, V_{pf,y} \quad \text{(B37)}$$

Integrating

$$\text{Ln } V_{pf,y} = -(\frac{\alpha}{M})\, t + \text{Constant} \quad \text{(B38)}$$

At $t = 0$,

$$V_{pf,y} = V_0 \sin\theta_0 \quad \text{(B39)}$$

$$\text{Constant} = \text{Ln}\,(V_0 \sin\theta_0) \quad \text{(B40)}$$

$$\text{Ln}(\frac{V_{pf,y}}{V_0 sin\theta_0}) = -(\frac{\alpha}{M})\, t \quad \text{(B41)}$$

$$\text{Or, } V_{pf,y} = V_0 \sin\theta_0\, e^{-(\alpha/M)\, t} \quad \text{(B42)}$$

$$d\,\frac{y_{pf}}{dt} = V_0 \sin\theta_0\, e^{-(\alpha/M)\, t} \quad \text{(B43)}$$

Integrating

$$y_{pf} = V_0 \sin\theta_0\,(-\alpha / M) e^{-(\alpha/M)t} + \text{Constant} \quad \text{(B44)}$$

$$\text{At } t = 0,\ y_{pf} = 0 \quad \text{(B45)}$$

$$0 = (-\frac{\alpha}{M}) V_0 \sin\theta_0 + \text{Constant} \quad \text{(B46)}$$

$$\text{Hence, } y_{pf} = (\frac{\alpha}{M})\, V_0 \sin\theta_0\, [\, 1 - e^{-(\alpha/M)\, t}\,] \quad \text{(B47)}$$

Similarly,

$$M\, d\frac{V_x}{dt} = -\alpha\,(V_{pn,x} - V_f) \tag{B48}$$

$$M\, d\frac{V_{pn,x}}{dt} = -\alpha\,(V_{pn,x} - V_f) \tag{B49}$$

Integrating

$$\text{Ln}\,(V_{pn,x} + V_f) = -\left(\frac{\alpha}{M}\right) t + \text{Constant} \tag{B50}$$

At $t = 0$,

$$V_{pn,x} = V_0 \cos\theta_0 \tag{B51}$$

$$\text{Constant} = \text{Ln}\,(V_0 \cos\theta_0 - V_f) \tag{B52}$$

$$\text{Or,}\quad V_{pn,x} = V_f + (V_0 \cos\theta_0 - V_f)\, e^{-(\alpha/M)\, t} \tag{B53}$$

$$d\frac{x_{pn}}{dt} = V_f + (V_0 \cos\theta_0 - V_f)\, e^{-(\alpha/M)\, t} \tag{B54}$$

Integrating

$$x_{pn} = V_f\, t - \left(\frac{\alpha}{M}\right)(V_0 \cos\theta_0 - V_f)\, e^{-(\alpha/M)\, t} + \text{Constant} \tag{B55}$$

$$\text{At}\quad t = 0,\ x_{pn} = 0 \tag{B56}$$

$$0 = 0 - \left(\frac{\alpha}{M}\right)(V_0 \cos\theta_0 - V_f) + \text{Constant} \tag{B57}$$

Hence,

$$x_{pn} = V_f\, t + \left(\frac{\alpha}{M}\right)(V_0 \cos\theta_0 - V_f)\,[1 - e^{-(\alpha/M)\, t}] \tag{B58}$$

$$y_{pn} = y_{pn} = \left(\frac{\alpha}{M}\right) V_0 \sin\theta_0\,[\,1 - e^{-(\alpha/M)\, t}\,] \tag{B59}$$

The trajectory is exponential as expected with $x_{pn}$ approaching infinity at time infinity and $y_{pn}$ approaching a constant at time infinity.

# APPENDIX C

# MATLAB PROGRAMS OF CONTACT ANGLE PLOT

## C.1. MATLAB PROGRAM FOR PLOTTING EQUATION (10) FOR $0^0<\theta<180^0$

The equation for contact angle measurement can be plotted in MATLAB to reduce calculations.

```
% x = -1:0.2:1;
% if x>=-1 && x<=0;
%     K=0;
% end
% if x>0 && x<=1
%     K=1;
% end
% y = [(24/pi)*(1-K*x^2)^1.5/(2-3*x+x^3)]^(1/3);
% plot(x,y,'--rs','LineWidth',2,...
%                 'MarkerEdgeColor','k',...
%                 'MarkerFaceColor','g',...
%                 'MarkerSize',10)
clc
clear all

for i=1:401
```

```
    x(i)=(i-1)*0.005-1;
y(i) = [(24/pi)*(1-x(i)^2)^1.5/(2-3*x(i)+x(i)^3)]^(1/3);
z(i)=acosd(x(i))/36;
end

plot(x,y,x,z)

for j=1:13
    X(j)=1;
    Y(j)=(j-1)*15/36;
    String(j)=(j-1)*15
end
for j=1:13
    str=num2str(String(j),'%3.0f');
    text(X(j)+0.01,Y(j),['---',str]);
hold on
end
```

# APPENDIX D

# TOOL WEAR AND MIST CHARACTERIZATION DATA

## D.1. TOOL MATERIAL: WC

Table D1. Tungsten carbide tool wear data for dry cutting

| Chip Load: 10μ/tooth | | | Coolant: Dry | | Material: 316L | | Tool: 1.016mm Dia | |
|---|---|---|---|---|---|---|---|---|
| Axial Depth: 0.348mm | | | Radial Depth: 0.56mm | | | | | |
| Tool # | Test # | Flank Wear (um) | Nose Wear(um) | Tool Dia(mm) | Incremental Pass | Pass Length (mm) | RPM | Linear Speed (m/min) |
| 1 | 1 | 19.3 | | | 5 | 16.25 | 10000 | 31.93 |
| | | 17.2 | | | | | | |
| | | *Chip 150u from nose* | | | | | | |
| | 2 | 21.8 | | | | | | |
| | | 17.7 | | | 10 | 16.25 | 10000 | |
| | 3 | 24.3 | | | 18 | 16.25 | 10000 | |
| | | 30.6 | | | | | | |
| | 4 | 33.4 | | | 22 | 20.5 | 10000 | |
| | | 27.8 | | | | | | |
| | 5 | 23.8 | | | 26 | 20.5 | 15000 | 47.89 |
| | | 29.2 | | | | | | |
| | 6 | *BUE* | 137um | | 30 | 20.5 | 15000 | |
| 2 | 1 | 17.6 | | | 8 | 16.25 | 20000 | 63.86 |
| | | 16.7 | | | | | | |
| | 2 | 18.5 | | | 16 | 16.25 | 20000 | |
| | | 20.8 | | | | | | |
| | 3 | 18 | | | 21 | 16.25 | 20000 | |
| | | 23.7 | | | | | | |
| | 4 | 28.6 | | | 28 | 20.5 | 20000 | |
| | | 25.2 | | | | | | |
| | 5 | 32.4 | | | 32 | 20.5 | 25000 | |
| | | 46.7 | | | | | | |
| | 6 | 37.1 | | | 36 | 20.5 | 25000 | |
| | | 33.6 | | | | | | |
| 3 | 1 | 21.2 | | | 5 | 20.5 | 30000 | 95.79 |
| | | 20.3 | | | | | | |
| | 2 | 18.6 | | | 10 | 20.5 | | |
| | | *Broken* | | | | | | |
| 4 | 1 | 15.2 | | | 9 | 20.5 | 40000 | 127.72 |
| | | 17.4 | | | | | | |
| | 2 | 17.6 | | | 13 | 20.5 | 40000 | |
| | | 16.3 | | | | | | |
| | 3 | *Broken* | | | 22 | 20.5 | 40000 | |

Table D2. Tungsten carbide tool wear data for mist cutting

| Chip Load: 10μ/tooth | | | Coolant: Mist | | Material: 316L | | Tool: 1.016mm Dia | |
|---|---|---|---|---|---|---|---|---|
| Axial Depth: 0.348mm | | | Radial Depth: 0.56mn | | Mist angle: (r, θ,φ)= (30mm, $60^0$, $55^0$) | | | |
| Tool # | Test # | Flank Wear (um) | Nose Wear(um) | Tool Dia(mm) | Incremental Pass | Pass Length (mm) | RPM | Linear Speed (m/min) |
| 5 | 1 | 4.8 | | | 4 | 20.5 | 6000 | 19.15 |
| | | 5.7 | | | | | | |
| | 2 | 16.3 | | | 8 | 20.5 | 6000 | |
| | | 11.7 | | | | | | |
| | 3 | 14.7 | | | 16 | 20.5 | 6000 | |
| | | 20 | | | | | | |
| | 4 | 23.7 | | | 20 | 20.5 | 6000 | |
| | | 18.4 | | | | | | |
| 6 | 0 | | | 1.0371 | | | | |
| | | | | 1.038 | | | | |
| | 1 | 7.2 | 4.8 | 1.029 | 4 | 20.5 | 4000 | 12.77 |
| | | 6.8 | 9.1 | 1.0239 | | | | |
| | 2 | 13.7 | 18.5 | 1.0248 | 12 | 20.5 | 4000 | |
| | | 11.9 | 20.6 | 1.0246 | | | | |
| | 3 | 12 | 11.8 | 1.0242 | 16 | 20.5 | 4000 | |
| | | 12.8 | 21.2 | 1.0239 | | | | |
| | | *small burs* | | | | | | |
| | 4 | 14.9 | 22.7 | 1.0231 | 20 | 20.5 | 6000 | 19.15 |
| | | 12.6 | 12.6 | 1.0239 | | | | |
| | 5 | 18.4 | 18.7 | 1.0221 | 28 | 20.5 | 6000 | |
| | | 17 | 14.9 | 1.0199 | | | | |
| | | *small burs* | | | | | | |
| | 6 | 20.2 | 23.8 | 1.0241 | 36 | 20.5 | 6000 | |
| | | 19 | 28.7 | 1.022 | | | | |
| | | | | | | | | |
| | 7 | 21.4 | 67.5 | 0.9943 | 42 | 20.5 | 6000 | |
| | | 23.4 | 47.7 | 1.003 | | | | |
| | | *attrition wear at nose* | | | | | | |
| 7 | 0 | | | 1.0352 | 0 | 20.5 | | |
| | | | | 1.0355 | | | | |
| | 1 | 8.1 | 14.1 | 1.0268 | 2 | 20.5 | 10000 | 31.93 |
| | | 7.9 | 15 | 1.0261 | | | | |
| | 2 | 9.7 | 18.8 | 1.0256 | 5 | 20.5 | 10000 | |
| | | 9.7 | 20.1 | 1.026 | | | | |
| | 3 | 9.8 | 29.6 | 1.0218 | 9 | 20.5 | 10000 | |
| | | 10.6 | 24.8 | 1.02 | | | | |
| | 4 | 11.9 | 41.7 | 1.0216 | 13 | 20.5 | 15000 | 47.89 |
| | | 9.9 | 39.7 | 1.022 | | | | |
| | | *Small BUE on flank* | | | | | | |
| | 5 | 11.7 | 42.1 | 1.0213 | 17 | 20.5 | 15000 | |
| | | 13 | 42.1 | 1.022 | | | | |
| | | *Large BUE on Nose* | | | | | | |
| | 6 | 13.1 | 42.7 | 1.022 | 21 | 20.5 | 15000 | |
| | | 12.1 | 42.3 | 1.0222 | | | | |
| | | *Large BUE on top view* | | | | | | |

D.2. TOOL MATERIAL: TiN--CT

Table D3. TiN tool wear data for dry cutting

| Chip Load: 10µ/tooth | | | Coolant: Dry | | Material: 316L | | Tool: 1.016mm Dia | |
|---|---|---|---|---|---|---|---|---|
| Axial Depth: 0.348mm | | | Radial Depth: 0.56mm | | | | | |
| Tool # | Test # | Flank Wear (um) | Nose Wear(um) | Tool Dia(mm) | Incremental Pass | Pass Length (mm) | RPM | Linear Speed (m/min) |
| 1 | 1 | *Edge Chipped* | | | 5 | 16.25 | 10000 | 31.93 |
| | | | | | | | | |
| 2 | 1 | 8.3 | | | 5 | 16.25 | | |
| | | 11.9 | | | | | | |
| | 2 | 23.1 | | | 10 | 16.25 | 20000 | 63.86 |
| | | 18.4 | | | | | | |
| | | *Tool Chipped* | | | | | | |
| 3 | 1 | *Large BUE* | | | 5 | 16.25 | 30000 | 95.79 |
| | | *Large BUE* | | | | | | |
| | 2 | *Large BUE* | | | 10 | 16.25 | 30000 | |
| | | *Large BUE* | | | | | | |

Table D4. TiN tool wear data for mist cutting

| Chip Load: 10µ/tooth | | | Coolant: Mist | | Material: 316L | | Tool: 1.016mm Dia | |
|---|---|---|---|---|---|---|---|---|
| Axial Depth: 0.348mm | | | Radial Depth: 0.56mm | | | Mist angle: (r, θ,φ)= (30mm, $60^0$, $55^0$) | | |
| Tool # | Test # | Flank Wear (um) | Nose Wear(um) | Tool Dia(mm) | Incremental Pass | Pass Length (mm) | RPM | Linear Speed (m/min) |
| 4 | 0 | | | 1.0266 | 0 | | | |
| | | | | 1.0257 | | | | |
| | 1 | 4 | 17.2 | 1.0229 | 4 | 20.5 | 4000 | 12.77 |
| | | 4.3 | 15.2 | 1.0264 | | | | |
| | 2 | 5 | 21.4 | 1.0217 | 8 | 20.5 | 4000 | |
| | | 6.7 | 21.9 | 1.0213 | | | | |
| | 3 | | 24.3 | 1.0209 | 16 | 20.5 | 4000 | |
| | | | 26.7 | 1.024 | | | | |
| | | *Chipped with a Microcrack* | | | | | | |
| 5 | 0 | | | 1.0264 | | | | |
| | | | | 1.0259 | | | | |
| | 1 | 19.5 | 47 | 0.9959 | 4 | 20.5 | 3000 | 9.57 |
| | | 17.8 | 28.3 | 1.0055 | | | | |
| | | *Coating Peel off on one Flank* | | | | | | |
| 6 | 0 | | | 1.0266 | 0 | | | |
| | | | | 1.0257 | | | | |
| | 1 | 8.3 | 48 | 0.9949 | 4 | 20.5 | 4000 | 12.77 |
| | | 12.3 | 42.8 | 0.996 | | | | |
| | | *Wear on back side of nose, BUE* | | | | | | |
| | 2 | 13.2 | 53 | 0.9962 | 5 | 20.5 | 4000 | 12.77 |
| | | 11 | 55 | 0.9937 | | | | |
| | | *Craters on nose.* | | | | | | |

D.3. TOOL MATERIAL : Ti-CN--CT

Table D5. Ti-CN--CT tool wear data for dry cutting

| Chip Load: 10µ/tooth | | | Coolant: Dry | | Material: 316L | | Tool: 1.016mm Dia | |
|---|---|---|---|---|---|---|---|---|
| Axial Depth: 0.348mm | | | Radial Depth: 0.56mm | | | | | |
| Tool # | Test # | Flank Wear (um) | Nose Wear(um) | Tool Dia(mm) | Incremental Pass | Pass Length (mm) | RPM | Linear Speed (m/min) |
| 1 | 1 | *Chipped corner* | | | 5 | 16.25 | 10000 | 31.93 |
| | | *Peeled Coating* | | | | | | |
| 2 | 1 | 15.7 | | | 5 | 16.25 | 20000 | 63.86 |
| | | *BUE* | | | | | | |
| | 2 | *Chipped* | | | 10 | 16.25 | | |
| 3 | 1 | *Peeled coating* | | | 5 | 16.25 | 30000 | 95.79 |
| | | *at corner, away* | | | | | | |
| | | *from cutting edge* | | | | | | |

Table D6. Ti-CN--CT tool wear data for mist cutting

| Chip Load: 10µ/tooth | | | Coolant: Mist | | Material: 316L | | Tool: 1.016mm Dia | |
|---|---|---|---|---|---|---|---|---|
| Axial Depth: 0.348mm | | | Radial Depth: 0.56mm | | | Mist angle: (r, θ,φ)= (30mm, $60^0$, $55^0$) | | |
| Tool # | Test # | Flank Wear (um) | Nose Wear(um) | Tool Dia(mm) | Incremental Pass | Pass Length (mm) | RPM | Linear Speed (m/min) |
| 4 | 0 | | | 1.0141 | 0 | | | |
| | | | | 1.011 | | | | |
| | 1 | 14.4 | 10.6 | 1.0155 | 4 | 20.5 | 4000 | 12.77 |
| | | 10.5 | 12 | 1.0167 | | | | |
| | 2 | 21.7 | 26.7 | 1.0124 | 8 | 20.5 | 4000 | |
| | | 17.7 | 13.8 | 1.0121 | | | | |
| | | *EdgePeeled* | | | | | | |
| 5 | 1 | 38.6 | 56.7 | 0.9423 | 4 | 20.5 | 3000 | 9.57 |
| | | 16.8 | 54.3 | 0.9416 | | | | |
| | | *Lot of burs, BUE* | | | | | | |
| | | *Nose Chip off* | | | | | | |

## D.4. TOOL MATERIAL: Ti-AlN—CT

Table D7. Ti-AlN--CT tool wear data for dry cutting

| Chip Load: 10µ/tooth | | | Coolant: Dry | | Material: 316L | | Tool: 1.016mm Dia | |
|---|---|---|---|---|---|---|---|---|
| Axial Depth: 0.348mm | | | Radial Depth: 0.56mm | | | | | |
| Tool # | Test # | Flank Wear (um) | Nose Wear(um) | Tool Dia(mm) | Incremental Pass | Pass Length (mm) | RPM | Linear Speed (m/min) |
| 1 | 1 | 15.3 | | | 5 | 16.25 | 10,000 | 31.93 |
| | | 19.5 | | | | | | |
| | 2 | 41.4 | | | 10 | 16.25 | | |
| | | 43.5 | | | | | | |
| 2 | 1 | *chipped edge* | | | 5 | 16.25 | 20,000 | 63.86 |
| | | *chipped edge* | | | | | | |
| 3 | 1 | *chipped edge* | | | 7 | 16.25 | 30,000 | 95.79 |
| | | *chipped edge* | | | | | | |

Table D8. Ti-AlN--CT tool wear data for mist cutting

| Chip Load: 10µ/tooth | | | Coolant: Mist | | Material: 316L | | Tool: 1.016mm Dia | |
|---|---|---|---|---|---|---|---|---|
| Axial Depth: 0.348mm | | | Radial Depth: 0.56mm | | | Mist angle: (r, θ,φ)= (30mm, $60^0$, $55^0$ | | |
| Tool # | Test # | Flank Wear (um) | Nose Wear(um) | Tool Dia(mm) | Incremental Pass | Pass Length (mm) | RPM | Linear Speed (m/min) |
| 4 | 0 | | | 1.0339 | 0 | | | |
| | | | | 1.0345 | | | | |
| | 1 | 12.6 | 35.2 | 0.9738 | 4 | 20.5 | 3,000 | 9.579 |
| | | | 35.8 | 0.9716 | | | | |
| | | *Flank Chipped* | | | | | | |
| 5 | 0 | | | 1.0342 | 0 | | | |
| | | | | 1.035 | | | | |
| | 1 | | 11 | 1.0333 | 4 | 20.5 | 4,000 | 12.77 |
| | | | 21 | 1.0285 | | | | |
| | | *Chipped Flank* | | | | | | |

## D.5. CONTACT ANGLE DATA

Table D9. Contact angle measurement data

| | Diameter (mm) | | Avg Dia | p/v^1/3 | contact angle |
|---|---|---|---|---|---|
| Coolant: | 2300 HD | | (mm) | | (Degrees) |
| Sl no. | vol: 2.5uL | | | | |
| 1 | 4.17 | 3.58 | 3.87 | 2.85 | 25.00 |
| 2 | 4.19 | 3.60 | 3.90 | 2.87 | 25.00 |
| 3 | 4.18 | 3.58 | 3.88 | 2.86 | 25.00 |
| Median: | | | 3.88 | 2.86 | |
| Coolant: | 2200.00 | | | | |
| Sl no. | vol: 2.5uL | | | | |
| 1 | 4.42 | 4.43 | 4.42 | 3.26 | 15.00 |
| 2 | 4.40 | 4.42 | 4.41 | 3.25 | 15.00 |
| 3 | 4.42 | 4.42 | 4.42 | 3.26 | 15.00 |
| Median: | | | 4.42 | 3.26 | |
| Coolant: | 2210EP | | | | |
| Sl no. | vol: .25uL | | | | |
| 1 | 2.43 | 2.28 | 2.35 | 3.74 | 12.00 |
| 2 | 3.00 | 2.82 | 2.91 | 4.62 | 5.00 |
| 3 | 2.88 | 2.43 | 2.66 | 4.22 | 10.00 |
| 4 | 3.23 | 3.17 | 3.20 | 5.08 | 2.50 |
| 5 | 3.33 | 3.24 | 3.29 | 5.22 | 1.00 |
| Median: | | | 2.91 | 4.62 | |
| Coolant: | 2210.00 | | | | |
| Sl no. | vol: .25uL | | | | |
| 1 | 2.26 | 1.84 | 2.05 | 3.25 | 17.50 |
| 2 | 1.86 | 1.94 | 1.90 | 3.02 | 22.50 |
| 3 | 1.88 | 1.74 | 1.81 | 2.87 | 27.50 |
| 4 | 2.02 | 1.72 | 1.87 | 2.97 | 22.50 |
| 5 | 1.80 | 1.80 | 1.80 | 2.86 | 27.00 |
| Median: | | | | 2.96 | |
| Coolant: | Coolube (1:30) | | | | |
| Sl no. | vol: .25uL | | | | |
| 1 | 1.26 | 1.26 | 1.26 | 2.00 | 60.00 |
| 2 | 1.22 | 1.22 | 1.22 | 1.93 | 65.00 |
| 3 | 1.22 | 1.22 | 1.22 | 1.94 | 65.50 |
| 4 | 1.21 | 1.21 | 1.21 | 1.92 | 67.50 |
| 5 | 1.23 | 1.23 | 1.23 | 1.96 | 61.00 |
| Median: | 1.22 | | | 1.94 | |
| Coolant: | Water | | | | |
| Sl no. | vol: .25uL | | | | |
| 1 | 1.18 | 1.18 | 1.18 | 1.87 | 70.00 |
| 2 | 1.17 | 1.17 | 1.17 | 1.86 | 70.00 |
| 3 | 1.18 | 1.18 | 1.18 | 1.88 | 69.00 |
| 4 | 1.22 | 1.22 | 1.22 | 1.94 | 64.00 |
| 5 | 1.19 | 1.19 | 1.19 | 1.88 | 69.00 |
| Median: | 1.18 | | | 1.88 | |

## D.6. PARTICLE SIZE DATA

Table D10. Particle size measurements of 2210 EP

| Coolant Type | 2210 EP | | | |
|---|---|---|---|---|
| | D1[µm] | D2[µm] | h[µm] | DAvg[µm] |
| | 2 | 2 | 0.8 | 2 |
| | 1.6 | 1.8 | 0.4 | 1.7 |
| | 1.9 | 2.1 | 0.3 | 2 |
| | 1.6 | 2.2 | 0.2 | 1.9 |
| | 1.5 | 2 | 0.2 | 1.75 |
| | 2.5 | 2.1 | 0.1 | 2.3 |
| Averages: | 1.85 | 2.03 | 0.33 | 1.94 |
| Average Volume: ($m^3$) | 7.42E-20 | | | |
| Average Radius(Microns) | 0.26 | | | |

Table D11. Particle size measurements of 2210

| Coolant Type | 2210 | | | |
|---|---|---|---|---|
| | D1[µm] | D2[µm] | h[µm] | DAvg[µm] |
| | 3.7 | 7.5 | 0.6 | 5.6 |
| | 4.1 | 6.8 | 0.4 | 5.45 |
| | 5.1 | 5.4 | 0.4 | 5.25 |
| | 8.3 | 3.1 | 0.6 | 5.7 |
| | 4.3 | 8.2 | 0.5 | 6.25 |
| | 6.8 | 4.7 | 0.5 | 5.75 |
| Averages: | 5.38 | 5.95 | 0.50 | 5.67 |
| Average Volume: ($m^3$) | 1.64E-18 | | | |
| Average Radius(Microns) | 0.73 | | | |

Table D12. Particle size measurements of 2300HD

| Coolant Type | 2300 HD | | | |
|---|---|---|---|---|
| | D1[µm] | D2[µm] | h[µm] | DAvg[µm] |
| | 29 | 35.1 | 1.1 | 32.05 |
| | 20.9 | 25 | 1.3 | 22.95 |
| | 24.6 | 21.5 | 1 | 23.05 |
| | 24.9 | 21.7 | 1.6 | 23.3 |
| | | | | |
| | | | | |
| Averages: | 24.85 | 25.83 | 1.25 | 25.34 |
| Average Volume: ($m^3$) | 4.93E-16 | | | |
| Average Radius(Microns) | 4.90 | | | |

Table D13. Particle size measurements of 2200

| Coolant Type | 2200 | | | |
|---|---|---|---|---|
| | D1[µm] | D2[µm] | h[µm] | DAvg[µm] |
| | 15.1 | 20.6 | 1.4 | 17.9 |
| | 12.1 | 19.8 | 1.1 | 16.0 |
| | 13.8 | 17.6 | 1.3 | 15.7 |
| | 14.3 | 18.6 | 1.4 | 16.4 |
| | 20.9 | 23.2 | 1.2 | 22.1 |
| | | | | |
| Averages: | 15.24 | 19.98 | 1.28 | 17.61 |
| Average Volume: ($m^3$) | 2.59E-16 | | | |
| Average Radius(Microns) | 3.95 | | | |

# APPENDIX E

# NC PROGRAM FOR TOOL WEAR MEASUREMENT

## E.1. NC PROGRAM FOR TOOL WEAR MEASUREMENT

The calculation of tool life requires measurement of tool wear at regular intervals. Tool life is defined as the length of time for which the cutting tool machines properly before starting to fail. Failure modes in micro-milling are due to abrasion or tool/cutting edge breakage. For a 1.016 mm diameter end mill, the tool failure criteria are set at: 1) 50 microns of flank wear; 2) 50 microns of nose wear; 3) chipping or breaking of cutting edge; whichever happens earlier. Machining is carried on till wear reaches the above mentioned limits. A sample program used for side milling over a pass length of 20.5mm is as follows:

```
%
O03201
( 4 passes at 4000 RPM to measure tool wear )
( POSTED FOR HAAS VF SERIES MILLS )
( BY FEATURECAM ON 7-30-2009 USING )
( Haas VF Series.CNC POSTPROCESSOR V9/99 )
N35 G00 G17 G40 G90
( TOOL: T1 = 0.04 dia. 0.04"  )
N45 T1 M6
N50 S4000 M03
```

N60 G54 X0.009 Y0.8271

N65 G43 H1 Z1.0

N70 Z0.1

N75 G01 Z-0.0137 F1.6

N80 X-0.002 Y0.808 F3.1

N85 Y0.

N90 X0.009 Y-0.0191

N95 G00 Z1.0

N100 X-0.013 Y0.8271

N105 Z0.1

N110 G01 Z-0.0137 F1.6

N115 X-0.024 Y0.808 F3.1

N120 Y0.

N125 X-0.013 Y-0.0191

N130 G00 Z1.0

N135 X-0.035 Y0.8271

N140 Z0.1

N145 G01 Z-0.0137 F1.6

N150 X-0.046 Y0.808 F3.1

N155 Y0.

N160 X-0.035 Y-0.0191

N165 G00 Z1.0

N175 G00 G17 G54 X-0.035 Y-0.0191 Z1.0 S4000 F1.6 M08

N180 X-0.057 Y0.8271

N185 Z0.1

N190 G01 Z-0.0137 F1.6

N195 X-0.068 Y0.808 F3.1

N200 Y0.

N205 X-0.057 Y-0.0191

N210 G00 Z1.0

( END OF PROGRAM )

N220 G28 G49 G91 Z0. M09

N225 G53 G90 X-20. Y0.

N230 M30

%

# VITA


| | |
|---|---|
| Name: | Saurabh Kajaria |
| Address: | C/O Department of Mechanical Engineering,<br>3123 Texas A&M University,<br>College Station, TX 77843. |
| Email Address: | saurabhkajaria@hotmail.com |
| Education: | B.E. Mechanical Engineering, Visvesvaraya Technological University, 2007.<br>M.S. Mechanical Engineering, Texas A&M University, 2009. |